

**Experimental analysis of heat transfer for
environmental control system in indoor plantation**

Napassawan Khammayom

A thesis submitted for the degree of

Doctor of Engineering

Division of System Engineering

Graduate School of Engineering

Mie University, Japan

March 2023

Abstract

An increasing in world population and climate changes including increasing the import of agricultural products in some countries as well resulted in increased demand for food and quality. Therefore, growing plants inside the greenhouse becomes increasing popular. The main advantages are high-energy efficiency of greenhouse and high-quality products. One key target to achieve the high-energy efficiency and product quality is the ability to control environmental conditions inside greenhouse. In all of the reviewed greenhouse, weather control system is air-conditioners. However, if the greenhouse space is huge, there is a great demand for air conditioner systems. Therefore, novel techniques that can control air temperature and reduce energy consumption are interesting. This research focused on microclimate weather control system for plantation. This aim to create suitable microclimate just around each plant while surrounding space inside greenhouse may have different weather conditions. Since the volume of the air to be controlled is smaller, both air conditioner system and energy consumption will be reduced.

The first objective was to study and research an energy analysis of an experimental greenhouse and determine how to control environmental conditions around plantation. Under this objective, a field experiment was performed in a small walk-in tunnel with a passive solar greenhouse for strawberry cultivation in a temperate area in central Japan. The energy required to maintain the optimum temperature for strawberry growth in the greenhouse was calculated. Furthermore, the impact of environmental factors on the strawberries was evaluated. The findings showed that the greenhouse can provide favorable environmental conditions for strawberry plants. Generally, supplemental heating is not required during the daytime because solar radiation is sufficient to maintain the temperature inside the greenhouse high enough for strawberry cultivation even in winter. The measured weather data indicated that the inside temperature was rather low during nighttime in winter; therefore, the use of a heating system is recommended during in this period. The calculated maximum heating requirement was from November 2020 to April 2021. The heat energy requirement was found to be maximum in January ($327.6 \text{ MJ/m}^2\text{-month}$ and $281.9 \text{ MJ/m}^2\text{-month}$ when $T_{de} = 10$ and 8°C , respectively). A 2°C reduction in heating temperature could reduce energy demand by up to 31%. The difference in air temperature between day and night may improve the sweetness and weight of strawberries.

The second objective was to control the local air temperature around plantation area. Under this objective, a cooling serpentine copper pipe heat exchanger is established for cooling in a laboratory-scale room. The experiments were carried out under various operating conditions, in which the inlet water temperature, water volume flow rate, and heat transfer surface area were controlled. Following the second objective, the last objective was to investigate the thermal performance and local air temperature distributions around a cooling serpentine copper pipe heat exchanger. The local air temperatures above and below the serpentine panel as well as the relative humidity were measured. Local air temperature contour graphs were also presented. The calculation and measurements showed that a cooling serpentine copper pipe heat exchanger can reduce local air temperatures. When room air temperature was 25°C , local air temperature was lower than room air temperature approximately 5 to 9°C under different inlet water temperatures and water flow rates. Based on the results, it can be seen that the temperature of inlet water and volume flow rate greatly influenced on total heat flux, condensation heat transfer and convective heat transfer. Increasing water volume flow rate and reducing inlet water temperature led to increase in rate of heat transfer. In

addition, heat transfer rate is directly proportional to the inlet water temperature and heat transfer rate is related with droplets size, number of droplets as well as film thickness. Thermal resistance increases with increasing film thickness and number of droplets on copper pipe. Condensation or the frozen ice around copper pipe could increase the reduction in local air temperature and increase rate of heat transfer. In conclusion, a serpentine copper pipe heat exchanger can help to control local air temperature and can be used to control the temperature in a small area as well as use less energy than conventional air conditioning.

Acknowledgements

First of all, I would like to express the deepest appreciation to Professor Naoki Maruyama for giving me the opportunity to conduct my work at such an inspiring and for his guidance, he continually and convincingly conveyed a spirit of adventure of regard research and scholarship and an excitement in regard to teaching. I can say that without his guidance this research would not have been possible. After more than 2 years staying at Mie, this period has been one of the most memorable experience in my life.

I would like to express my thank to my patient and supportive supervisor, Assistant Professor Chatchawan Chaichana of the Faculty of Engineering, Chiang Mai University, Thailand, for introducing me to Professor Naoki Maruyama and for his kind encouragement. In addition, financial support was provided by Energy Technology for Environment Research Center (ETE) and I also thank to all member staffs of ETE for their kind support.

I am indebted to Professor Masafumi Hirota and Associate Professor Akira Nishimura of the Division of Mechanical Engineering, Mie University for their every valuable suggestion, in order to conduct the experiment. Their unassuming approach to research and engineering is a source of inspiration.

My sincere thanks go to the students at Thermal Energy System Laboratory of Mie University for their assistance when I have been at Mie University. Moreover, I would like to thank to my friends “Thai Students” at Mie University. I enjoyed every moment we were together.

Finally, my deepest thanks go to my mom and family; thank you for always being there for me and supporting me from the start, and for continuing to encourage me to achieve my dream. Aong, no words can explain how grateful and appreciative I am to you and your family. Thank you for always cheering me up and for all your support, encouragement and patience.

Napassawan Khammayom

March, 2023

Table of contents

Abstract	i
Acknowledgements	iii
List of figures	viii
List of tables	xi
Nomenclature	xii

1. Introduction

1.1 Research motivation	1
1.2 Literature reviews	
1.2.1 Literature review on cooling system for plant factory applications	2
1.2.2 Literature review on spot cooling system in plantation area	6
1.2.3 Literature review on heat exchanger applications	8
1.3 Research objective	11
1.4 Scopes of research	11
1.5 Significance of research	11
1.6 Outline of the thesis	12
Reference in chapter 1	12

2. Principle and theories

2.1 Energy balance of walk-in tunnel	16
2.1.1 Statistical analysis	19
2.2 Principle of natural convection	19
2.2.1 Physical mechanism of natural convection	19
2.2.2 Natural convection over surface	23
2.3 Internal forced convection	25
2.3.1 Laminar and turbulent flow in tube	25
2.3.2 General thermal analysis	25

2.3.3 Pressure drop	26
2.4 Heat exchanger	
2.4.1 Heat exchanger type	27
2.4.2 Analysis of heat exchanger	29
2.5 Condensation heat transfer	30
2.5.1 Film condensation	31
2.5.2 Dropwise condensation	33
Summary	33
Reference in chapter 2	33

3. Research methodology

3.1 Introduction of overall experiment	35
3.2 Experimental greenhouse	35
3.2.1 Greenhouse description	36
3.2.2 Temperature control using ventilation fan	37
3.2.3 Greenhouse environmental monitoring	38
3.2.4 Greenhouse strawberry cultivation and measurement	41
3.2.5 Measurement sensor and equipment	42
3.3 Laboratory-scale experiment	46
3.3.1 Experimental set-up	46
3.3.2 Environmental factors monitoring	48
Temperature measurement	48
Volume water flow rate measurement	52
Relative humidity measurement	53
Water pressure measurement	54
3.3.3 Equipment and sensor specification	54
3.3.4 Experimental conditions	58

3.3.5 Experimental procedure conditions	59
Reference in chapter 3	60
4. Results and discussion of the experiment in the greenhouse	
4.1 Introduction	61
4.2 Climate under greenhouse	
4.2.1 Monthly environmental parameters	62
4.2.2 Daily environmental parameters	63
4.3 Heat loss through greenhouse	
4.3.1 Daytime heat loss	68
4.3.2 Nighttime heat loss	69
4.4 Greenhouse heating requirement	71
4.5 Statistical analysis results	75
4.6 Effect of environmental on strawberries production	
4.6.1 The environment factors on pick up dates	75
4.6.2 Harvest on 20 February 2021	78
4.6.3 Harvest on 5 April 2021	79
Summary	81
Reference in chapter 4	82
5. Results and discussion of the experiment in the heat exchanger	
5.1 Introduction	84
5.2 Analysis of serpentine heat exchanger	
5.2.1 Effect of inlet water temperature on water temperature difference	86
5.2.2 Pressure drop and pumping power	86
5.2.3 Rate of heat transfer	87
5.2.4 Convective heat transfer coefficient on the surface	88

5.3 Condensation heat transfer	90
5.4 Local air temperature profiles	95
Summary	101
Reference in chapter 5	102
6. Conclusions	103

Appendix

List of publications

List of figures

Figures	Page
Figure 1-1 Showing natural ventilation process in the greenhouse	3
Figure 1-2 Schematic view of fan-pad cooling system	4
Figure 1-3 Photographic view of the greenhouse and main components	5
Figure 1-4 Root zone cooling system of strawberry nurseries	7
Figure 1-5 Cross-sectional investigation of the two different soil container types	8
Figure 1-6 Classification of the radiant cooling system	9
Figure 1-7 A temperature-entropy diagram for condensation process	9
Figure 1-8 Vertical air temperature gradients measured in a test section for different heating systems	10
Figure 2-1 Energy balance of experimental greenhouse	17
Figure 2-2 The cooling of a hot box in a cooler environment by natural convection	20
Figure 2-3 The buoyancy force keeps the ships afloat in water	21
Figure 2-4 The Grashof number Gr is a measure of the relative magnitudes of the buoyancy force and the opposing viscous force acting on the fluid	22
Figure 2-5 Typical velocity and temperature profiles for natural convection flow over a hot vertical plate	23
Figure 2-6 The heat transfer of fluid flowing through a tube	26
Figure 2-7 Types of flow path configuration through heat exchanger	28
Figure 2-8 A shell-and-tube heat exchanger	29
Figure 2-9 Two types of condensation (a) film condensation and (b) dropwise condensation	31
Figure 2-10 Laminar steady film condensation on vertical plate	32
Figure 3-1 The methodological procedures	35
Figure 3-2 Greenhouse layout and measurement location	36
Figure 3-3 (a) The external view of experimental greenhouse	36
Figure 3-3 (b) The internal view of experimental greenhouse	37
Figure 3-4 (a) Wind duct and additional vinyl sheet	37
Figure 3-4 (b) Ventilation fan	38
Figure 3-5 Data logger and electric circuit	39
Figure 3-6 Measurement of relative humidity, solar radiation and air temperature inside the greenhouse	40
Figure 3-7 (a) Measurement of solar radiation outside the greenhouse	40
Figure 3-7 (b) Measurement of humidity outside the greenhouse	40
Figure 3-8 Example of strawberry: (a) saccharimeter; (b) strawberry weight; (c) shape	41
Figure 3-9 T-type thermocouple	42
Figure 3-10 Humidity sensor	43

Figure 3-11 Pyranometer	44
Figure 3-12 Refractometer PAL-1	45
Figure 3-13 Hioki 8422-50 data logger	45
Figure 3-14 (a) Schematic diagram of a serpentine copper pipe heat exchanger	47
Figure 3-14 (b) Showing a serpentine copper pipe heat exchanger place on the stand (Top view)	47
Figure 3-14 (c) System configuration	48
Figure 3-15 (a) Air temperature measurement layout	49
Figure 3-15 (b) Measurement of air temperatures around the pipe	49
Figure 3-16 (a) Surface temperature measurement layout	50
Figure 3-16 (b) Measurement of copper pipe surface temperature	50
Figure 3-17 (a) Installation picture of Styrofoam sheet (completely closed)	51
Figure 3-17 (b) Installation picture of Styrofoam sheet (open windows)	51
Figure 3-18 Room temperature measurement	52
Figure 3-19 Measurement of inlet and outlet water temperature	52
Figure 3-20 (a) Flow meter with monitor	52
Figure 3-20 (b) Flow meter without monitor	53
Figure 3-21 Glove valve	53
Figure 3-22 (a) Humidity sensor placed above a pipe (with and without monitor)	53
Figure 3-22 (b) Humidity sensor placed below a pipe (with and without monitor)	53
Figure 3-23 Pressure gauge	54
Figure 3-24 Photo of THD-R-V (left) and THD-DD2-V (right) humidity sensors	55
Figure 3-25 Photo of digital pressure gauge	56
Figure 3-26 Photo of air-cooled chiller	57
Figure 4-1 Monthly inside and outside environmental data of greenhouse from December, 2020 to February, 2021	63
Figure 4-2 Environmental data: (a) air temperature, (b) solar radiation, and (c) relative humidity during February 15–18, 2021	65
Figure 4-3 Environmental parameters recorded on February 18, 2021	67
Figure 4-4 Heat transfer process in the greenhouse	68
Figure 4-5 Heat loss through the greenhouse as a function of the time of the day (February 18, 2021) ..	69
Figure 4-6 Heat loss through the greenhouse as a function of the time of nighttime (February 18, 2021)	70
Figure 4-7 The temperature difference between the inside and ambient air temperatures	70
Figure 4-8 Estimated maximum monthly heating required to maintain the greenhouse temperature at 10°C	72
Figure 4-9 Estimated maximum monthly heating required to maintain the greenhouse temperature at 8°C	72
Figure 4-10 (a) Comparison of design and measured temperatures ($T_{de} = 10^{\circ}\text{C}$)	74

Figure 4-10 (b) Comparison of design and measured temperatures ($T_{de} = 8^{\circ}\text{C}$)	74
Figure 4-11 Standard deviation and mean value of inside air temperature as a function of day (February 15–18, 2021)	75
Figure 4-12 (a) The comparison of the temperatures inside and outside the greenhouse at different times	76
Figure 4-12 (b) The comparison of solar radiation between inside and outside greenhouse at different times	77
Figure 4-12 (c) The comparison of relative humidity between inside and outside greenhouse at different times	78
Figure 4-13 (a) Strawberry fruits harvested on 20 February 2021	79
Figure 4-13 (b) Strawberry fruits harvested on 5 April 2021	80
Figure 5-1 Showing water and dew-point temperatures along with temperature difference between outlet and inlet water temperatures when inlet water temperature was set above dew-point temperature	85
Figure 5-2 The variation of water temperature difference with inlet water temperature for different water flow rate	86
Figure 5-3 (a) The variation of pressure drops with inlet water temperature for different water flow rates	87
Figure 5-3 (b) Pumping power versus flow rate curves	87
Figure 5-4 Rate of heat transfer versus inlet water temperature at different water flow rates	88
Figure 5-5 Variation in the convective heat transfer coefficient with inlet water temperature for different water flow rate	89
Figure 5-6 Variation in the convective heat transfer with inlet water temperature for different water flow rate	89
Figure 5-7 Condensation heat transfer with inlet water temperature for different water flow rate	91
Figure 5-8 Condensation heat transfer coefficient with inlet water temperature for different water flow rate	91
Figure 5-9 Photo of moist air condensing on copper pipe (at $T_{inlet,t} = 4^{\circ}\text{C}$)	92
Figure 5-10 Photo of moist air condensing on copper pipe (at $T_{inlet,t} = 2^{\circ}\text{C}$)	93
Figure 5-11 Photo of moist air condensing on copper pipe (at $T_{inlet,t} = 0^{\circ}\text{C}$)	93
Figure 5-12 Photo of moist air condensing on copper pipe (at $T_{inlet,t} = -2^{\circ}\text{C}$)	94
Figure 5-13 Photo of moist air condensing on copper pipe (at $T_{inlet,t} = -4^{\circ}\text{C}$)	94
Figure 5-14 Photo of moist air condensing on copper pipe (at $T_{inlet,t} = -6^{\circ}\text{C}$)	95
Figure 5-15 Showing the plotting positions of air temperature contour plots	96
Figure 5-16 Air temperature distribution over time under different inlet water temperatures and flow rates	98
Figure 5-17 Air temperature contour graphs	101

List of tables

Tables	Page
Table 2-1 Empirical correlations for the average Nusselt number for natural convection over surfaces ..	24
Table 3-1 Specification of ventilation fan	38
Table 3-2 Specifications of sensors and accuracy	42
Table 3-3 Specifications of hygrometer	43
Table 3-4 Specifications of pyranometer	44
Table 3-5 Specifications of refractometer	45
Table 3-6 Specifications of data logger	46
Table 3-7 Specifications of the serpentine copper pipe	47
Table 3-8 Instruments and sensors	54
Table 3-9 Specifications of humidity sensor	55
Table 3-10 Specifications of digital pressure gauge	56
Table 3-11 Specifications of flow sensor	56
Table 3-12 Specifications of chiller	57
Table 3-13 Test cases	58
Table 4-1 Parameters used in calculation for each month	71
Table 4-2 Required heat energy under different design temperatures and percentage reduction of energy	73
Table 4-3 Mean and design temperatures of the air inside and outside greenhouse	74
Table 4-4 Strawberry quality parameters on 20 February 2021	79
Table 4-5 Strawberry quality parameters on 5 April 2021	80
Table 4-6 Mean and standard deviation of strawberry samples ($s = 8$) on different days of harvest	81
Table 4-7 The comparison of climatic parameters at different days	81

Nomenclature

A_c	total area of the covering material, m ²
A_{gr}	plantation area, m ²
A_s	surface area, m ²
c_p	specific heat of the fluid, kJ/(kg·K)
c_{pl}	specific heat of liquid at the average film temperature, kJ/(kg·K)
D	diameter, m
D_i	inner diameter, m
E_m	the monthly heating requirement, kJ/month
e_m	the monthly heating requirement per plantation area, kJ/(m ² ·month)
f	friction factor
$F_{buoyancy}$	buoyancy force, N
g	gravitational acceleration, m/s ²
G_{in}	solar radiations inside the greenhouse, W/m ²
G_{amb}	solar radiations outside the greenhouse, W/m ²
Gr	Grashof number
H	the daily heating duration, h/d,
h	convection heat transfer coefficient, W/(m ² ·K)
$h_{dropwise}$	heat transfer coefficient for dropwise, W/(m ² ·K)
h_{fg}	latent heat of vaporization, kJ/kg
h_{fg}^*	modified latent heat of vaporization, kJ/kg
h_{horiz}	heat transfer coefficient for film condensation, W/(m ² ·K)
h_L	head loss, m
k	thermal conductivity of air at film temperature, W/(m·K)
k_l	thermal conductivity of liquid, W/(m·K)
L_c	characteristic length, m
m	number of thermocouple points inside the greenhouse
\dot{m}	mass flow, kg/s
N	number of days per month, d/month
n	number of the data point
Nu	Nusselt number
p	perimeter, m
P_1	pressure at the inlet tube, kPa
P_2	pressure at the outlet tube, kPa
ΔP	pressure drop, kPa

Pr	Prandtl number
\dot{Q}_c	heat loss through the covering material, W
\dot{Q}_{cond}	condensation heat transfer, W
\dot{Q}_{conv}	convective heat transfer, W
\dot{Q}_{gr}	heat loss to the ground, W
\dot{Q}_{rad}	net rate of radiation heat transfer, W
\dot{q}_s	constant surface heat flux, W
\dot{Q}_{total}	rate of the total heat loss, W
$\dot{Q}_{total,c}$	heat flux through heat exchanger, W
\dot{Q}_v	the ventilation heat loss, W
R	radius, m
Ra_L	Rayleigh number
Re	Reynolds number
s	number of thermocouple points outside the greenhouse
T_{amb}	ambient air temperature, °C
$T_{chiller}$	chiller set-point temperature, °C
T_{de}	design or heating temperature, °C
T_{dif}	temperature difference between outlet and inlet water temperatures, °C
T_{dp}	dew point temperature, °C
T_e	average temperature at the exit °C
T_i	average temperature at the inlet, °C
T_{in}	air temperature inside the greenhouse, °C
$\overline{T_{in}}$	average of air temperature inside greenhouse in daytime, °C
$T_{in,j}$	inside air temperature at time interval j , °C
T_{inlet}	inlet water temperature, °C
$T_{inlet,t}$	target inlet water temperature, °C
T_{in_day}	average inside air temperature during the day, °C
T_{in_night}	average inside air temperature at night, °C
T_l	dataset of values inside the greenhouse
T_m	mean temperature, °C
T_{mean_in}	average air temperature inside the greenhouse, °C
T_{mean_out}	average air temperature outside the greenhouse, °C
T_{outlet}	outlet water temperature, °C
T_{room}	room air temperature, °C
T_s	surface temperature, °C
T_{sat}	saturation temperature, °C
T_{∞}	temperature of the fluid sufficiently far from the surface, °C

U_c	overall heat transfer coefficient of the covering material, $W/(m^2 \cdot K)$
U_{gr}	ground heat transfer coefficient, $W/(m^2 \cdot K)$
V	volume of the greenhouse, m^3
\dot{V}	volume flow rate, m^3/s
\dot{V}_a	air volume flow rate, m^3/s
V_{avg}	average velocity for incompressible flow in a circular pipe, m/s
V_{body}	volume of the portion of the body immersed in the fluid, m^3
ν	kinematic viscosity of the fluid, m^2/s
$\dot{W}_{pump,L}$	pumping power to overcome the pressure loss,

Greek letters

β	coefficient of volume expansion, $1/K$
μ	dynamic viscosity, $Pa \cdot s$
μ_l	dynamic viscosity of liquid, $Pa \cdot s$
ρ_{body}	density of the body, kg/m^3
ρ_{fluid}	density of the fluid, kg/m^3
ρ_l	density of liquid, kg/m^3
ρ_v	density of vapor, kg/m^3
σ_i	the standard deviation of inside air temperature, $^{\circ}C$
τ	time, minute, hour
τ_w	shear stress, N/m^2
ϑ	flow velocity, m/s
φ_{in}	humidity inside the greenhouse, %
φ_{out}	humidity outside the greenhouse, %

Abbreviations

<i>ACH</i>	air change per hour, $1/h$
<i>G</i>	solar radiation, W/m^2
<i>RH</i>	relative humidity, %
<i>SD</i>	standard deviation
<i>SSC</i>	soluble sugar contents

Subscript

c	cold fluid
h	hot fluid
i	inside
in	inlet

max	maximum
o	outside
out	outlet
wi	inlet water
wo	outlet water

Chapter 1

Introduction

1.1 Research motivation

The rapid growth of population and the climate change in the last few decades are challenging to enhance food resource, water, and energy efficiency [1]. In order to get high yield and improve products quality, greenhouse or plant factory are used. Growing plant inside completely closed room, so-called “plant factory” or “greenhouse” is widely popular due to the increasing in world population. Greenhouse technology is considered to overcome the problem of high temperature during summer times. The greenhouse is one of the most profitable sectors as it can provide very high yields when compared to traditional farming [2]. Cultivation of crops in a completely closed room has many advantages such as growing seasons can be extended, creating an optimum growing environment, protection from insects and pesticide as well as reduced energy consumption [3]. The main advantages of indoor plantation are high energy efficiency and high-quality products. One key factor to achieve the high energy efficiency and product quality is the ability to control environmental conditions inside plantation area. It appeared that controllable environmental conditions are the keys. The environmental conditions that are controlled include air temperature, humidity and light.

In tropical and subtropical climates stand particular design challenges because of high temperature and high humidity during the summer seasons. So, cooling systems are considered as the key to create proper environmental conditions for growing plants inside plantation area [4]. Central air-conditioners is used to control air to an optimal level. After controlled, the air is distributed to plantation space. In this way, suitable microclimate for each plant inside plantation is created. However, air-conditioners consume large quantities of energy, if the plantation area is large. So, large size of air-conditioner and large amount of energy are required.

Due to the energy sustainability issues nowadays, different cooling systems have been proposed to provide a suitable indoor condition for plants such as mechanical cooling systems, natural ventilation, evaporative cooling systems, combined systems and so on [5]. Generally, traditional central air-conditioning systems adopt the heat and moisture coupling treatment approach to control indoor environments [6]. This treatment inevitably leads to wasted energy [7]. Thus, many researchers are currently focusing on various projects in order to determine the best solutions to these challenges.

For many years, method of cooling within a small space so called, “spot cooling” has become popular. Spot cooling is commonly used to cool air in a large space such as factory, office and so no. It exactly directs a small stream of cool air in the desired location. For cool air, spot cooling can be achieved by radiation which lowers the mean radiant temperature or by convection which increases air velocity or the combination of both methods [8]. Moreover, spot cooling, which is used in nurseries, has recently become widespread method of increasing energy efficiency [9]. Spot cooling inside greenhouse is not only air temperature but also the temperature of soil. This method, so called “root zone cooling” means installing of cooling tube in the soil to reduce soil temperature while the shoots are exposed to ambient temperature. Optimization of root zone cooling and the air temperature is very important in plant cultivation which affects the quality and yield of fruit. Root zone cooling has been researched by many studies as a technology to promote plant growth and energy conservation in greenhouses.

Controlling air temperature in a controlled room consumes a large amount of energy. In particular, cooling a large space such as the inside of a greenhouse consumes more electricity than a small or local area. It is crucial to develop feasible techniques for lowering energy use while remaining an optimum environmental condition in local space. In order to understand the impact of the environment on the cultivation of sensitive crops, the energy balance in greenhouse was studied. Thus, a field experiment was performed in a small walk-in greenhouse to study an energy analysis and to determine how it affected the local environmental around plantation area. After that, a microclimate weather management system for indoor plantation was studied and experimented. This aims to create an appropriate microclimate around each plant. Accordingly, a cooling serpentine copper pipe heat exchanger is introduced to control local environmental conditions that can reduce energy consumption compared to traditional cooling system. This evaluation method may reduce the energy used that can control the desired environment in a small area or microclimate area.

1.2 Literature reviews

This part presents previous studies and contains three parts, including cooling technologies for greenhouse, heat exchanger applications and spot cooling methods. The literature review of previous studies will be described in detail below.

1.2.1 Literature review on cooling systems for greenhouse applications

In this section, a comprehensive review of cooling systems in hot regions was presented. A critical discussion and the comparison between the several cooling systems was also showed in detail. It is necessary to find a novel, high energy efficiency technology for greenhouse that is suitable for growing plant. In addition, the development of applicable cooling systems is a necessary research challenge.

Compared to an open field agricultural, a modern greenhouse can provide a high degree of environmental control factors in terms of air temperature, relative humidity, and solar radiation, etc. In addition, greenhouse can protect plant from inverse climatic conditions. Cooling systems are considered as a solution to create suitable environmental conditions, particularly to guarantee the required range of relative humidity and temperature inside greenhouse. Cooling systems can be divided into two types, passive cooling system and active cooling system. Passive cooling system refer to design strategy including orientation, shape, shading, and covering materials. On the other hand, active cooling system prefers to the cooling systems that use electricity or water to reduce air temperature inside greenhouse. Generally, a combined system is used that prefers to both passive and active cooling system due to it can provide adequate conditions for plant and reduce the use of electricity [10].

One key target for using passive cooling system is to decrease cooling requirement inside greenhouse. There are many strategies namely the shape and orientation design for greenhouse and covering materials. Sethi, V.P. et al. [11] studied the effect of greenhouse shapes on the temperature and solar capture. According to the results, Quonset shape received a minimum value in temperature and solar radiation. In contrast, uneven-span shape received a higher solar radiation and heat absorb. Many previous studies confirmed that E-W orientation relative to N-S axis could reduce cooling and heating requirements in both cooling and heating seasons [12-14]. However, there are many factors that lead to the optimum selection of design and orientation of greenhouse, for example, wind direction, location, the requirement of solar radiation, and plant type.

In hot and humid areas, covering materials plays an important role in the requirement of energy, economics and the yield of the greenhouse. Covering materials of greenhouse can be divided into many categories, such as glass, polyethylene (PE), polycarbonate (PC), and fiberglass. To avoid over heat entering the greenhouse and to reduce cooling requirement, shading and reflection are generally used. The air temperature inside greenhouse is reduced by 10% when using 50% of shaded roof [15]. Abdel-Ghany et al. [16] investigated the several shading methods such as roof shading, external shading. The results showed that the external shading is more effective in a reduction in solar radiation inside a greenhouse than the conventional greenhouse. In addition, white roof painted and external black shading nets are an alternative way to effectively reduce heat entering the greenhouse [17]. In terms of thermal and optical properties, there are many experimentally studies to improve covering material thermal performance. NIRS covering film (Near Infrared Spectroscopy) is one of options used for extreme weather because it can reflect near infrared radiation without the impact on photosynthesis and crop growth. The results demonstrated that a reduction in air temperature inside greenhouse is approximately 5°C and the energy consumption of cooling requirement is reduced by 8% [18,19]. Murakami et al. [20] experimentally studied two new NIRS cutting nets that high absorption in near infrared wave lengths and strong transmittance of visible light. The results showed that air temperature inside greenhouse could be reduced by 5°C in sunny day and sugar accumulation of melon also increased.

Natural ventilation is one of the most basic methods for reducing the temperature difference between the outside and inside air. The difference in pressure leads to natural ventilation or internal air buoyancy. Natural or passive ventilation requires very little electricity use and equipment. In application, window openings at side wall and roof are necessary for the external cool air entering the greenhouse as shown in figure 1-1 [21].

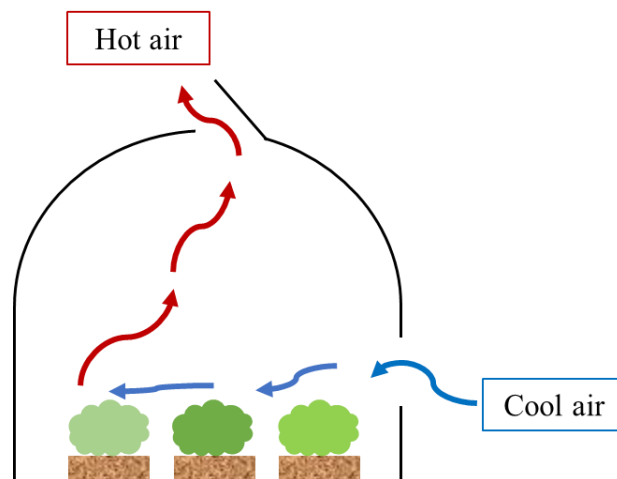


Figure 1-1 Showing natural ventilation process in the greenhouse

Espinoza et al. [22] evaluated the influence of ventilation configuration on the flow pattern in multi-span greenhouse with an obstacle to airflow such as a neighboring greenhouse. It was found that the ventilation system's obstructions and the distribution of ventilation surfaces affect the flow pattern through the greenhouse. The surrounding greenhouse on the leeward side decreased the ventilation capacity. Also, two roof and side vents configuration improved air movement at the crop zone but the overall volumetric flow rate was lower than the three roof and side vents. Moreover, many researchers state that the environment around a greenhouse significantly affect

the rate of air change which mainly depends on an opening area. Thus, the total area of vents should be 15-30% of ground area [23]. However, natural convection is insufficient to cool down and remove heat from greenhouse. Thus, forced ventilation is ensured by fans or ventilators that are used for control air temperature and relative humidity. In hot and humid areas, forced ventilation is commonly used to reduce overheating and provide suitable growing conditions and it is easily replaced other cooling systems such as fans and pads system [24,25].

Evaporative cooling is one of the most potential technologies for providing suitable weather conditions of the greenhouse in hot climates. These systems are based on conversion of sensible heat into latent heat of evaporated water with water supplied mechanically [26]. During the process, water supplied directly into the greenhouse by mist or fog system, sprinklers and fan-pad evaporative cooling. The technique can significantly decrease temperature below the ambient temperature and increase humidity inside the greenhouse. Fan and pad system are considered to be an efficient control and cool down inside air temperature for greenhouse climate where the outside temperature exceeds more 40°C. Fan and pad system generally consist of fans on sidewall and pad on another sidewall of the greenhouse. The principle of this system is applied by running water over the pad and consequent withdrawal of air through it by fans on the opposite side as shown in figure 1-2. Fan-pad cooling produces two changes in the condition of the air exiting the pads. During the process, air temperature becomes cooler and its humidity is also raised [27]. From the reviewed literatures, it can be said that the fan-pad system can effective for the greenhouse cooling and humidification in hot climates. In order to achieve optimum cooling, water flow rate and distribution system, capacity of pump, recirculation and output rate of the system must be carefully calculated and designed to provide adequate wetting of the pad and to avoid accumulation of pads. In addition, this system may achieve by the combination fan-pad with other systems such as shading screen in terms of cooling achievement. However, there are many disadvantages of fan-pad systems: temperature and humidity distributions will be uneven across the greenhouse. It may be not effective in those areas where high humidity and increased maintenance of greenhouse operation.

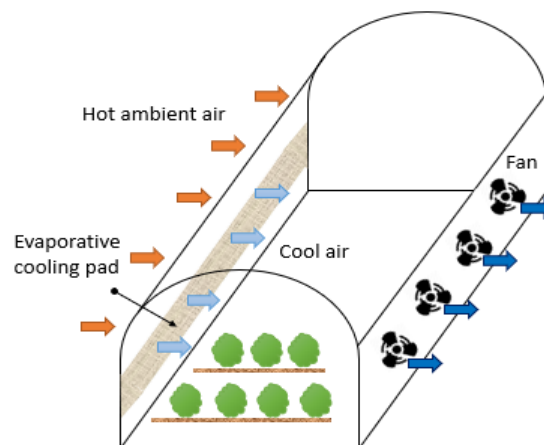


Figure 1-2 Schematic view of fan-pad cooling system

One of evaporative cooling systems is fogging system. This system provides spraying water as small droplets of 10-30 μm through tiny nozzles at high pressure to create micro-fine mist above the crops inside greenhouse. Cooling is achieved by evaporative of droplets. Typically, a fogging system is employed in addition to the

conventional cooling process, especially during the hottest portion of the year and it shows better results in hot and dry conditions [28]. Fogging can also be used to create increasing relative humidity beside from cooling greenhouse. It is said that fogging system can achieve high efficiency of water evaporation while also keeping leaf dry. Moreover, fogging system can lead a more uniform distribution and humidity in a greenhouse as compared to natural ventilation with roof opening [29]. However, there are disadvantages when compared to the fan-pad evaporative cooling system such as the lower air saturation efficiency, cost, water and energy consumption.

Mechanical cooling systems in one of the most widely used systems in hot regions with high ambient temperature and high solar levels. Mechanical cooling systems consist of utilizes fan, heat pumps, and heat exchanger which can maintain greenhouse temperature at low levels. Many researchers focused on an investigation and assessment greenhouse mechanical cooling system in hot areas. The main advantages of mechanical cooling system are efficient at controlling air temperature, humidity and also CO₂ especially in fully-closed greenhouse resulted in improve microclimate, water consumption, and increased crop yields. However, this system is a major consumer of energy and return poor investment in hot regions. Moreover, some technologies are cumbersome and require costly maintenance [30]. One cooling system may not be sufficient to provide the optimum weather conditions under hot and dry regions. To achieve the optimal cooling in hot climates, cooling techniques can be combined. As an example, combined cooling systems and the components of greenhouse are shown in figure 1-3. This greenhouse is combination of many cooling techniques consisting with fan and pad system, ventilation fan, external shading net and circulation fan. Combined or hybrid technique can decrease energy consumption especially solar powered has been proposed in hot regions to reduce energy cost while improving greenhouse cooling performance. During the last years, many researchers have studied combinations of different cooling techniques.

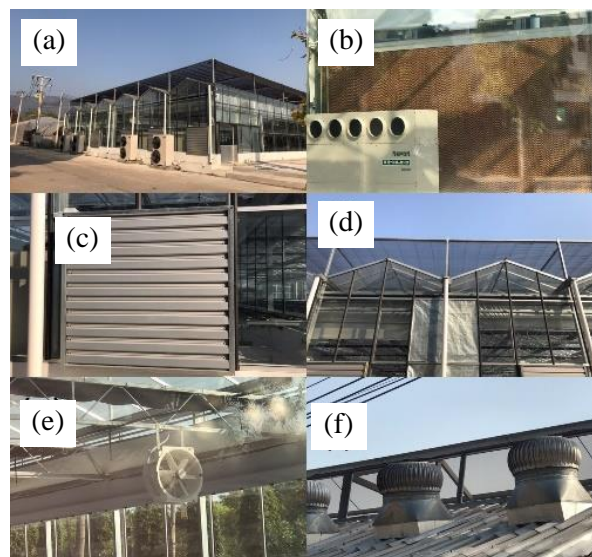


Figure 1-3 Photographic view of the greenhouse and main components (a) external view; (b) evaporative cooling pad; (c) extracting fan; (d) external shading net; (e) circulation fan; and (f) ventilation fan

This section presented the available worldwide cooling systems for agricultural greenhouse in regions with hot climates. The detailed review highlighted that none of the currently available technologies that can provide all cooling requirements of the greenhouse is perfect. The selection of system is based on many parameters such as greenhouse location, cost, type of the crops, and so on. In order to grow crops outside of the growing season and

achieve the highest yields, the most effectively cooling greenhouse technology must satisfy these requirements. There is essential to improve the cost and effective technology appropriate to local climatic conditions. Based on critical review of works of various researchers, it can be seen that the combination of natural ventilation, evaporative cooling and shading has potential to decrease greenhouse energy requirement and provide suitable conditions for crop production throughout the year. For the future works, the research should be focused on greenhouse design, improved water efficiency in protected cultivation and understanding of thermal behavior of the greenhouse. Moreover, the research should be considered about new cladding materials to reduce heat load. Finally, the development of cooling technology suitable for tropical and subtropical is necessary for effective cooling performance in local conditions.

1.2.2 Literature review on spot cooling system in plantation area

In the previous section, several cooling techniques are aimed to reduce air temperature inside greenhouse. However, due to high energy demand for crop production under normal tropical, many researchers are finding out cooling technique to reduce energy consumption and also decrease air temperature during hot climate. The spot cooling system is thought to utilize energy more effectively than any other technology for cooling the entire greenhouse. Spot cooling inside greenhouse refers to both soil and air temperatures reduction. In soil, root zone cooling method means installing of cooling tube in the soil to reduce soil temperature while the shoots are exposed to ambient temperature.

Many previous studies have been conducted and tested on different plants. Yurina Kwack et al. [31] studied on root zone cooling for paprika transplants. This study compared two different types of cold-water supply pipes, including plastic pipes and stainless-steel pipes, to reduce rockwool cubes (planting media). The root zone temperature of rockwool cubes, growth and development of paprika transplants as effected by root zone cooling were investigated. When supply cool water at 17°C, plastic pipes could reduce rockwool cubes temperature by 3.6°C during the day time on sunny day. In plastic pipes, the root-zone was most effective. Due to the plastic pipe have low thermal conductivity, cooling efficiency was increased by allowing water to circulate at a lower temperature. In addition, spot cooling of root zone improved root growth and increased number of flowers compared as with uncooled rock wool cubes. According to a study [32], butterhead lettuce growth and development in a containerized planting system were investigated in relation to the impacts of root zone cooling (RZC). Polyvinyl chloride (PVC) pipes were used to circulate cold water to cool the root zone, while their shoots were exposed to the hot ambient temperature. In this study, PVC pipes were buried through media at depth of 100 mm and cool water temperature was varied from 4-16°C. The temperature of the root zone was measured at different depths (50 mm, 100 mm, 150 mm and 200 mm). Butterhead lettuce grew better under the conditions provided by the cooling pipes that were buried 100 mm below the surface. In addition, the root zone media had a minimum temperature of 14.4°C at 18:00 and a mean daily temperature of 19°C. At the end of the growth stage, the root zone cooling treatment had considerably greater lettuce canopy diameter and number of leaves compared to the control plants. This part can be seen that the use of plastic pipes for root zone cooling is very popular. Due to the low cost and easy to handle. Thus, it allowed to construct a more efficient and economic system for root zone cooling.

Root zone cooling techniques have been developed to reduce root zone temperature and increase fruit production in hot season. Shinji Mizuno et el. [33] used the New Root-zone Environmental Control System

(N.RECS) to cool the root zone of strawberry nurseries planted in pots in late summer and investigated the effects on flowering and yield in a super-forcing culture. In experiment, heat exchanger panels and polyethylene pipes with outside diameter of 1 cm were buried of depth at 8 cm. Heat pump was used to generate chilled water to 7°C at 1.6-1.8 L/min, as shown in figure 1-4. The root zone temperature was measured at 5 cm below soil surface and crown temperature was also monitored. The results show that during root-zone cooling, the soil's average surface temperature, where the crown is located, was around 23°C, which initiated flowering. Furthermore, soil temperature was about 19°C, while air temperature inside nurseries exceeded more than 26°C. However, Root-zone cooling did not affect the development of new leaves during treatment.

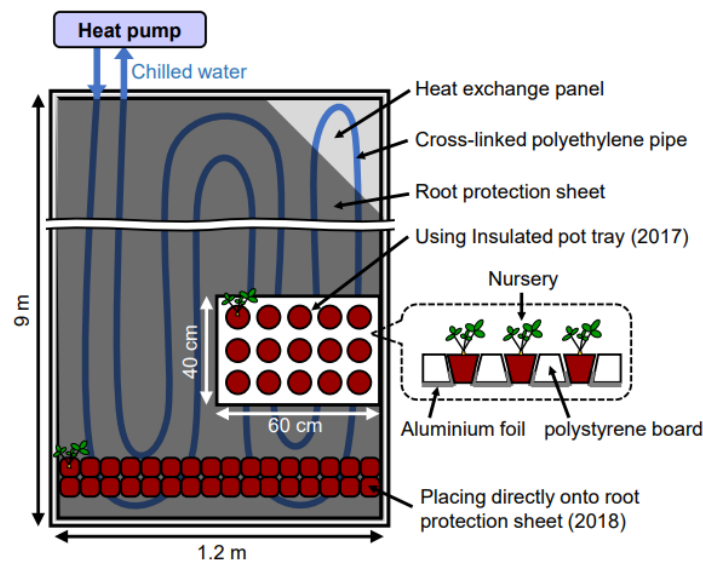
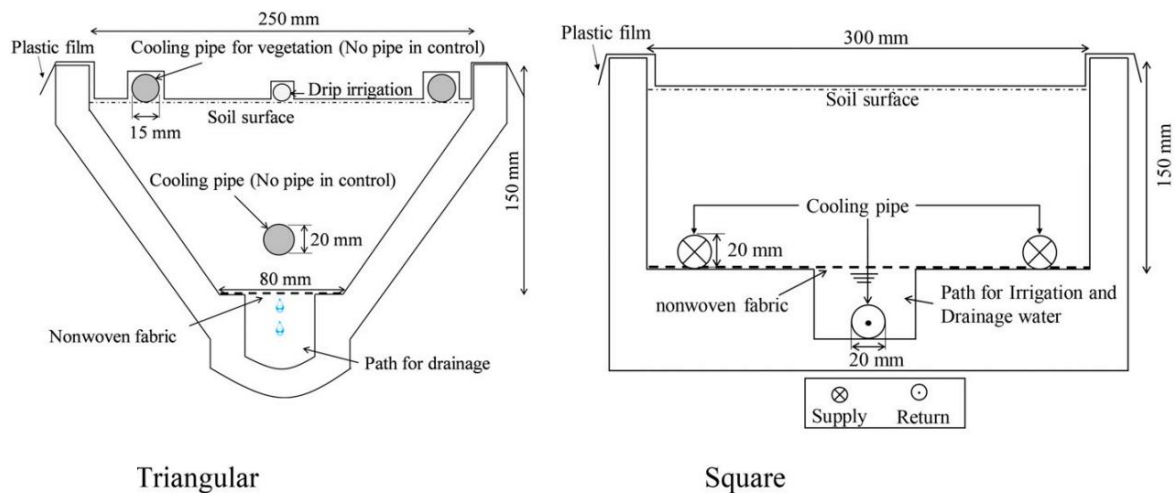


Figure 1-4 Root zone cooling system of strawberry nurseries [33]

Shigeoki Moritani et al. [34] proposed Ground-source heat pumps (GSHPs) to chill water to facilitate cooling of strawberry cultivated in pots during the summer. There have been two different soil container types and cooling methods examined. In one cooling system, tubes transporting cold water were placed both above and below the soil, while the other cooling system used cold water passing through tubes placed under the soil and within the irrigation channel to facilitate bottom irrigation, as shown in figure 1-5 (A) and figure 1-5 (B), respectively. The results found that rapid transfer of cold water through the bottom irrigation channel into the root zone, which was facilitated by the reduction in soil moisture content driven on by plant transpiration as well as heat conduction from the soil to the cooling tube, allowed for more cooling. Measured soil temperatures for the buried-tube system were found to be coldest when the tube was chilled considerably (9.4°C). Compared to the scenario where no GSHPs was used, both systems successfully provided decreased soil temperatures.



Triangular

Square

Figure 1-5 Cross-sectional investigation of the two different soil container types [34]

The zone cooling system is thought to utilize energy more effectively than any other technology for cooling the entire greenhouse. In a previous study, Herry Suhardiyanto and Takahisa Matsuoka [35] reported that the fresh weight of the top part of the spinach plants in the cooled zone exceeded double that of the normally ventilated environment on the 45th day after sowing. Cooling method is that two similar spot coolers were used to provide cool air, and 23.2 cm diameter perforated polyethylene tubes were used to transport the cool air into the lower (plant) zone. The total blowing rate of cool air coolers was 6.9 m³/min. These tubes were insulated to prevent direct solar radiation. This cooling methods was operated manually when four sensors in the plant zone exceeded 30°C and turn off when all sensors decreased of 27°C. During sunny days, spot cooling method was able to maintain the daily maximum air temperature in plant zone from 30.4°C to 36.8°C compared to from 32.0°C to 39.0°C in the natural ventilated plant zone.

In previous studies, spot cooling system in plantation area can be divided into 2 categories. Firstly, temperature control of the rooting area, so called “root zone temperature” and secondly, temperature control of local air temperature that delivers conditioned air directly to a plantation area. Spot cooling can be more energy-efficient than traditional central air conditioning systems due to they are use less energy than using the entire greenhouse. This has provided the lead for the research methodology in this study.

1.2.3 Literature review on heat exchanger applications

Nowadays, the used of conventional air-conditioner has increased. Excessive fossil and electricity are the main energy used and caused energy crises as well as climate problems. The sustainable development requires high-efficiency cooling technology to satisfy user requirements for indoor environmental control with low energy consumption. Thus, many researchers are now focusing on novel cooling techniques to find out the best solutions to these challenges. Radiant cooling system panel that is used as spot cooling has been gaining much popularity. Thus, in this section, a critical review for radiant cooling system was proposed in details.

Over the few year, radiant heating and cooling systems are potential alternatives to conventional air-conditioning systems, and they have received a lot of interest in Eastern Asian and European countries [36]. The application of radiant cooling has been widely used not only residential but also in non-residential buildings such as office buildings, school, department store, etc. Radiant cooling and heating systems are the alternative systems

used to meet the demand and has many advantages in the application such as reducing energy consumption, improving thermal comfort, offering simple and effective zone control, saving space and reducing noise [37,38].

Radiant cooling systems are defined as air-conditioners systems in which more than half of heat transferred by radiation [39]. Generally, radiant cooling provides cooling by the combination of radiation and convection [40,41]. Radiant cooling systems are usually classified into three types depending on their structures: (1) embedded surface systems, (2) thermally activated building systems and (3) radiant panel systems as shown in figure 1-6.

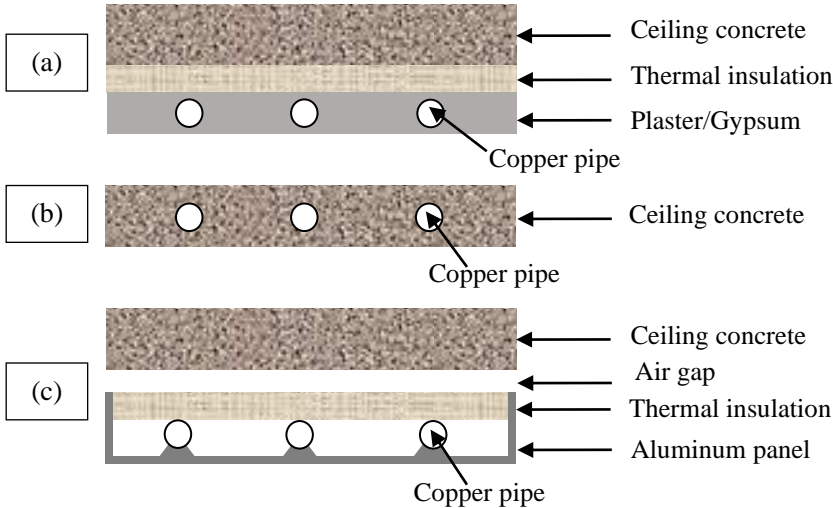


Figure 1-6 Classification of the radiant cooling system [41]: (a) embedded surface system, (b) thermally activated building system and (c) radiant panel system

Basically, radiant system only deals with sensible heat. Thus, it needs to be supplemented with a ventilation system. In hot and humid areas, condensation is the common problem. A low radiant surface temperature will easily lead to condensation on the radiant surface when humidity is not reduced accordingly. The condensation of air can be represented by a temperature-entropy diagram, as is shown in figure 1-7. From figure 1-7, point 1 is the beginning state of indoor air, and point 2 is the initial stage of condensation. Line 2-3 is condensation process of indoor air on the low radiant surface. It can see that the condensation is occurred by the temperature difference and driven by pressure difference. This problem results in the reduce in cooling capacity. Thus, the temperature control of the radiant surface and air-contact surface is coupled to enhance the cooling capacity [42,43]

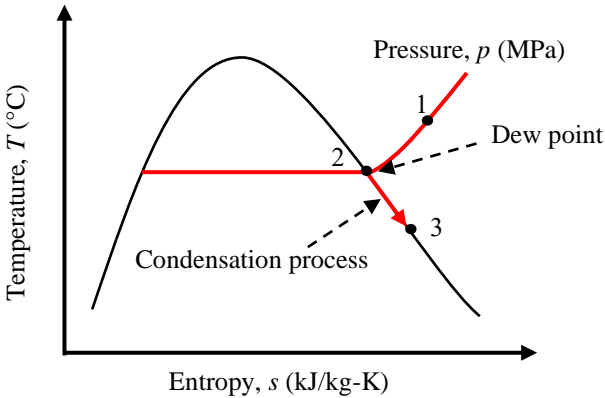


Figure 1-7 A temperature-entropy diagram for condensation process [44]

The thermal medium of radiant cooling system is usually water which can achieve high energy efficiency because of reduced distribution losses and possibility of using high-temperature water for cooling. Moreover, water can transport approximately 3,500 times more heat than the same volume of air [45]. Therefore, the transportation energy for thermal medium can be reduced compared to conventional air-conditioning systems. Owing to this, radiant cooling system can achieve a high energy-efficiency with low energy consumption.

Utilizing radiant heat transfer and large surfaces for heat transfer can provide an ideal vertical air temperature gradient [46,47] as presented in figure 1-8. From figure 1-8, it can be seen that heating radiant floor and heating radiant panel under window seems to be steady at different vertical positions.

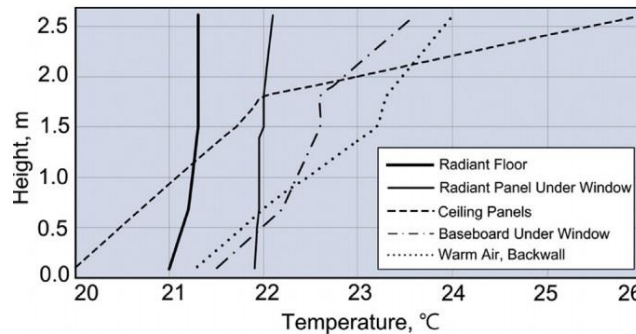


Figure 1-8 Vertical air temperature gradients measured in a test section for different heating systems [46]

Many researchers have focused on the use of radiant cooling panels in real applications. Guoqing Yu et al. [48] developed a simplified model for top insulated metal ceiling radiant cooling panels with serpentine tube to predict the average panel temperature, outer water temperature and cooling capacity. They found that 1) The tube spacing significantly affects cooling capacity, within the appropriate range of tube spacing from 0.05 m to 0.3 m, 2) If the tube thermal conductivity is less than 1.0 W/(m·K), the cooling capacity will be considerably affected and 3) The water flowrate has to be high enough to maintain a turbulent flow. Meanwhile, Minzhi Ye et al. [49] experimentally investigated the thermal performance of ceiling radiant cooling panel by assessing the heat conditions in a lab-scale room with this new panel installed. The results found that the average air temperature dropped by over 1.5°C and the total heat flux increased by 50% when the inlet water temperature decreased from 24°C to 15°C at the same flow rate of 4 L/min. Variations in the temperature of the inlet water had a significant impact on the heat flux, although changes in flow rate had less of an effect. In addition, the panel achieved the same air temperature with a lower flow rate, which shows the potential for energy saving.

Besides, Y.L. Yin et al. [50] experimentally studied comprehending detailed performance of radiant cooling panel when it used as an air conditioning system. A constant temperature and humidity environment chamber was used to simulate the various indoor thermal environments while three radiant cooling panels with a combined surface area of 0.16 m² were prepared for investigation. The results showed that the performance of the radiant cooling panels' heat transfer was most significantly impacted by the flow state of chilled water. Despite the fact found that moisture condensation on the radiant cooling panels increased the amount of heat transfer, but posed a challenge in using of radiant cooling panels. Recently, Gallardo and Berardi. [51] examined the phase change material-integrated radiant panel system's thermal performance. The results demonstrated that a radiant cooling system in an office

building produced energy savings of about 48% when compared to a traditional air conditioning system. Results further demonstrate that the proposed system can only be used at night, which increases plant productivity.

This section presented a comprehensive review of radiant cooling system panel. The detailed review highlighted that even the utilizing of radiant cooling system has been widely applied in both residential and non-residential buildings. On the other hands, no studies have been conducted on the use of heat exchanger in plantation area. Many works have been accomplished applied radiant cooling/heating systems for controlling environmental inside the buildings. In the previous works, the combination of a ventilation system to deal with latent load, the radiant cooling system has proven to be feasible in hot and humid climates such as China, India, Thailand, Singapore, and so on [45].

1.3 Research objective

Modern control heating/cooling technologies play an important role in enhancing the energy efficiency and economically feasible alternatives to conventional systems. It has driven the development of feasible techniques for lowering energy use while remaining an optimum environmental condition in local space. In particular, cooling a large space such as the inside of a greenhouse consumes more electricity than a small or local area. In order to achieve that, this study focused on a microclimate weather management system for indoor plantation. This aims to reduce energy consumption. Hence, three objectives were developed as follows:

- 1.3.1 To study and research an energy analysis of an experimental greenhouse and determine how to control environmental conditions around plantation area. Under this objective, a field experiment was performed in a small walk-in greenhouse and the impact of environmental factors on the strawberries was evaluated.
- 1.3.2 To control the local air temperature around plantation area. Under this objective, a cooling serpentine copper pipe heat exchanger is established for cooling in a laboratory-scale room. For this propose, this novel technique may reduce the energy used in cooling and serve as a model for further development of cooling for small space.
- 1.3.3 To investigate the thermal performance and local air temperature distributions around a cooling serpentine copper pipe heat exchanger. Finally, the optimum working condition such as volume flow rate and inlet temperature of working fluid for environmental control system is proposed.

1.4 Scopes of research

- 1.4.1 A field experiment was performed in a small walk-in tunnel with a passive solar greenhouse for strawberry cultivation in a temperate area in central Japan.
- 1.4.2 The serpentine copper pipe heat exchanger was experimentally studied inside laboratory room and room air temperature was controlled by air-conditioning at specific points.

1.5 Significance of research

- 1.5.1 This study provides insight into the effect of environmental factors on the quality of sensitive fruit (such as strawberry) in the indoor plantation.
- 1.5.2 This novel cooling technique can reduce energy consumption compared with a conventional greenhouse that can control the desired air temperature in a small scale or microclimate area.

1.5.3 This evaluation methods used in this study can be applied to areas that require cooling such as tropical or temperate areas.

1.5.4 To produce high quality crops even in off-season cultivation in tropical areas with energy saving.

1.6 Outline of the Thesis

This chapter provided the motivation of this study and outlined the brief background including cooling systems for greenhouse applications that help to understand the advantages and disadvantages of each current cooling technology. The literature review of heat exchanger and spot cooling was also presented. Research objective, scopes of research, and significance of this study were also shown in this chapter.

In chapter 2, this chapter contains of the principle and theories used in this study that includes energy balance of the experimental greenhouse as well as the heat and mass transfer theorems, thermodynamic theorems and the calculation of heat transfer through a serpentine copper pipe heat exchanger.

In chapter 3, this chapter describes the methodology and equipment used in this study that includes two main experiments. Firstly, an experimental site in a small walk-in tunnel was constructed to study the energy analysis and study how it affected the local environmental around plantation area. Secondly, experimental analysis of environmental control system in a laboratory-scale room. In each experiment explains the experimental set-up and test procedures. Besides that, the specification of sensor and equipment will be presented in details.

In chapter 4, this chapter explains the experiment on the impact of environmental factors on energy balance of experimental greenhouse. For this purpose, the estimation of the greenhouse of energy balance is proposed and the energy required to heat the greenhouse is calculated. Besides that, the quality of strawberries was evaluated in this section.

In chapter 5, this chapter presents the experiment on the heat transfer performance, air temperature gradients and the condensation of moisture on a serpentine copper pipe heat exchanger in a laboratory-scale room. In addition, local air temperature contour graphs were presented.

Finally, chapter 6 provides the conclusions remarks on the work carried out in this thesis.

References in chapter 1

- [1] United Nations. (2019). World Population Prospects 2019. In Department of Economic and Social Affairs. World Population Prospects 2019. Retrieved from <http://www.ncbi.nlm.nih.gov/pubmed/12283219>.
- [2] Mohammadi, B., Ranjbar, S. F. & Ajabshirchi, Y. (2018). Application of dynamic model to predict some inside environment variables in a semi-solar greenhouse. *Information Processing in Agriculture*, 5(2), 279–288.
- [3] Katsoulas, N., Sapounas, A., De Zwart, F., Dieleman, J. A. & Stanghellini, C. (2015). Reducing ventilation requirements in semi-closed greenhouses increases water use efficiency. *Agricultural Water Management*, 156, 90–99.
- [4] Cuce, P. M. & Riffat, S. (2016). A state-of-the-art review of evaporative cooling systems for building applications. *Renewable and Sustainable Energy Reviews*, 54, 1240–1249.
- [5] Ghoulem, M., El Moueddeb, K., Nehdi, E., Boukhanouf, R. & Kaiser Calautit, J. (2019). Greenhouse design and cooling technologies for sustainable food cultivation in hot climates: Review of current practice and future status. *Biosystems Engineering*, 183, 121–150.

- [6] Chiang, W., Wang, C. & Huang, J.S. (2012). Evaluation of cooling ceiling and mechanical ventilation systems on thermal comfort using CFD study in an office for subtropical region. *Building and Environment*, 48, 113–127.
- [7] Ferkl, L. & Siroky, J. (2010). Ceiling radiant cooling: comparison of ARMAX and subspace identification modelling methods. *Building and Environment*, 45(1), 205–212.
- [8] Melikov, A.K., Helkjær, A., Arakelian, R. & Fanger, P.O. (1994). Spot Cooling - Part 2: Recommendations for design of spot cooling systems. *Ashrae Transactions*, 100, 500–510.
- [9] Yamasaki, A. (2013). Recent progress of strawberry year-round production technology in Japan. *Japan Agricultural Research Quarterly*, 47, 37–42.
- [10] Soussi, M., Chaibi, M.T., Buchholz, M. & Saghrouni, Z. (2022). Comprehensive review on climate control and cooling systems in greenhouses under hot and arid conditions. *Agronomy*, 12(3), 626.
- [11] Sethi, V.P. (2009). On the selection of shape and orientation of a greenhouse: Thermal modeling and experimental validation. *Solar Energy*, 83, 21–38.
- [12] Panwar, N.L., Kaushik, S. & Kothari, S. (2011). Solar greenhouse an option for renewable and sustainable farming. *Renewable and Sustainable Energy Reviews*, 15, 3934–3945.
- [13] Dragičević, S.M. (2011). Determining the optimum orientation of a greenhouse on the basis of the total solar radiation availability. *Thermal Science*, 15, 215–221.
- [14] El-Maghlany, W.M., Teamah, M.A. & Tanaka, H. (2015). Optimum design and orientation of the greenhouses for maximum capture of solar energy in North Tropical Region. *Energy Conversion and Management*, 105, 1096–1104.
- [15] Kittas, C., Bartzanas, T. & Jaffrin, A. (2000). Greenhouse evaporative cooling: Measurement and data analysis. *Acta Horticulture*, 534, 67–74.
- [16] Abdel-Ghany, A.M., Picuno, P., Al-Helal, I., Alsadon, A., Ibrahim, A. & Shady, M. (2015). Radiometric Characterization, Solar and Thermal Radiation in a Greenhouse as Affected by Shading Configuration in an Arid Climate. *Energies*, 8, 13928–13937.
- [17] Kittas, C., Baille, A. & Giaglaras, P. (1999). Influence of Covering Material and Shading on the Spectral Distribution of Light in Greenhouses. *Journal of Agricultural Engineering Research*, 73, 341–351.
- [18] Abdel-Ghany, A.M., Al-Helal, I.M., Alzahrani, S.M., Alsadon, A.A., Ali, I.M. & Elleithy, R.M. (2012). Covering Materials Incorporating Radiation-Preventing Techniques to Meet Greenhouse Cooling Challenges in Arid Regions: A Review. *The Scientific World Journal*, 2012, 906360.
- [19] Stanghellini, C., Dai, J. & Kempkes, F. (2011). Effect of near-infrared-radiation reflective screen materials on ventilation requirement, crop transpiration and water use efficiency of a greenhouse rose crop. *Biosystems Engineering*, 110, 261–271.
- [20] Murakami, K., Fukuoka, N. & Noto, S. (2017). Improvement of greenhouse microenvironment and sweetness of melon (*Cucumis melo* L.) fruits by greenhouse shading with a new kind of near-infrared ray-cutting net in mid-summer. *Scientia Horticulturae*, 218, 1–7.
- [21] Sethi, V. P. & Sharma, S. K. (2007). Survey of cooling technologies for worldwide agricultural greenhouse applications. *Solar Energy*, 81(12), 1447–1459.

- [22] Espinoza, K., López, A., Valera, D. L., Molina-Aiz, F. D., Torres, J. A. & Peña, A. (2017). Effects of ventilator configuration on the flow pattern of a naturally-ventilated three-span Mediterranean greenhouse. *Biosystems Engineering*, 164, 13–30.
- [23] Ganguly, A. & Ghosh, S. (2011). A Review of Ventilation and Cooling Technologies in Agricultural Greenhouse Application. *Iranica Journal of Energy & Environment*, 2, 32–46.
- [24] Kittas, C., Karamanis, M. & Katsoulas, N. (2005). Air temperature regime in a forced ventilated greenhouse with rose crop. *Energy and Buildings*, 37, 807–812.
- [25] Nikolaou, G., Neocleous, D., Katsoulas, N. & Kittas, C. (2009). Effects of Cooling Systems on Greenhouse Microclimate and Cucumber Growth under Mediterranean Climatic Conditions. *Agronomy*, 9, 300.
- [26] Sethi, V. P. & Sharma, S. K. (2007). Survey of cooling technologies for worldwide agricultural greenhouse applications. *Solar Energy*, 81(12), 1447–1459.
- [27] Ghani, S., Bakochristou, F., ElBialy, E.M.A.A., Gamaledin, S.M.A., Rashwan, M.M., Abdelhalim, A.M. & Ismail, S.M. (2018). Design challenges of agricultural greenhouses in hot and arid environments-A review. *Engineering in Agriculture, Environment and Food*, 12, 48–70.
- [28] Ishii, M., Okushima, L., Moriyama, H., Sase, S., Takakura, T. & Kacira, M. (2014). Effects of natural ventilation rate on temperature and relative humidity in a naturally ventilated greenhouse with high pressure fogging system. *Acta Horti*, 1037, 1127–1132.
- [29] Katsoulas, N., Kittas, C. & Bartzanas, T. (2012). Microclimate Distribution in a Greenhouse Cooled by a Fog System. *Acta Horticulturae*, 927, 773–778.
- [30] Kittas, C., Katsoulas, N., Bartzanas, T. & Bakker, S. (2013). Greenhouse climate control and energy use. In *FAO plant production and protection paper*. 217. *Good Agricultural Practices for greenhouse vegetable crops: Principles for Mediterranean climate areas* (pp. 63–95) (Rome).
- [31] Yurina, K., Dong Sub, K. & Changboo, C. (2014). Root-zone cooling affects growth and development of paprika transplants grown in rockwool cubes. *Horticulture Environment and Biotechnology*, 55, 14–18.
- [32] Fazlil Ilahi, W.F., Ahmad, D. & Husain, M.C. (2017). Effects of root zone cooling on butterhead lettuce grown in tropical conditions in a coir-perlite mixture. *Horticulture Environment and Biotechnology*, 58, 1–4.
- [33] Mizuno, S., Muramatsu, Y., Tateishi, A., Watanabe, K., Shinmachi, F., Koshioka, M. & Kubota, S. (2022). Effects of Root-zone Cooling with Short-day Treatment in Pot-grown Strawberry (*Fragaria × ananassa* Duch.) Nurseries on Flowering and Fruit Production. *The Horticulture Journal*, 91(1), 1–7.
- [34] Moritani, S., Nanjo, H., Itou, A. & Imai, T. (2018). Root-zone Cooling Evaluation Using Heat Pump for Greenhouse Strawberry Production. *Horttechnology*, 28(5), 570–577.
- [35] Herry, S. & Takahisa, M. (1992). Evaluation of a System for Microclimate Modification in a Plastic Greenhouse during Hot Weather. *Environment Control in Biology*, 30(4), 143–151.
- [36] Song, M., Mao, N., Xu, Y. & Deng, S. (2019). Challenges in, and the development of, building energy saving techniques, illustrated with the example of an air source heat pump. *Thermal Science and Engineering Progress*, 10, 337–356.
- [37] Borong, L., Zhe, W., Hongli, S., Yingxin, Z. & Qin, O. (2016). Evaluation and comparison of thermal comfort of convective and radiant heating terminals in office building. *Building and Environment*, 106, 91–102.

- [38] Niu, J., Kooi, J.V., & Rhee, H. (1995). Energy saving possibilities with cooled-ceiling systems. *Energy and Buildings*, 23, 147–158.
- [39] Kyu-Nam R. & Kwang Woo, K. (2015). A 50 year review of basic and applied research in radiant heating and cooling systems for the built environment. *Building and Environment*, 91, 166–190.
- [40] CIBSE. (2007). *CIBSE Guide B-heating, Ventilating, Air Conditioning and Refrigeration: the Chartered Institution of Building Services Engineers*, London.
- [41] Helmut, E. & Corina, S. (1995). Hydronic radiant cooling - preliminary assessment. *Energy and Buildings*, 22, 195–205.
- [42] Jingjuan, F., Stefano, S. & Fred B. (2013). Cooling load differences between radiant and air systems. *Energy and Buildings*, 65, 310–321.
- [43] Yin, Y., Wang, R., Zhai, X. & Ishugah, T. (2014). Experimental investigation on the heat transfer performance and water condensation phenomenon of radiant cooling panels. *Building and Environment*, 71, 15–23.
- [44] Novoselac, A. & Srebric, J. (2002). A critical review on the performance and design of combined cooled ceiling and displacement ventilation systems. *Energy and Buildings*, 34, 497–509.
- [45] Claus, B. & Richard, E.S. (2013). *Fundamentals of Thermodynamics*, eighth ed., University of Michigan, Willey.
- [46] Kyn-Nam, R., Bjarne, W.O. & Kwang, W.K. (2017). Ten questions about radiant heating and cooling systems. *Building and Environment*, 112, 367–381.
- [47] Bjarne, W.O. (2002). Radiant floor heating in theory and practice. *ASHRAE J.* 44, 19–26.
- [48] Guoqing, Y., Le, X., Chengjun, D. & Hengtao, C. (2018). Simplified model and performance analysis for top insulated metal ceiling radiant cooling panels with serpentine tube arrangement. *Case Studies in Thermal Engineering*, 11, 35–42.
- [49] Minzhi, Y., Ahmed, A. S., Ali, R., Hideki, S. & Katsunori, N. (2021). Thermal performance of ceiling radiant cooling panel with a segmented and concave surface: Laboratory analysis. *Applied Thermal Engineering*, 196, 117280.
- [50] Yin, Y.L., Wang, R.Z., Zhai, X.Q. & Ishugah, T.F. (2014). Experimental investigation on the heat transfer performance and water condensation phenomenon of radiant cooling panels. *Building and Environment*, 71, 15–23.
- [51] Gallardo, A. & Berardi, U. (2019). Analysis of the energy and thermal performance of a radiant cooling panel system with integrated phase change materials in very hot and humid conditions. *IOP Conference Series: Material and Science Engineering*, 609(5), 052025.

Chapter 2

Principle and theories

Environmental factors such as temperature, photoperiod, and light intensity have significant effects on growth, yield and fruit quality. Thus, cultivation in a greenhouse is the solution to overcome climatic diversity. Strawberry production in Japan is mostly done in greenhouses, which not only provide a suitable environment for cultivation but also prevent any likely damage to the strawberry crop from the extreme environment. The climate of the main production area in Japan is temperate. This means that the temperature remains above freezing during the coldest month and can often reach over 30°C in summer. For commercial and economic considerations, the quality of strawberry produce and energy consumption for producing it are critical.

Active solar heating systems have been widely used worldwide in greenhouses during winter. However, no energy analysis has been performed on the use of double vinyl sheets in solar greenhouses without supplemental heating. The objectives of this study were to perform an energy analysis of an experimental greenhouse and determine how it affected the local environment around the plantation area in terms of temperature, relative humidity, and solar radiation. A field experiment was performed in a small walk-in tunnel with a passive solar greenhouse for strawberry cultivation in a temperate area in central Japan. Based on the study, the optimum energy requirement for controlling the optimum environment for sensitive plant cultivation is proposed. The evaluation methods used in this study can be applied also to tropical regions to achieve the suitable conditions for energy management.

2.1 Energy balance of walk-in tunnel

The energy balance of the greenhouse was derived under steady-state conditions. In this present study, four components played significant roles: the greenhouse covering, inside air temperature, floor, and plants [1]. Figure 2-1 depicts the heat transfer cycle in the experimental greenhouse. This figure indicates that radiation is the source of the energy flow entering the greenhouse, whereas the energy flow exiting the greenhouse is by way of heat losses through the covering material, ventilation, and ground.

Therefore, the following assumptions are made:

- 1) Heat absorption by greenhouse covering material is negligible.
- 2) Evaporation from the ground is negligible.
- 3) Transpiration from strawberry plants is negligible.
- 4) Radiation heat exchange between the greenhouse covering material and inside air is negligible.

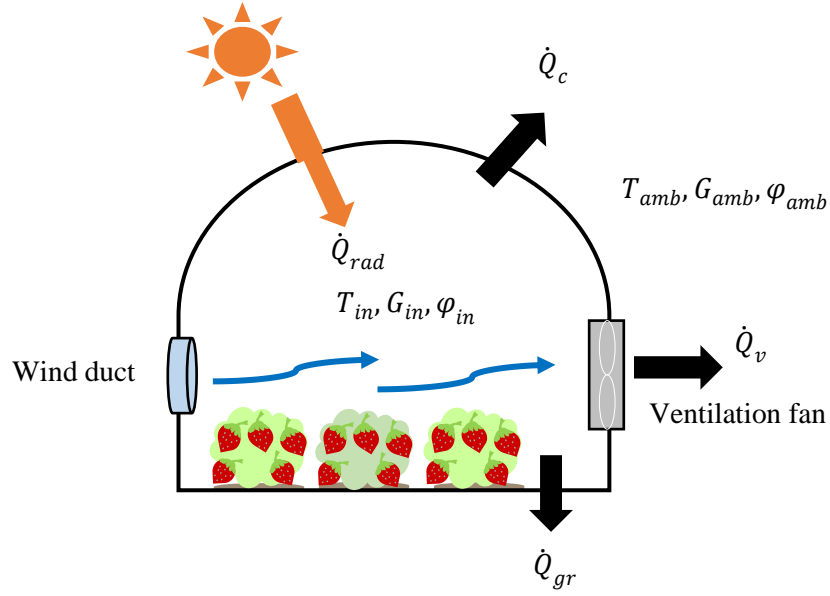


Figure 2-1 Energy balance of experimental greenhouse

The variables in the figure above are described as follows: T_{in} and T_{amb} are the air temperatures inside and outside the greenhouse, ϕ_{in} and ϕ_{out} are the humidity inside and outside the greenhouse as well as G_{in} and G_{out} are the solar radiations inside and outside the greenhouse.

Using the first law of thermodynamics, the energy balance in the present study is derived as

$$\dot{Q}_{rad} = \dot{Q}_c + \dot{Q}_{gr} + \dot{Q}_v \quad (2.1)$$

where \dot{Q}_{rad} is the net rate of radiation heat transfer to the greenhouse surface exposed to solar and atmospheric radiation, \dot{Q}_c is the heat loss through the covering material, \dot{Q}_{gr} is the heat loss to the ground, and \dot{Q}_v is the ventilation heat loss.

In this study, the experimental greenhouse is located in Matsusaka city, Mie in central Japan. The climate of the Matsusaka city has a variety of characteristics. The annual average temperature is 15°C, which is relatively high for Japan. Furthermore, solar radiation resources are substantial [2]. The solar radiation during the daytime is sufficient to maintain the air temperature inside the greenhouse at the desired level for optimal growth of the strawberry plants even during the winter season. The present study assumed that heat loss through the greenhouse is a major factor during winter, particularly when there is no solar radiation. To estimate the heat energy required for maintaining the optimum inside temperature for plant health and growth, the total heat loss through the small walk-in tunnel was considered.

The rate of the total heat loss (\dot{Q}_{total}) through the small walk-in tunnel comprised the heat losses through the covering material, ground, and ventilation exhaust and was calculated as follows [3,4]:

$$\dot{Q}_{total} = \dot{Q}_c + \dot{Q}_{gr} + \dot{Q}_v \quad (2.2)$$

$$\dot{Q}_c = U_c A_c (T_{in} - T_{amb}) \quad (2.3)$$

$$\dot{Q}_{gr} = U_{gr} A_{gr} (T_{in} - T_{amb}) \quad (2.4)$$

$$\dot{Q}_v = 0.33ACHV(T_{in} - T_{amb}) \quad (2.5)$$

where U_c is the overall heat transfer coefficient of the covering material, $W/(m^2 \cdot K)$

A_c is the total area of the covering material, m^2

T_{in} is the inside air temperature, $^{\circ}C$

T_{amb} is the ambient air temperature, $^{\circ}C$

U_{gr} is the ground heat transfer coefficient, $W/(m^2 \cdot K)$

A_{gr} is the plantation area, m^2

ACH is air change per hour, $1/h$

V is the volume of the greenhouse, m^3

The value of U_c depends on many factors such as the type and thickness of the covering material, size of the greenhouse, specifications of the heating system, and wind speed. Therefore, the value of U_c was determined experimentally instead of being based on theoretical calculations in the range of $6.0\text{--}8.0 W/(m^2 \cdot K)$ as determined in reference 5. Considering the heat transfer through the cover material by conduction, convection, and radiation of polyvinyl chloride, the value of U_c was calculated to be $6.2 W/(m^2 \cdot K)$ in this study.

To compensate for the ventilation heat loss, the inside air needs to be heated by the temperature difference between the inside and the ambient environment. The energy required to raise the temperature of 1 cubic meter of air by 1 K is 0.33 Wh. Therefore, the heat capacity per cubic meter is $0.33 Wh/(m^3 \cdot K)$ [6].

Air changes per hour (ACH) is a measure of how many times the volume of air within a greenhouse will be replaced with fresh air. The size of the greenhouse and the temperature difference between the inside air and outside air are the principal factors that affect the ventilation requirement for temperature control. From reference 7, $ACH = 0.75\text{--}2 h^{-1}$ for double-wall plastic greenhouses. ACH can vary widely based on the type of construction and age of the greenhouse. The ACH can be calculated by dividing the air flow rate (\dot{V}_a) of the ventilation fan by the volume of the greenhouse (V). In this study, ACH was calculated to be $150 h^{-1}$. This value is significantly different from that reported in the existing literature. This difference is attributed to the capacity of the fan, which is excessive for the size of the greenhouse.

For the energy required to heat the experimental greenhouse in this study. The monthly heating requirement was calculated by adding the daily heat losses. Heating is necessary at night, when there is no solar radiation. Similarly, the ventilation fan does not operate unless the inside air temperature exceeds $25^{\circ}C$. Therefore, the heat loss by ventilation is ignored when the ventilation fan is off or when the inside air temperature is low. In addition, the heat loss or gain to the ground is assumed to be negligible and is ignored. Furthermore, the ground was also covered with a single black plastic sheet. Therefore, the monthly heating requirement E_m (kJ/month) was calculated as follows [8-10]:

$$E_m = \dot{Q}_c \cdot HN \quad (2.6)$$

equation (2.6) can be rewritten as

$$E_m = 3.6U_cA_c(T_{de} - T_{amb,min}) \cdot HN \quad (2.7)$$

$$e_m = E_m/A_{gr} \quad (2.8)$$

where T_{de} is design temperature for optimal growth of the strawberry plants in the greenhouse, $T_{amb,min}$ is the monthly minimum ambient air temperature, °C, H is the daily heating duration, h/d, N is the number of days per month, d/month and e_m is monthly heating requirement per plantation area, kJ/(m²·month).

2.1.1 Statistical analysis

To evaluate the fluctuation in the inside air temperature in the greenhouse, statistical analysis in terms of the standard deviation (SD) was analyzed. The standard deviation (SD) is a measure of the dispersion in a set of data from its average. The more dispersed the data, the higher the deviation. Oppositely, a low SD indicates that the data set points tend to close to the average [21]. That is to say that the fluctuation in air temperature must be the lowest. Therefore, the SD should be minimum. The SD for inside air temperature is calculated by equation (2.9)

$$\sigma_i = \sqrt{\frac{1}{n} \sum_{j=1}^n (T_{in,j} - \overline{T_{in}})^2} \quad (2.9)$$

where σ_i is the standard deviation of inside air temperature, °C

$T_{in,j}$ is the inside air temperature at time interval j , °C

$\overline{T_{in}}$ is the average of air temperature inside greenhouse in daytime, °C

n is the number of the data point

2.2 Principle of natural convection

Cooling a large space such as the inside of a greenhouse consumes more electricity than a small or local area. Method of cooling or heating within a small space or local space has become popular due to the use of less energy. In order to achieve that, this study focused on a microclimate weather management system for indoor plantation. In particular, local temperature control is very important for strawberry cultivation. Therefore, a cooling serpentine copper pipe heat exchanger is the point of interest. Serpentine heat exchangers are the most compact and are minimal in terms of the volume of the microchannel coils, without manifolds in their design. This arrangement allows for serpentine coils that are suitable for compact, lightweight cooling applications. In addition, a serpentine heat exchanger does not block light in plant photosynthesis, unlike a fin and tube heat exchanger, which is important in cultivation. Under this objective, a cooling serpentine copper pipe heat exchanger is established for cooling in a laboratory-scale room. So that, the study of natural convection and heat transfer on heat exchanger is therefore important.

2.2.1 Physical mechanism of natural convention

A hot box on a horizontal plate eventually cools to the room air temperature, as shown in figure 2-2. Consider about a hot object in a cold environment. The temperature of the outside of the object will drop, while the temperature of the air around it will increase. As a result, a small layer of warmer air surrounds the object, and heat will be transported from this layer to the outer layers of air. The cooling process is slow in this situation because the

box is always surrounded by warm air and has no direct contact with cooler air further away. It may not be observed any air movement near the box, but thorough measurements would show otherwise.

The rise of heated air and flow of cooler air into its place continues until the box is cooled to the surrounding air temperature. Natural convection current refers to the motion caused by the constant replacement of warm air in the region of the box with cooler air nearby, and natural convection heat transfer refers to the heat transfer that is enhanced as a result of this natural convection current.

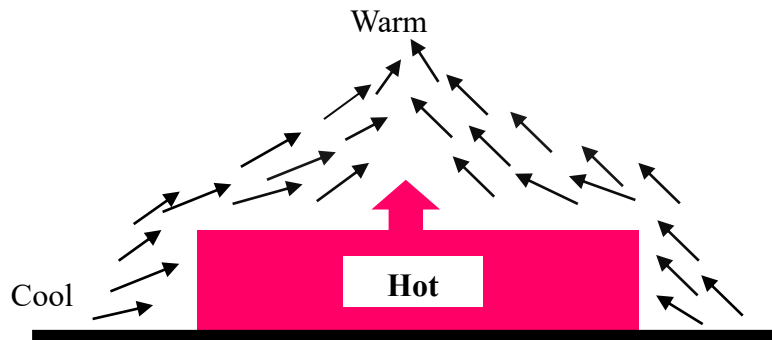


Figure 2-2 The cooling of a hot box in a cooler environment by natural convection

There is a net force in a gravitational field that pushes a light fluid placed in a heavy fluid upward. The upward force exerted by a fluid on a body completely or partially immersed in it is called the buoyancy force. The buoyancy force is equal to the weight of the fluid displaced by the body. That is,

$$F_{buoyancy} = \rho_{fluid} V_{body} g \quad (2.10)$$

where ρ_{fluid} is the density of the fluid, V_{body} is the volume of the portion of the body immersed in the fluid, and g is the gravitational acceleration. The net vertical force acting on a body in the absence of other forces is the difference between the body's weight and the buoyancy force. That is to say,

$$F_{net} = W - F_{buoyancy} \quad (2.11)$$

$$F_{net} = (\rho_{body} - \rho_{fluid}) V_{body} g \quad (2.12)$$

Note that the net force is proportional to the difference in the densities of the fluid and the body. This is known as Archimedes' principle. There are several applications of the buoyancy effect in daily life. One reason is because heat transfer between a hot (or cold) surface and the fluid around it would occur by conduction instead of natural convection in the condition of buoyancy. Buoyancy is essential for the natural convection currents that exist in the seas, lakes, and atmosphere. Additionally, buoyancy allows both light and heavy warships made of steel to float on water (figure 2-3).

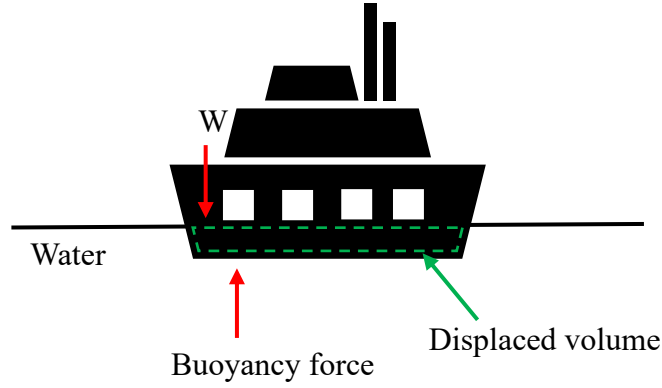


Figure 2-3 The buoyancy force keeps the ships afloat in water ($W = F_{buoyancy}$ for floating objects)

Since density is a function of temperature, the variation of density of a fluid with temperature at constant pressure can be expressed in terms of the volume expansion coefficient β , defined as,

$$\beta \approx -\frac{1}{\rho} \frac{\Delta\rho}{\Delta T} = -\frac{1}{\rho} \left(\frac{\rho_\infty - \rho}{T_\infty - T} \right) \quad (\text{at constant pressure}) \quad (2.13)$$

where ρ_∞ is the density and T_∞ is the temperature of quiescent fluid away from surface.

It can also be shown that for an ideal gas

$$\beta_{ideal} \approx \frac{1}{T} \quad (1/K) \quad (2.14)$$

where T is the thermodynamic temperature. Note that the parameter β represents the fraction of volume change of a fluid that corresponds to a temperature change ΔT at constant pressure. Also note that the buoyancy force at constant pressure is proportional to the difference in density, which is proportional to the variation in temperature. Therefore, the buoyancy force and natural convection currents are stronger and the temperature difference between a fluid near a hot (or cold) surface and a fluid away from it is larger, resulting in a higher rate of heat transfer.

The Grashof number Gr

Grashof number is a dimensionless group. It presents the natural convection effects and represents the ratio of the buoyancy force to the viscous force acting on the fluid.

$$Gr = \frac{\text{buoyancy forces}}{\text{viscous forces}} = \frac{g\Delta\rho V}{\rho\nu^2} \quad (2.15)$$

It is also expressed as

$$Gr = \frac{g\beta(T_s - T_\infty)L_c^3}{\nu^2} \quad (2.16)$$

where

- g is gravitational acceleration, m/s^2
- β is coefficient of volume expansion, $1/K$
- T_s is temperature of the surface, $^\circ C$

T_{∞} is temperature of the fluid sufficiently far from the surface, °C

L_c is characteristic length of the geometry, m

ν is kinematic viscosity of the fluid, m²/s

The dimensionless Grashof number, which measures the ratio of the buoyancy force to the viscous force acting on the fluid, controls the flow regime in natural convection, as shown in figure 2-4.

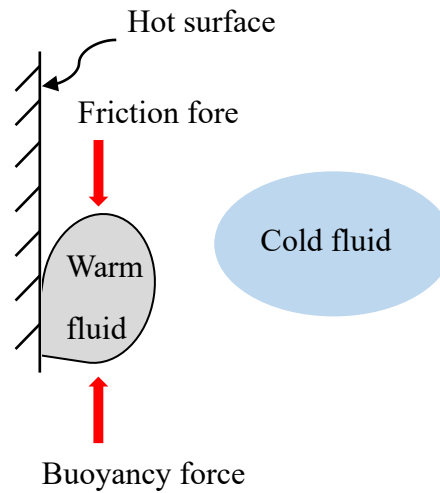


Figure 2-4 The Grashof number Gr is a measure of the relative magnitudes of the buoyancy force and the opposing viscous force acting on the fluid

In natural convection, the Grashof number plays the role that the Reynolds number does in forced convection. As a result, in natural convection, the Grashof number is the primary criteria for evaluating whether the fluid flow is laminar or turbulent. For vertical plates, for example, the critical Grashof number is observed to be approximately 10^9 . Therefore, the flow regime on a vertical plate starts to become turbulent at Grashof numbers greater than 10^9 .

2.2.2 Natural convection over surfaces

Natural convection heat transfer on a surface is affected by the geometry as well as the direction of the surface. It is also influenced by variations on the surface and the thermophysical parameters of the fluid involved. For example, the velocity and temperature profile for natural convection over a hot vertical plate are shown in figure 2-5.

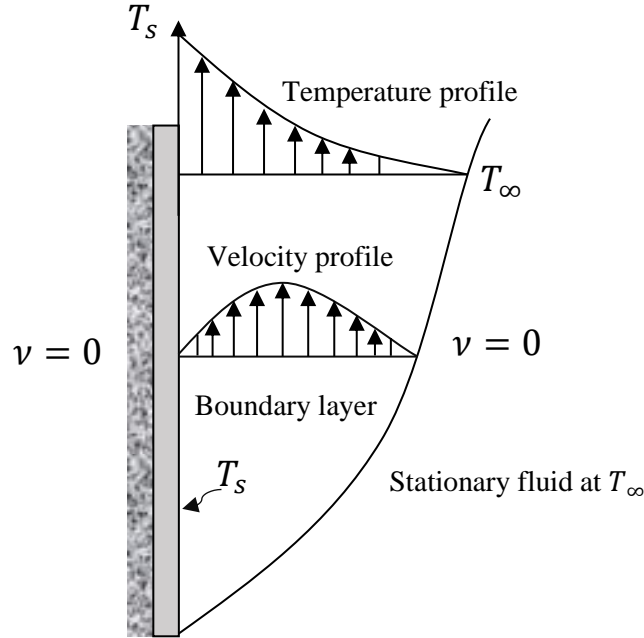


Figure 2-5 Typical velocity and temperature profiles for natural convection flow over a hot vertical plate
(Source: N. Necati Özisik. Heat transfer: a basic approach. McGraw-Hill, 1985)

Nusselt number Nu

$$Nu = \frac{hL_c}{k} = C(Gr_L Pr)^a = C Ra_L^a \quad (2.17)$$

where h is heat transfer coefficient ($W/m^2 \cdot K$), k is thermal conductivity of air at film temperature ($W/m \cdot K$), Ra_L is the Rayleigh number, which is the product of the Grashof number, which explains the relationship between buoyancy and viscosity within the fluid, and the Prandtl number, which describes the relation between momentum diffusivity and thermal diffusivity. C is constant coefficient and a is constant exponent, and both of values depend on the geometry of the surface and the flow regime, which is defined by the range of Rayleigh number. Note that, the value of a is usually $\frac{1}{4}$ for laminar and $\frac{1}{3}$ for turbulent flow. Normally, the value of the constant C is less than 1.

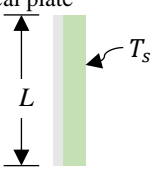
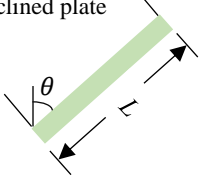
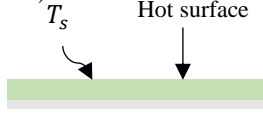
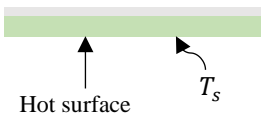
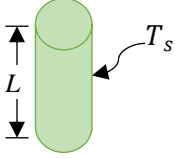
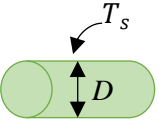
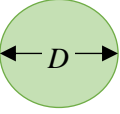
Rayleigh number Ra_L

Here, the Rayleigh number is defined as

$$Ra_L = Gr_L Pr = \frac{g\beta(T_s - T_\infty)L_c^3}{\nu^2} Pr \quad (2.18)$$

Table 2-1 provides simple relations for the average Nusselt number for a variety of shapes. The typical geometries' lengths and the ranges of Rayleigh numbers where the relation applies are also shown in this table. All fluid properties are to be evaluated at the film temperature $T_f = \frac{1}{2}(T_s + T_\infty)$.

Table 2-1 Empirical correlations for the average Nusselt number for natural convection over surfaces

Geometry	Characteristic length, L_c	Range of Ra_L	Nu
<p>Vertical plate</p> 	L	10^4 - 10^9 10^{10} - 10^{13} Entire range	$Nu = 0.59Ra_L^{1/4}$ (2.19) $Nu = 0.1Ra_L^{1/3}$ (2.20) $Nu = \left\{ 0.825 + \frac{0.387Ra_L^{1/6}}{[1+(0.492/Pr)^9/16]^{1/4}} \right\}^2$ (2.21) (Note: complex but more accurate)
<p>Inclined plate</p> 	L		Use vertical plate equations for the upper surface of a cold plate and the lower surface of a hot plate. Replace g by $g \cos \theta$ for $0 < \theta < 60^\circ$
<p>Horizontal plate</p> <p>(Surface area A_s and perimeter p)</p> <p>(a) Upper surface of a hot plate (or lower surface of a cold plate)</p>  <p>(b) Lower surface of a hot plate (or upper surface of a cold plate)</p> 	A_s/p	10^4 - 10^7 10^7 - 10^{11} 10^5 - 10^{11}	$Nu = 0.59Ra_L^{1/4}$ (2.22) $Nu = 0.1Ra_L^{1/3}$ (2.23) $Nu = 2.7Ra_L^{1/4}$ (2.24)
<p>Vertical cylinder</p> 	L		A vertical cylinder can be treated as a vertical plate when $D \geq \frac{35L}{Gr_L^{1/4}}$
<p>Horizontal cylinder</p> 	D	$Ra_D \leq 10^{12}$	$Nu = \left\{ 0.6 + \frac{0.387Ra_D^{1/6}}{[1+(0.559/Pr)^9/16]^{1/4}} \right\}^2$ (2.25)
<p>Sphere</p> 	D	$Ra_D \leq 10^{11}$ $(Pr \geq 0.7)$	$Nu = 2 + \frac{0.589Ra_D^{1/4}}{[1+(0.469/Pr)^9/16]^{1/4}}$ (2.26)

The rate of heat transfer by natural convection from a solid surface at a uniform temperature (T_s) to the surrounding fluid is expressed by Newton's law of cooling as once the average Nusselt number and thus the average convection coefficient is known.

$$\dot{Q}_{conv} = hA_s(T_s - T_\infty) \quad (2.27)$$

where A_s is the heat transfer surface area and h is the average heat transfer coefficient on the surface.

2.3 Internal forced convection

Flow sections are frequently referred to as pipes, ducts, or conduits. Flow sections with a circle cross section are typically referred to as pipes (particularly when the fluid is a liquid), while flow sections with a noncircular cross section are typically referred to as ducts (especially when the fluid is a gas). Tubes are the common name for small-diameter pipes.

Fluid distribution networks and heating and cooling applications frequently involve liquid or gas movement through pipes or ducts. In these applications, the fluid is typically forced to flow through a flow section by a fan or pump. Thus, friction must be considered due to it is directly related to pressure drop and head loss during pipe and duct flow. The pressure drop is then used to determine the pumping power requirement.

2.3.1 Laminar and turbulent flow in tube

Depending on the flow conditions, flow in a tube can be laminar or turbulent. At low velocities, fluid flow is streamlined and therefore laminar, but turns turbulent as the velocity is increased beyond a critical point. In practice, turbulent pipe flows are the usual. When highly viscous fluids, like oils, flow through tubes with small diameters or through enclosed spaces, laminar flow occurs.

For flow in circular tube, the Reynolds number Re is defined as

$$Re = \frac{V_{avg}D}{\nu} = \frac{\rho V_{avg}D}{\mu} = \frac{\rho D}{\mu} \left(\frac{\dot{m}}{\rho \pi D^2 / 4} \right) = \frac{4\dot{m}}{\mu \pi D} \quad (2.28)$$

where V_{avg} is the average flow velocity, D is the diameter of the tube and $\nu = \mu/\rho$ is the kinematic viscosity of the fluid. The friction factor, Nusselt number, and Reynolds numbers for flow in noncircular tubes are based on the hydraulic diameter D_h .

Although precise Reynolds numbers for laminar, transitional, and turbulent flows are desirable, this is not always the case in practice. This is due to the fact that the transition from laminar to turbulent flow is also affected by the degree of flow disturbance caused by surface roughness, pipe vibrations, and flow fluctuations. Under most practical conditions, the flow in a tube is laminar for $Re < 2,300$, fully turbulent for $Re > 10,000$ and transition in between.

2.3.2 General thermal analysis

The conservation of energy equation for the constant flow of a fluid in a tube can be expressed in the absence of any work interactions as (figure 2-6)

$$\dot{Q}_{total,c} = \dot{m}c_p(T_e - T_i) \quad (2.29)$$

where T_i and T_e are the average fluid temperatures at the inlet and exit of the tube, respectively, and \dot{Q} is the rate of heat transfer to or from the fluid.

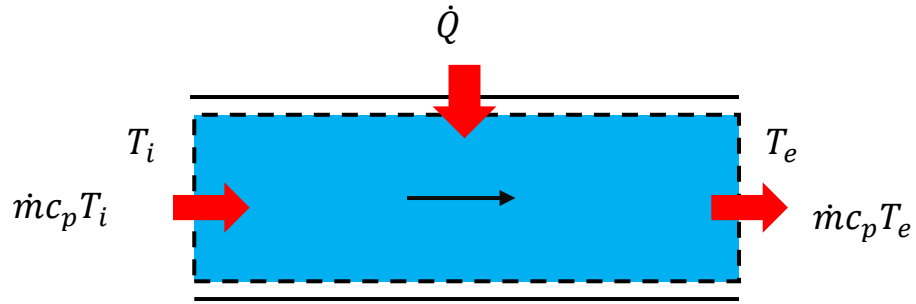


Figure 2-6 The heat transfer of fluid flowing through a tube

2.3.3 Pressure drop ΔP

The pressure drop ΔP is a quantity of importance in the study of pipe flow since it is directly related to the amount of power needed by the fan or pump to keep the flow going. Pressure drop is defined as the difference in total pressure between two points in a fluid carrying network. Note that, P_1 is the pressure at the inlet tube, P_2 is the pressure at the exit tube and L is the length of the tube.

$$\frac{dP}{dx} = \frac{P_1 - P_2}{L} \quad (2.30)$$

and the pressure drop across laminar flow in terms of V_{avg} is expressed as

$$\Delta P = P_1 - P_2 = \frac{8\mu L V_{avg}}{R^2} = \frac{32\mu L V_{avg}}{D^2} \quad (2.31)$$

The pressure drop is proportional to the viscosity μ of the fluid, and ΔP would be zero if there were no friction. Therefore, the drop of pressure from P_1 to P_2 in this case is due entirely to viscous effects and equation (2.31) represents the pressure loss ΔP_L , when viscosity μ of the fluid pass through a pipe at constant diameter D and constant length L at average velocity V_{avg} . In practice, expressing the pressure loss for all types of fully developed internal flows is convenient as

$$\Delta P_L = f \frac{L}{D} \frac{\rho V_{avg}^2}{2} \quad (2.32)$$

where ρV_{avg}^2 is the dynamic pressure and f is the Darcy friction factor and can be expressed as

$$f = \frac{8\tau_w}{\rho V_{avg}^2} \quad (2.33)$$

where τ_w is shear stress. Taking equation (2.31) and (2.32) and solving for f yields the friction factor for fully developed laminar flow in a circular tube.

$$f = \frac{64\mu}{\rho D V_{avg}} = \frac{64}{Re} \quad (2.34)$$

The equation above shows the friction factor is a function of the Reynolds number only and is independent from the roughness of the pipe surface. In the analysis of pipe systems, pressure losses are frequently described in terms of the equivalent fluid column height, or head loss h_L . Knowing that, $\Delta P = \rho gh$ so that a fluid height is equal to $h = \Delta P / \rho g$, the pipe heat loss is obtained by dividing ΔP_L by ρg to get

$$h_L = \frac{\Delta P_L}{\rho g} = f \frac{L}{D} \frac{V_{avg}^2}{2g} \quad (2.35)$$

The head loss h_L is the additional height that a pump must raise the fluid to overcome frictional losses in the pipe. The head loss is caused by viscosity and is proportional to the wall shear stress. Therefore, the required pumping power to overcome the pressure loss is expressed as

$$\dot{W}_{pump,L} = \dot{V} \Delta P_L = \dot{V} \rho g h_L = \dot{m} g h_L \quad (2.36)$$

where \dot{V} is the volume flow rate and \dot{m} is mass flow rate.

The average of laminar flow in horizontal tube is,

$$V_{avg} = \frac{(P_1 - P_2) R^2}{8\mu L} = \frac{(P_1 - P_2) D^2}{32\mu L} = \frac{\Delta P D^2}{32\mu L} \quad (2.37)$$

Thus, the volume flow rate for lamina flow through a horizontal tube of constant diameter D and length L gives [11]

$$\dot{V} = V_{avg} A_c = \frac{(P_1 - P_2) R^2}{8\mu L} \pi R^2 = \frac{(P_1 - P_2) D^4}{128\mu L} = \frac{\Delta P D^4}{128\mu L} \quad (2.38)$$

2.4 Heat exchanger

Heat exchangers are often used in practice for a variety of purposes, such as chemical processes, engineering processes, power plants, and air conditioning. In a heat exchanger, heat transfer typically occurs through conduction through the wall separating the two fluids and convection in each fluid. There are no external thermal energy and work interactions. Among the various types of heat exchangers, serpentine heat exchangers are the most compact and are minimal in terms of the volume of the microchannel coils, without manifolds in their design. This arrangement allows for serpentine coils that are suitable for compact, lightweight cooling applications. Serpentine tubes can be used in laminar flow heat exchange systems, since straight tube heat exchangers allow limited mixing in the laminar flow regime. In addition, a serpentine heat exchanger does not block light in plant photosynthesis, unlike a fin and tube heat exchanger, which is important in cultivation. The heat transfer theory with respect to heat exchanger is described below.

2.4.1 Heat exchanger types

The design of heat exchangers is a challenging issue. It goes beyond just focusing at heat transmission. From the perspective of total cost of ownership, weight, size, and cost of manufacturing and installation all have a significant impact on the final design. Although cost is usually a crucial factor, size and footprint tend to be the determining factors when choosing a design.

Most heat exchangers may be classified as one of several basic types. Heat exchangers can classify four common types. Most heat exchangers may be classified as one of several basic types. Based on the configuration of the flow path, the four most typical types are shown in figure 2-7 below [12].

In a double-pipe heat exchanger, there are two different flow configurations that are possible: in parallel flow, at one end, the two fluid streams enter together, pass through in the same direction, and exit together. On the other hands, in counter flow, the hot and cold fluids enter the unit from opposite ends and flow in the opposite directions. The two fluids in compact heat exchangers often move perpendicular to each other, and this flow configuration is known as cross-flow. Depending on the flow configuration, cross-flow is further classified as unmixed and mixed flow. In unmixed crossflow units one fluid stream shuttles back and forth across the flow path of the other fluid stream, usually giving a crossflow approximation to counterflow. In addition, in mixed crossflow units one fluid moves through the heat transfer matrix at right angles to the flow path of the other fluid.

The shell-and-tube heat exchanger may be the type of exchanger used most commonly in industrial applications. This type consists of round tubes mounted on a cylindrical shell with their axes parallel to that of the shell. Figure 2-8 demonstrates the main characteristics of a shell-and tube exchanger having one fluid flowing inside the tubes and the other flowing outside the tubes.

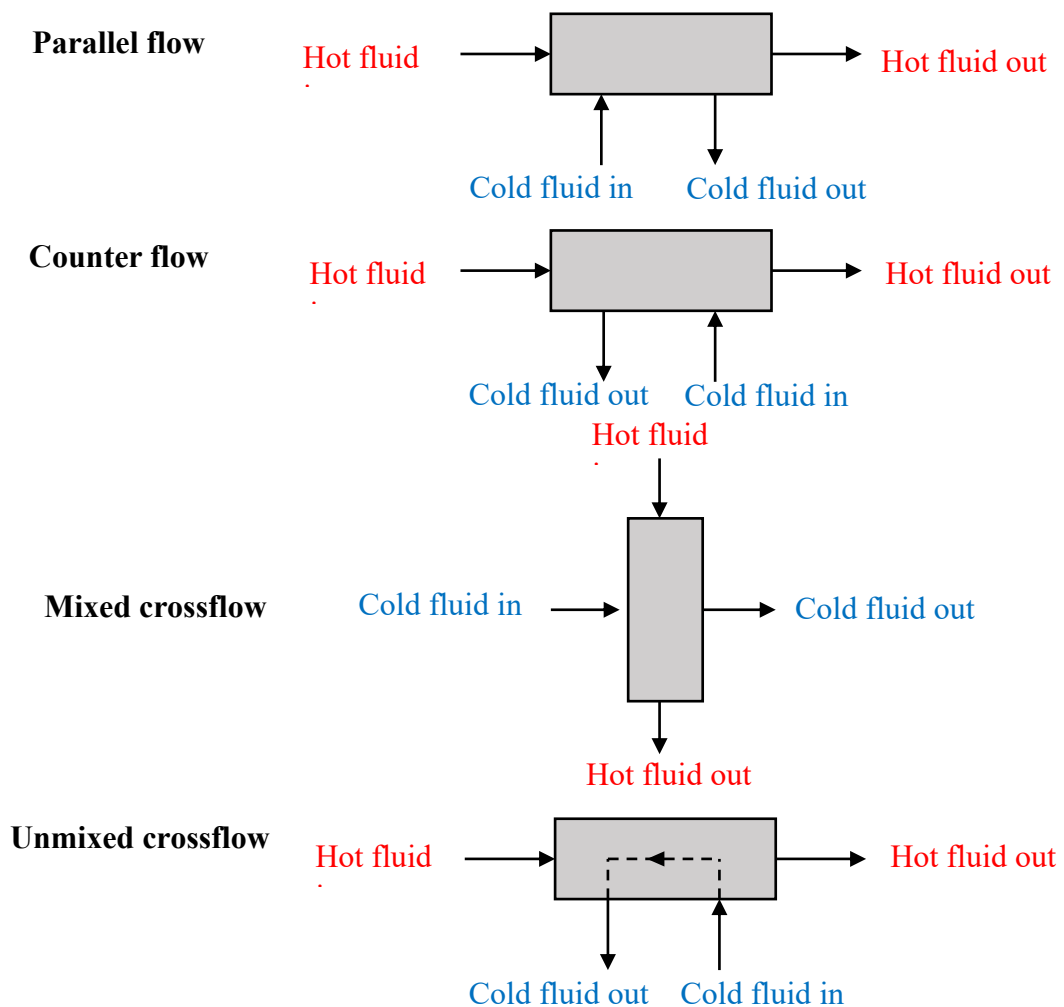


Figure 2-7 Types of flow path configuration through heat exchanger

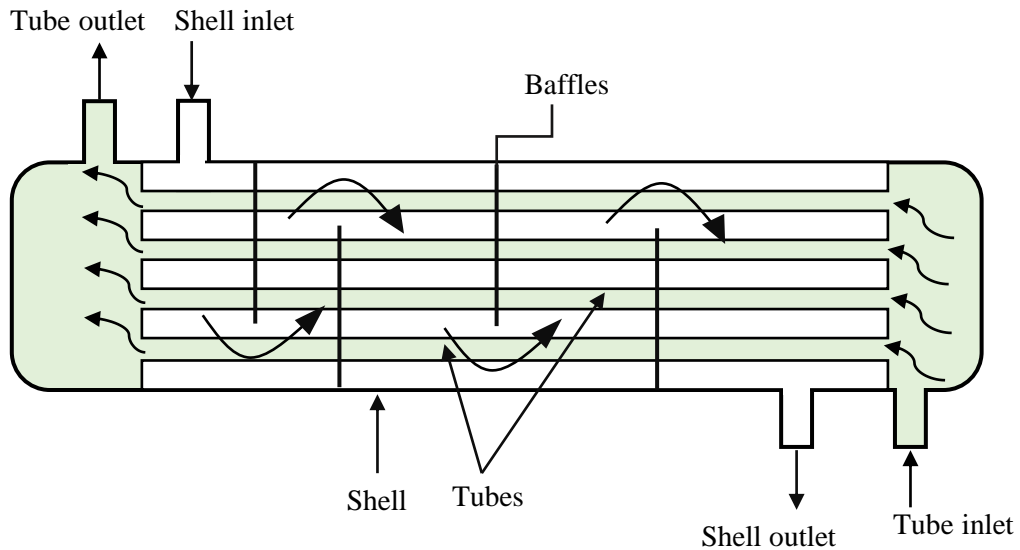


Figure 2-8 A shell-and-tube heat exchanger

(Source: Yunus A. Cengel and Afshin J. Ghajar. Heat and mass transfer. McGraw-Hill, 2015)

The tube bundle, shell, front and rear end headers, and baffles are this type of shell-and-tube exchanger's main parts. The tubes are supported by the baffles, which also help to increase the turbulence of the shell fluid and direct fluid flow roughly in a normal direction to the tubes. There are different baffle kinds, and the choice of baffle type, spacing, and shape depends on the flow rate allowed shell-side pressure drop, the necessity of tube support, and the flow-induced vibrations. There are numerous shell-and-tube exchanger variations; the differences are found in the organization of the flow configurations and the specifics of construction.

2.4.2 Analysis of heat exchangers

Typically, the operating conditions of heat exchangers remain constant over long periods of time. They are therefore suitable for modeling as steady-flow devices. As a result, each fluid continues to flow at a constant mass rate, and its temperature and velocity are constant at all inlets and outlets. Additionally, the velocities and elevations of the fluid streams change very little or not at all, which results in negligible kinetic and potential energy changes. In general, temperature affects a fluid's specific heat. But with little loss in accuracy, it can be treated as a constant at some average value within a given temperature range. In most cases, axial heat conduction along the tube is negligible and insignificant. Finally, the outer surface of the heat exchanger is assumed to be completely insulated, so that there is no heat loss to the surrounding medium, and any heat transfer occurs between the two fluids only. In practice, the idealizations stated above are closely approximated, and they greatly simplify the analysis of a heat exchanger while sacrificing little accuracy. As a result, they are widely used. Therefore, they are commonly used. Under these assumptions, the first law of thermodynamics requires that the rate of heat transfer from the hot fluid be equal to the rate of heat transfer to the cold one. That is,

$$\dot{Q}_{total,c} = \dot{m}_c c_{pc} (T_{c,out} - T_{c,in}) \quad (2.39)$$

and

$$\dot{Q}_{total,c} = \dot{m}_h c_{ph} (T_{h,in} - T_{h,out}) \quad (2.40)$$

where the subscripts h and c mean for hot and cold fluids, respectively, and \dot{m} is mass flow rate, c_p is specific heats, T_{out} is outlet temperature and T_{in} is inlet temperature.

In accordance with the second law of thermodynamics, the heat transfer rate Q is assumed to be a positive quantity, and its direction is understood to be from the hot fluid to the cold one. In heat exchanger analysis, heat capacity rate is a product from the mass flow rate and specific heat of a fluid and is defined for hot and cold fluids as

$$C_h = \dot{m}_h c_{ph} \quad (2.41)$$

and

$$C_c = \dot{m}_c c_{pc} \quad (2.42)$$

With the definition of heat rate above, Equation (39) and (40) can be expressed as

$$\dot{Q}_{total,c} = C_c (T_{c,out} - T_{c,in}) \quad (2.43)$$

and

$$\dot{Q}_{total,c} = C_h (T_{h,in} - T_{h,out}) \quad (2.44)$$

2.5 Condensation heat transfer

Condensation occurs one of two ways, first, either the air is cooled to its dew-point temperature T_{dp} which is the temperature at water in the air condenses to create water droplets. Secondly, the temperature of a vapor is reduced below its saturation temperature T_{sat} that the air cannot hold any more water. In addition, cold air can hold less water vapor than warm air. This is usually done by bringing the air into contact with a solid surface that temperature T_s is below the saturation temperature T_{sat} of the vapor.

The dew point temperature T_{dp} is defined by the Magnus formula, that is

$$T_{dp} = \frac{243.12 \times \left\{ \ln\left(\frac{RH}{100}\right) + \frac{17.62 \times T_{amb}}{243.12 + T_{amb}} \right\}}{17.62 - \left\{ \ln\left(\frac{RH}{100}\right) + \frac{17.62 \times T_{amb}}{243.12 + T_{amb}} \right\}} \quad (2.45)$$

where RH is relative humidity in present and T_{amb} is ambient air temperature.

There are two types of condensation observed: film condensation and dropwise condensation. In film condensation, the condensate wets the surface, creating a liquid coating that slides down due to gravity. The thickness of the liquid film increases in the flow direction as more vapor condenses on the film. In dropwise condensation, the condensed vapor produces droplets on the surface during dropwise condensation, and the surface is totally covered by all these many droplets of various sizes as shown in figure 2-9.

2.5.1 Film condensation

The film condensation on vertical plate is considered, as shown in figure 2-9 The liquid film begins to form at the top of the plate and moves downward due to gravity. The thickness of the film δ increases in the flow direction x because of continued condensation at the liquid–vapor interface. Condensation releases heat in the amount of the latent heat of vaporization h_{fg} , which is transported through the film to the plate surface at temperature.

The velocity and temperature profiles of the condensate are also given in figure 2-10. In this case, velocity at the wall is zero because of non-slip and reaches a maximum where liquid and vapor meet. The temperature of the condensate is T_{sat} at the interface and decreases steadily to T_s at the wall. As was the case in forced convection involving a single phase, heat transfer in condensation also depends on whether the condensate flow is laminar or turbulent. Again the criterion for the flow regime is provided by the Reynolds number, which is defined as

$$Re = \frac{D_h \rho_l V_l}{\mu_l} = \frac{4A_c \rho_l V_l}{p \mu_l} = \frac{4 \rho_l V_l \delta}{\mu} = \frac{4 \dot{m}}{p \mu_l} \quad (2.46)$$

where D_h is hydraulic diameter of the condensate flow, m

p is wetted perimeter of condensate, m

A_c is cross-sectional area of the condensate flow at the lowest part of the flow, m²

ρ_l is density of the liquid, kg/m³

μ_l is viscosity of the liquid, kg/m·s

V_l is average velocity of the condensate at the lowest part of the flow, m/s

\dot{m} is mass flow rate of the condensate at the lowest part, kg/s

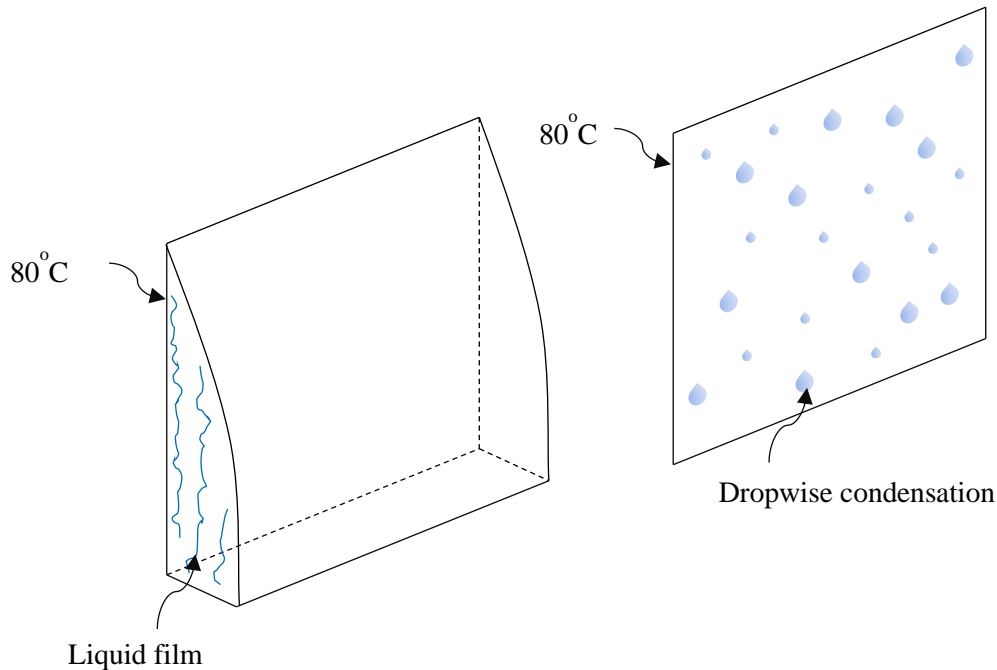


Figure 2-9 Two types of condensation (a) film condensation and (b) dropwise condensation
(Source: Yunus A. Cengel and Afshin J. Ghajar. Heat and mass transfer. McGraw-Hill, 2015)

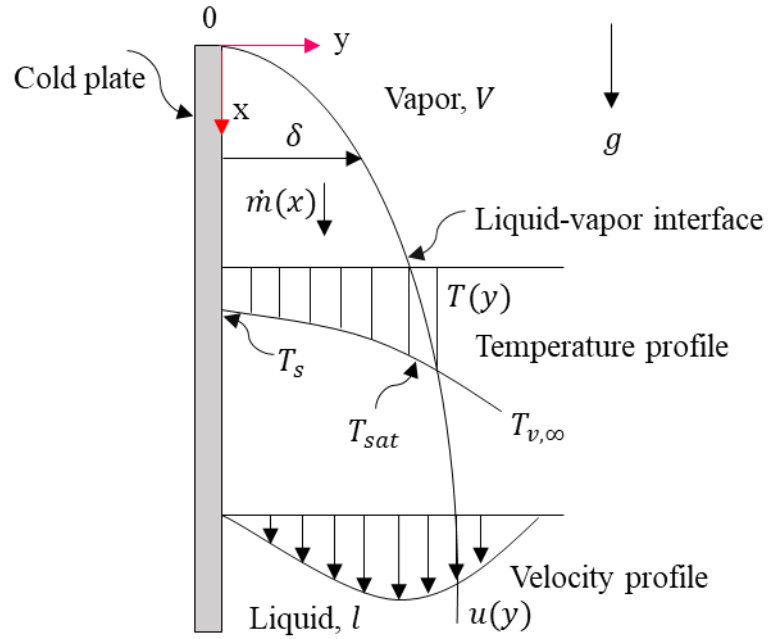


Figure 2-10 Laminar steady film condensation on vertical plate

(Source: Yunus A. Cengel and Afshin J. Ghajar. Heat and mass transfer. McGraw-Hill, 2015)

Note that the hydraulic diameter is specified once again such that it reduces to the normal diameter for flow in a circular tube.

The heat released as a unit mass of vapor condenses is known as the latent heat of vaporization h_{fg} , and it is typically used to represent heat transfer per unit mass of condensate formed during condensation. Nonetheless, the condensate in an actual condensation process is cooled to an average temperature between T_{sat} and T_s . Thus, the actual heat transfer will be larger. The h_{fg} can be replaced by the modified latent heat of vaporization h_{fg}^* , defined as

$$h_{fg}^* = h_{fg} + 0.68c_{pl}(T_{sat} - T_s) \quad (2.47)$$

where c_{pl} is the specific heat of liquid at the average film temperature.

With these considerations, the rate of heat transfer can be defined as

$$\dot{Q}_{cond} = hA_s(T_{sat} - T_s) = \dot{m}h_{fg}^* \quad (2.48)$$

where A_s is the heat transfer area. Solving for \dot{m} from the equation (2.48) and substituting it into equation (2.46) gives another relation for the Reynolds number,

$$Re = \frac{4\dot{Q}_{cond}}{\rho\mu_l h_{fg}^*} = \frac{4A_s h (T_{sat} - T_s)}{\rho\mu_l h_{fg}^*} \quad (2.49)$$

Horizontal tubes and spheres

The average heat transfer coefficient for film condensation on the outer surfaces of a horizontal tube is determined to be

$$h_{horiz} = 0.729 \left[\frac{g\rho_l(\rho_l - \rho_v)h_{fg}k_l^3}{\mu_l(T_{sat} - T_s)D} \right]^{1/4} \quad (2.50)$$

where D is the diameter of the horizontal tube. Equation (2.50) can be easily converted to a sphere by substituting the constant 0.729 with 0.815.

2.5.2 Dropwise condensation

Dropwise condensation occurs when small droplets formed at surface nucleation sites increase as a result of ongoing condensation, coalesce into large droplets, then slide down when they reach a particular size, clearing the surface and exposing it to vapor. There is no liquid coating to resist heat transfer in this case. As a result, dropwise condensation can obtain heat transfer coefficients that are more than ten times greater than those associated with film condensation. P. Griffith (1983) [13] recommends these simple correlations for dropwise condensation of steam on copper surfaces, That is

$$h_{dropwise} = 51,104 + 2044T_{sat}, \quad 22^\circ\text{C} < T_{sat} < 100^\circ\text{C} \quad (2.51)$$

$$h_{dropwise} = 255,510, \quad T_{sat} > 100^\circ\text{C} \quad (2.52)$$

where T_{sat} is in $^\circ\text{C}$ and the heat transfer coefficient $h_{dropwise}$ is in $\text{W}/\text{m}^2 \cdot \text{K}$.

Summary

A serpentine copper pipe heat exchanger is used to control microclimate in the greenhouse in this study. So, the increasing of its heat transfer enhancement is very important. Heat transfer enhancement is the practice of improving heat transfer coefficients, increasing surface area for heat transfer, or both. Surface roughness, turbulence promoters, and fins are example of practical heat transfer enhancements. Electrostatic fields, mechanical assistance, surface or fluid vibration, and other factors can greatly enhance heat transfer. These latter procedures, as opposed to surface treatments, are known as active enhancement techniques since they require external power. The enhancement of natural convection can be achieved by expanding the surface or surface roughness. Extended surfaces are surface extensions, like fins, where main purpose is to increase the surface area for heat transfer. Surface roughness can include any of several roughness elements that generally do not provide a substantial increase in surface area but, rather, increase the heat transfer coefficient by modifying fluid flow in the boundary layer.

References in chapter 2

- [1] Fitz-Rodríguez, E., Kubota, C., Giacomelli, G. A., Tignor, M. E., Wilson, S. B. & McMahon M. (2010). Dynamic modeling and simulation of greenhouse environments under several scenarios: a web-based application. *Computers and Electronics in Agriculture*, 70(1), 105–116.
- [2] Mie Prefectural Government, Mie Climate, Available at: <https://www.pref.mie.lg.jp/ENGLISH/> (accessed 10 May, 2021).

- [3] Lazaar, M., Bouadila, S., Kooli, S. & Farhat, A. (2015). Comparative study of conventional and solar heating systems under tunnel Tunisian greenhouses: Thermal performance and economic analysis. *Solar Energy*, 120, 620–635.
- [4] Ihoume, I., Tadili, R., Arbaoui, N., Bazgaou, A., Idrissi, A., Benchrifa, M. & Fatnassi, H. (2022). Performance study of a sustainable solar heating system based on a copper coil water to air heat exchanger for greenhouse heating. *Solar Energy*, 232, 128–138.
- [5] Papadakis, G., Briassoulis, D., Scarascia Mugnozza, G., Vox, G., Feuilloy, P. & Stoffers, J. A. (2000). Radiometric and thermal properties of, and testing methods for, greenhouse covering materials. *Journal of Agricultural Engineering Research*, 77(1), 7–38.
- [6] The Open University, Cutting ventilation losses, Available at: <https://www.open.edu/openlearn/nature-environment/energy-buildings/content-section-2.3> (accessed 10 August, 2021)
- [7] Takakura, T. (1982). Heating, Ventilating and Cooling Greenhouses. *Journal of Agricultural Meteorology*, 38(1), 65–70.
- [8] Abdel-Ghany, A.M., Al-Helal, I.M., Alzahrani, S.M., Alsadon, A.A., Ali, I.M. & Elleithy, R.M. (2012). Covering Materials Incorporating Radiation-Preventing Techniques to Meet Greenhouse Cooling Challenges in Arid Regions: A Review. *The Scientific World Journal*, 906360.
- [9] Stanghellini, C., Dai, J. & Kempkes, F. (2011). Effect of near-infrared-radiation reflective screen materials on ventilation requirement, crop transpiration and water use efficiency of a greenhouse rose crop. *Biosystems Engineering*, 110, 261–271.
- [10] Murakami, K., Fukuoka, N. & Noto, S. (2017). Improvement of greenhouse microenvironment and sweetness of melon (*Cucumis melo* L.) fruits by greenhouse shading with a new kind of near-infrared ray-cutting net in mid-summer. *Scientia Horticulturae*, 218, 1–7.
- [11] Yunus A. Cengel and Afshin J. Ghajar. (2015). Heat and mass transfer. McGraw-Hill.
- [12] Fraas, Arthur P. (1989). Heat exchangers design, 2nd ed. Hoboken, NJ: Wiley Interscience.
- [13] Griffith, P. (1983). “Dropwise Condensation.” In *Heat Exchanger Design Handbook*, ed. E. U. Schlunder, Vol 2, Ch. 2.6.5. New York: Hemisphere.

Chapter 3

Research methodology

3.1 Introduction of the overall experiment

In this chapter, the material and methods used in this study are presented. The experiment was divided into two experiments, including an experimental in a laboratory room and experimental greenhouse in practice. The methodological procedures of this study can be described as shown in figure. 3-1.

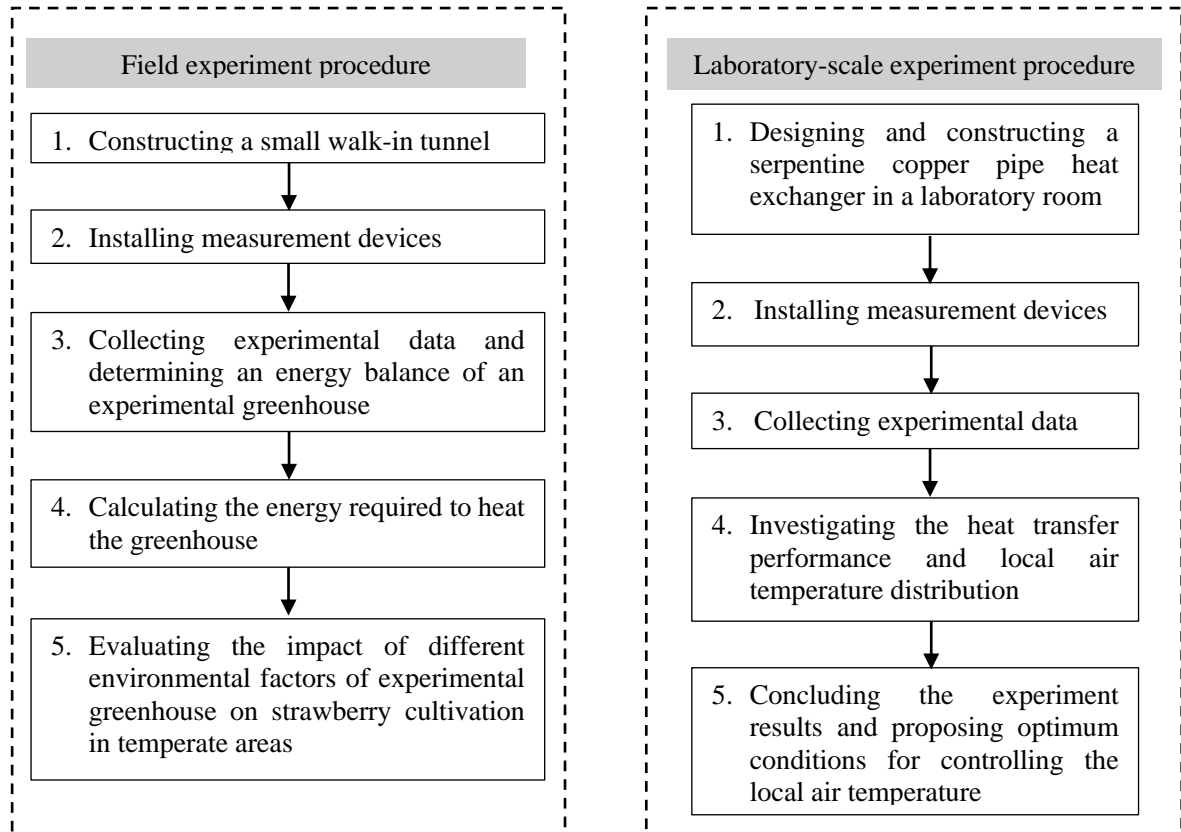


Figure 3-1 The methodological procedures

To achieve research objectives, experiments are carried out in greenhouse and in laboratory. The details of this study are described below as follows.

3.2 Experimental greenhouse

This section explains how to study and research an energy analysis of experimental greenhouse. Firstly, an experimental greenhouse was constructed and greenhouse description will be explained in details below. In this study, strawberry plants were grown in cultivation beds under the greenhouse. To research the effect of climatic conditions on the quality of strawberry, environmental factors such as temperature, relative humidity and solar radiation for strawberry cultivation were investigated. Thus, many measurement sensors were installed. Collected data were used as parameters to calculate the energy balance of this greenhouse and to see how it effected to

strawberry cultivation as well. The study of greenhouse energy balance leads to inspiration for energy reduction and environmental control in plantation area.

3.2.1 Greenhouse description

A small walk-in greenhouse was built in Mie prefecture, Japan (latitude 34°34' N, longitude 136°53' E). The greenhouse (11.0 m long × 5.2 m wide × 2.5 m high) was constructed with steel frames and was covered with a double vinyl sheet. The schematic of the greenhouse and sensor locations are depicted in figure 3-2. The greenhouse was located in a field without shading. The external and internal views, taken in October, 2020, are shown in figure 3-3 (a) and figure 3-3 (b), respectively.

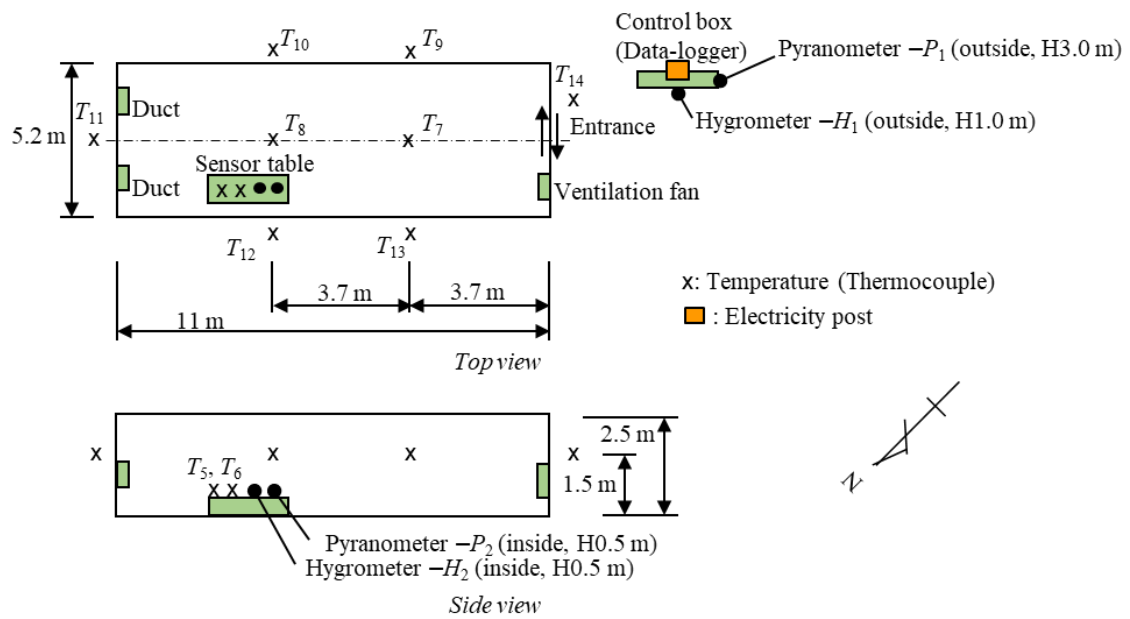


Figure 3-2 Greenhouse layout and measurement location

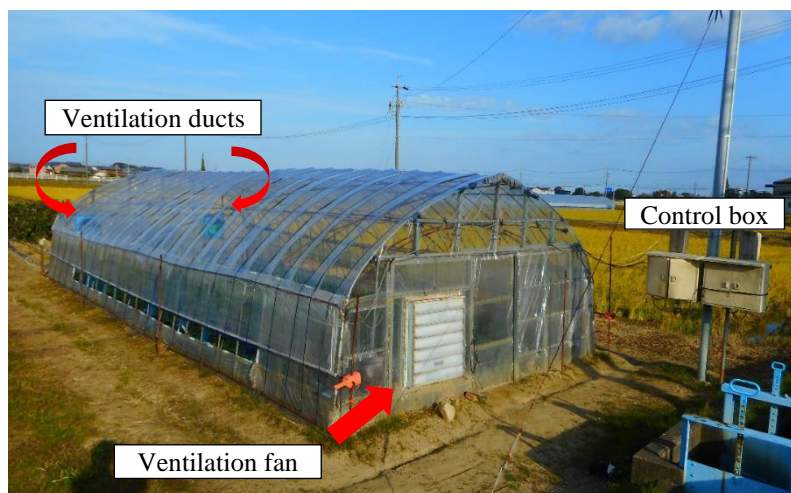


Figure 3-3 (a) The external view of experimental greenhouse



Figure 3-3 (b) The internal view of experimental greenhouse

3.2.2 Temperature control using ventilation fan

To maintain the optimum temperature for strawberry cultivation and reduce energy consumption in the small walk-in greenhouse during the winter season, an additional PVC sheet was introduced inside the greenhouse to reduce night-time heat dissipation from the ground to the outside, as shown in figure 3-4 (a). Due to this structure, supplemental heating was not required during cold weather conditions in this study. However, when the inside air temperature exceeded more than 25°C, wind ducts as well as a ventilation fan automatically opened and turned on, as shown in figure 3-4 (a) and figure 3-4 (b), respectively. The specifications of the ventilation fan are given in table 3-1. This fan is suitable for greenhouses up to 50 m long. Therefore, its capacity is large relative to the volume of the greenhouse used in this study.



Figure 3-4 (a) Wind duct and additional vinyl sheet



Figure 3-4 (b) Ventilation fan

Table 3-1 Specification of ventilation fan

Designation	Specification
Model	HF-80ETG-60 (Mitsubishi Electric Corp.)
Size	H 950 mm × V 900 mm
Blade diameter	800 mm
Motor	3 phase 200 V, 60 Hz, 0.4 kW
Air flow rate	290 m ³ /min

3.2.3 Greenhouse environmental monitoring

The air temperature, relative humidity, and solar radiation inside and outside the cultivation tunnel were measured at 1-min intervals during the cultivation period from November 2020 to April 2021. All of these sensors were connected and were recorded by a multi-channel data logger as shown in figure. 3-5. The placements of sensors are given in figure 3-2. There were four thermocouple sensors inside the tunnels: sensors T_5 and T_6 were all 0.5 m above the ground, while T_7 and T_8 were hung at 1.0 m from the ceiling to measure the mean inside air temperature. Furthermore, six sensors, T_9 to T_{14} , were located at a height of 1.5 m on the outside of the small walk-in tunnels to measure the mean outside temperature.

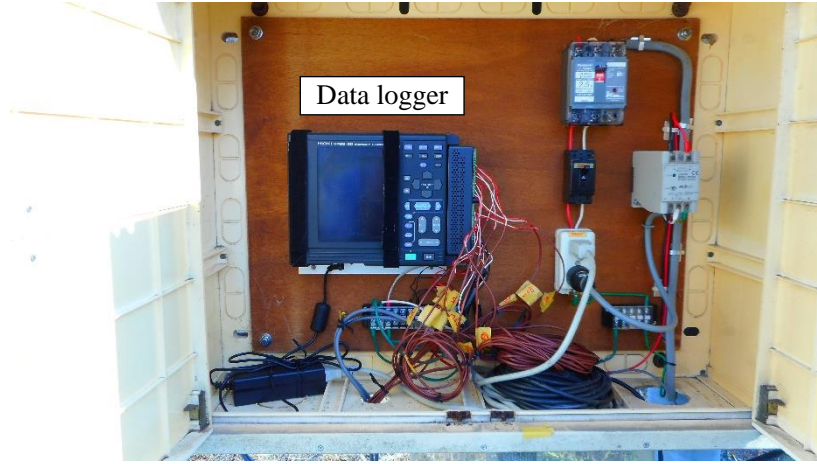


Figure 3-5 Data logger and electric circuit

The average inside temperature was obtained by averaging the values from four sensors (T_5-T_8). Meanwhile, the average outside temperature was calculated by averaging the values from sensors T_9-T_{14} , as shown in equation (3.1) and equation (3.2), respectively. During this study, daytime was defined as when the solar radiation was greater than 0 W/m^2 , while nighttime was defined as taking place when the solar radiation was equal to 0 W/m^2 .

$$T_{mean_in} = \frac{1}{m} \sum_{l=5}^8 T_l \quad (3.1)$$

$$T_{mean_out} = \frac{1}{s} \sum_{l=9}^{14} T_l \quad (3.2)$$

where T_{mean_in} is the average air temperature inside the greenhouse, °C

T_{mean_out} is the average air temperature outside the greenhouse, °C

T_l is the dataset of values inside the greenhouse

m is the number of thermocouple points inside the greenhouse

s is the number of thermocouple points outside the greenhouse.

The solar radiation in the horizontal plane outside and inside of the greenhouse was measured with a pyranometer at the positions P_1 and P_2 , respectively. Moreover, humidity sensors were placed at the positions H_1 and H_2 to measure the relative humidity outside and inside, respectively. Figure 3-6 shows the measurement of relative humidity and solar radiation inside the greenhouse. A pyranometer and humidity sensor outside the greenhouse was shown in figure 3-7 (a) and figure 3-7 (b), respectively.

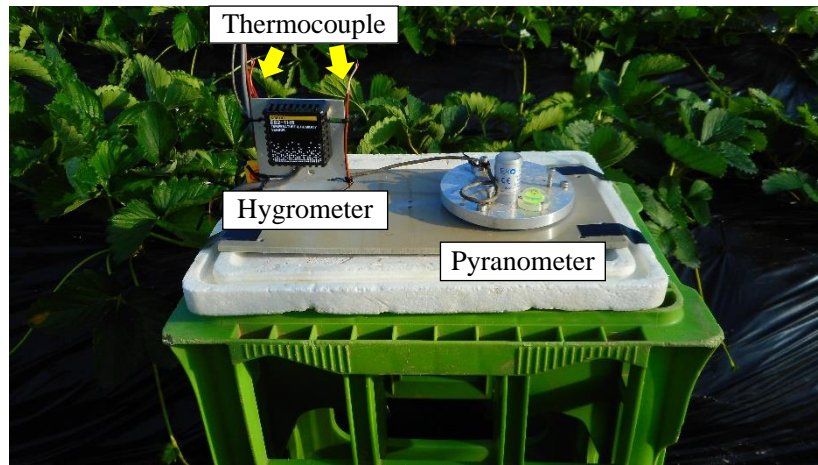


Figure 3-6 Measurement of relative humidity, solar radiation and air temperature inside the greenhouse



Figure 3-7 (a) Measurement of solar radiation outside the greenhouse

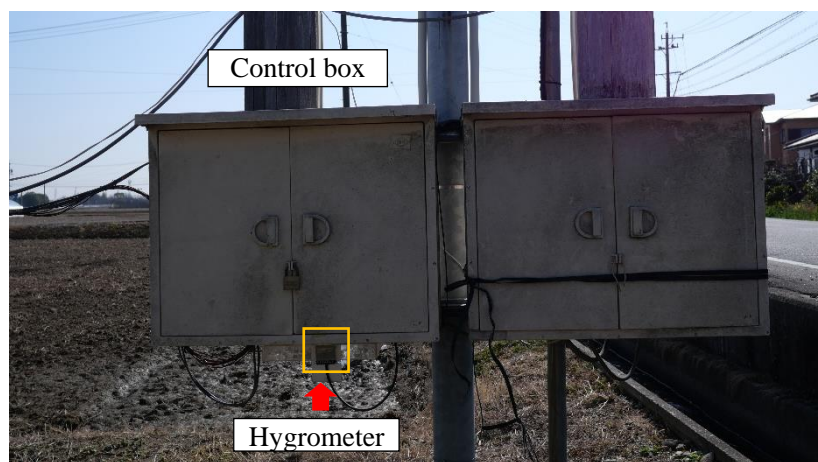


Figure 3-7 (b) Measurement of humidity outside the greenhouse

3.2.4 Greenhouse strawberry cultivation and measurement

In 1967, a new variety, known as “Harunoka”, was promoted across Japan because it had very low temperature requirement. Therefore, this variety has gained wide acceptance in cold areas [1]. Moreover, this variety can be harvested right from December to June. Therefore, owing to the popularity of Harunoka strawberries, we selected it for this study.

Strawberry plants were grown in cultivation beds in the designed tunnel from mid September 2020. There were five beds in the greenhouse, as shown in figure 3-3 (b). The three beds in the center were 11 m long, 0.95 m wide, and 0.25 m high at the center, while the other beds were 11 m long, 0.68 m wide, and 0.25 m high at the center. All of the beds were covered with a single black plastic sheet to prevent weeds as well as heat dissipation and water evaporation. The distances between the bed centers were 1.2 m for the central beds and 1.0 m for the side beds, respectively. Drip irrigation was used for all beds because it helps in maintaining humidity at a desired level to prevent fungal diseases. Furthermore, it prevents excess or deficit water supply, which is critical to the sensitive strawberry plants [2]. Depending on the weather, the frequency of irrigation can vary significantly. In this study, drip irrigation was supplied twice a week during planting in winter.

Soluble sugar contents (*SSC*) is the collection concentration of sugars, acids and other substances dissolved in the cell sap. The main soluble sugar components in strawberries are glucose and fructose, which comprise over 80%–90% of the total sugar and 40% of the total dry weight [3]. Generally, the *SSC* of strawberries can vary from 4% to 11%, depending on cultivar and environment [4]. It has been found that temperature can affect to *SSC* [5]. Growing temperatures above 25°C can reduce fruit set and decrease fruit *SSC*.

The fruit weight, width, length and *SSC* of strawberries were measured at room temperatures as a reference. “Harunoka” strawberries were selected as the sample to obtain juice for *SSC* measurements. *SSC* was measured with a digital saccharimeter (see figure 3-8 (a)). The strawberry juice sample, of approximately 0.3 mL, was dropped onto the prism of the digital saccharimeter. Each sample was repeatedly tested 3 times. A digital scale was used for strawberry weight measurement, with 0.1 g precision measurement (see figure 3-8(b)). Moreover, strawberry fruit size (width and length) was measured in mm with perpendicular-angle rulers, as shown in figure 3-8 (c). In this work, there were a lot of strawberries in the greenhouse. Additionally, there were many different shapes and sizes. So, the exact size of each sample was not necessary to obtain. In order to display the typical shape and size only, perpendicular-angle rulers were used to compare them.

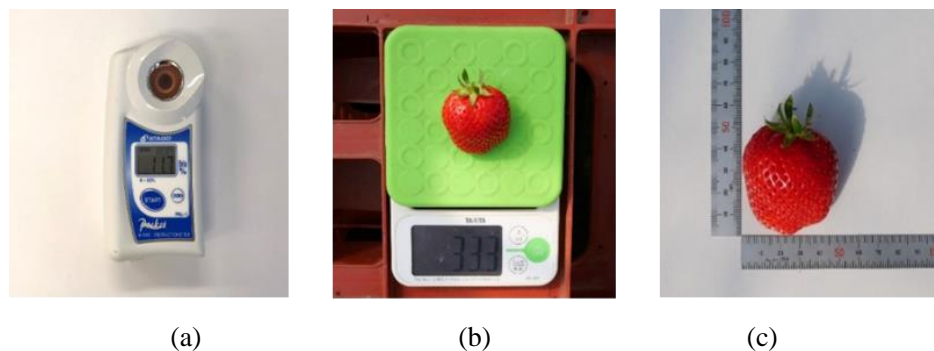


Figure 3-8 Example of strawberry: (a) saccharimeter; (b) strawberry weight; (c) shape

3.2.5 Measurement sensor and equipment

To measure the environmental factors around plantation area, many measurement sensors were used. The specification and accuracy of the measurement sensors are shown in table 3-2. The details of the measuring devices will be described below.

Table 3-2 Specifications of sensors and accuracy

Parameter	Instrument name	Model/Type	Measurement range	Accuracy
Temperature	Thermocouple	T-type	-250 to 350°C	$\pm 1^\circ\text{C}$ or $\pm 0.75\%$ (f.s.) (Standard accuracy)
Relative humidity	Humidity sensor	ES2-THB	20 to 95%	$\pm 3\%$
Solar radiation	Pyranometer	ML-01	0 to 1000 W/m ²	$\pm 1.70\%$
Soluble sugar contents	Digital refractometer	PAL-1	0 to 53%	$\pm 0.2\%$ Brix

Thermocouple

T-type thermocouples were used to measure the temperature of air in this experiment. It is very stable thermocouple and is used in extremely low temperature. It consists of copper wire for positive leg and a constantan (55% Copper and 45% Nickel) alloy wire for the negative leg, joined together at one end. A voltage is produced that is linked to the temperature when the junction of the two metals is heated or cooled. The measurement range is between -250 to 350°C. Figure 3-9 shows the picture of T-type thermocouple.

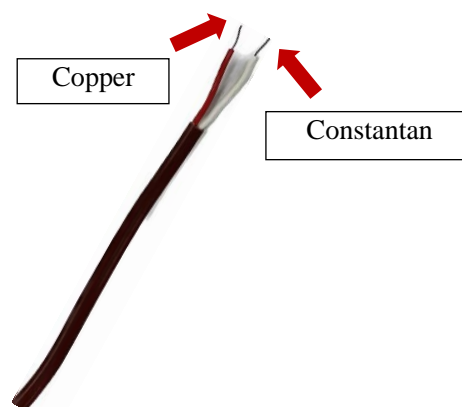


Figure 3-9 T-type thermocouple

Hygrometer

For measurement the relative humidity both inside and outside the greenhouse, Omron humidity sensors (ES2-THB model) were used. They can detect humidity within an accuracy of $\pm 3\%$. The photo of hygrometer is shown in figure 3-10 and the specifications of the hygrometer are shown in table 3-3.



Figure 3-10 Humidity sensor

Table 3-3 Specifications of hygrometer

Description	Specification
Humidity detection range	20 to 95%
Humidity detection accuracy	$\pm 3\%$ (25 °C, 40 to 80%)
Power supply voltage	24 VDC
Operating voltage range	85% to 110% of power supply voltage
Current consumption	10 mA max.
Humidity output	1 to 5 V (for humidity of 0% to 100%) Permissible load impedance: 100 k Ω min.
Operating temperature and humidity range	0 to 55°C, humidity of 95% max.
Storage temperature and humidity range	-20 to 60°C, humidity of 95% max.
Weight	Approximately 43 g

Pyranometer

To measure solar radiation both inside and outside the greenhouse, ML-01 silicon pyranometers were used. This model is made for high-quality irradiance measurements. Fast response, light, tough and easy to install. The sensor can be installed in the horizontal position for global horizontal measurement applications with a standard removable mounting plate levelling feet. The photo of pyranometer is shown in figure 3-11 and the specifications of the pyranometer are shown in table 3-4.



Figure 3-11 Pyranometer

Table 3-4 Specifications of pyranometer

Description	Specification
Measurement range	0 ~ 200 W/m ²
Spectral range	400 ~ 1,000 nm
Response time	< 1ms
Sensitivity	49.3 $\mu\text{V}/\text{W}\cdot\text{m}^{-2}$ (Pyranometer placed inside the greenhouse)
	41.5 $\mu\text{V}/\text{W}\cdot\text{m}^{-2}$ (Pyranometer placed outside the greenhouse)
Output	0 ~ 100 mV
Internal resistance	48 Ω
Operating temperature	-30 ~ 70°C
Weight	30 g

Digital refractometer

Soluble sugar contents (SSC) is one of common parameters for defining fruit quality of greenhouse strawberry. A widely used measurement to evaluate sugar content is Brix (unit is %). In this study, digital refractometer was used to measure brix. It has a compact and durable unit offering easy and accurate Brix readings. The photo of digital refractometer is shown in figure 3-12 and the specifications of the digital refractometer are shown in table 3-5.



Figure 3-12 Refractometer PAL-1

Table 3-5 Specifications of refractometer

Description	Specification
Measurement range	Brix 0 to 53%
Resolution	Brix 0.1%
Accuracy	±0.2%
Sample volume	2 to 3 drops
Measurement time	About 3 seconds
Dimensions and weight	5.5× 3.1× 10.9 cm 100g

Datalogger

In this study, Hioki model 8422-50 is electronic devices which automatically monitor and record multiple channels over time. It has 32-channels isolated, so there is no need to be concerned about potential differences among measurement objects. This data logger can record in real time to a large memory card. The photo of data logger is shown in figure 3-13 and the specifications of the data logger are shown in table 3-6.



Figure 3-13 Hioki 8422-50 data logger

Table 3-6 Specifications of data logger

Measurement Items	Temperature, voltage, cumulative pulses, rotations
Input Channels	Analog 32 channels isolated PHOTO-MOS relays Pulse Inputs: 4 channels Logic Inputs: 16 channels (using the 8993 DIGITAL I/O UNIT)
Thermocouple Types	K, E, J, T, N, W (WRe5-26), R, S, and B
Analog Voltage Input	4 ranges: 100 mV, 1 V, 10 V, 100 V and 1-5 V f.s.
Recording Interval	100 ms to 1 hour (200 ms to 1 hour when using more than 17 channels). Note: All input channels are scanned at high speed during each recording interval.
Memory Capacity	Internal: 32 MB (16MW data points) External: up to 528 MB (Flash ATA Card)

3.3 Laboratory-scale experiment

This study will focus on a microclimate weather management system for a greenhouse. This aims to create an appropriate microclimate just around each plant, despite the fact that the surrounding space inside the greenhouse may have different weather conditions. Thus, in this study, controlling local air temperatures around a plantation area was experimentally investigated. In addition, a serpentine copper pipe heat exchanger for cooling was introduced. The details of experiment will be explained in details as follows.

3.3.1 Experimental set-up

The objective of this experiment was to control microclimate environmental conditions around plantation area. To achieve this objective, an experimental model was designed and built as a serpentine copper pipe heat exchanger for cooling. Heat exchangers are often used in practice for a variety of purposes, such as chemical processes, engineering processes, power plants, and air conditioning. In a heat exchanger, heat transfer typically occurs through conduction through the wall separating the two fluids and convection in each fluid. There are no external thermal energy and work interactions [6]. Among the various types of heat exchangers, serpentine heat exchangers are the most compact and are minimal in terms of the volume of the microchannel coils, without manifolds in their design. This arrangement allows for serpentine coils that are suitable for compact, lightweight cooling applications. Serpentine tubes can be used in laminar flow heat exchange systems, since straight tube heat exchangers allow limited mixing in the laminar flow regime [7]. In addition, a serpentine heat exchanger does not block light in plant photosynthesis, unlike a fin and tube heat exchanger, which is important in cultivation. Thus, a serpentine copper pipe heat exchanger was introduced and studied to control local environmental factors around plantation area.

A copper pipe with an outer diameter of 12.7 mm and a thickness of 0.8 mm was used. A serpentine copper pipe heat exchanger was constructed in a laboratory-scale room under air-conditioned, and the length and width were 870 mm and 330 mm, respectively, as shown in figure 3-14 (a). Table 3-7 shows specifications of the serpentine copper pipe heat exchanger. The length was estimated based on the length of the straight regions and did not include

the bend regions. The serpentine copper pipe was placed horizontally on a stand inside an experiment room, as shown in figure 3-14 (b).

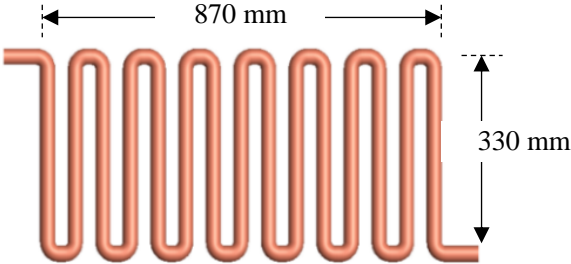


Figure 3-14 (a) Schematic diagram of a serpentine copper pipe heat exchanger



Figure 3-14 (b) Showing a serpentine copper pipe heat exchanger place on the stand (Top view)

Table 3-7 Specifications of the serpentine copper pipe

Details	Size (mm)
Outer diameter	12.7
Thickness	0.8
Total length	870
Total width	330
Distance between copper pipes	50

A water-cooled chiller was used to generate cold water and to circulate cold water to a serpentine copper pipe heat exchanger. The supply water temperature and volume flow were controlled during the experiments by adjusting the chiller and globe valve, respectively. Figure 3-14 (c) shows the water loop control.

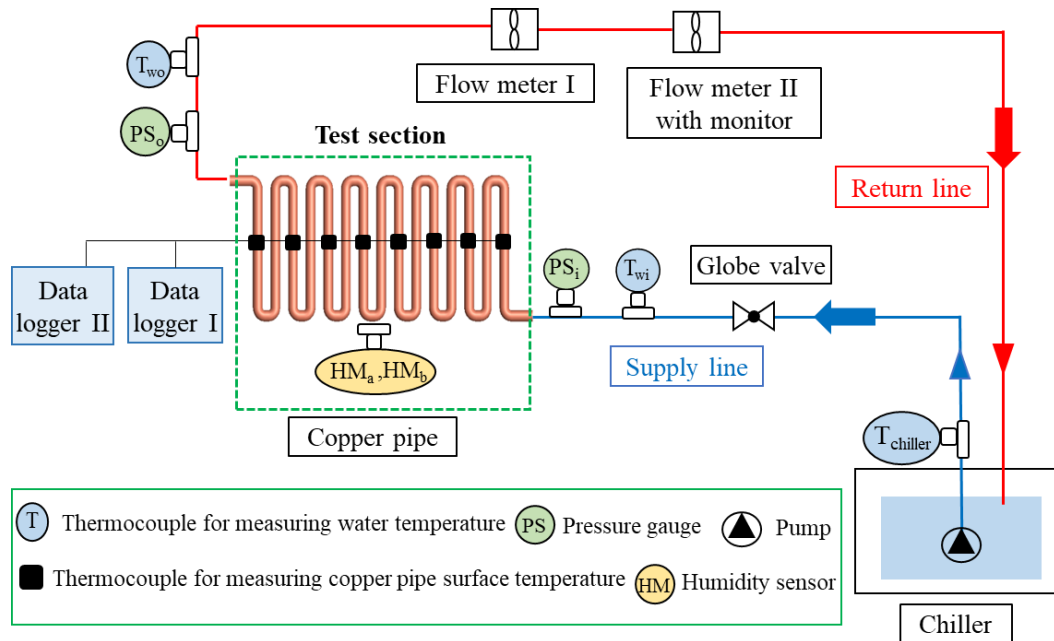


Figure 3-14 (c) System configuration

3.3.2 Environmental factors monitoring

In this experiment, there were several environmental factors to be measured, including air temperature, water temperature, volume water flow rate, relative humidity and water pressure. The measurements for each variable are described below in the following.

Temperature measurement

To control local air temperatures and investigate thermal performance around a serpentine copper pipe heat exchanger, air temperature, copper pipe surface temperature and circulating water temperature were measured as calculating parameters. The measurement of temperature in this experiment were divided into three variables: 1) air temperature, 2) surface temperature and 3) water temperature.

Air temperatures were measured both above and below the serpentine copper pipe at different vertical positions using T-type thermocouple. There are two vertical different positions above the pipe and three verticals different positions below a pipe. In each vertical position used six thermocouples. Thus, there were totally thirty sensors around a serpentine copper pipe heat exchanger. The air temperatures above the pipe were defined at -50 and -100 mm. The air temperatures below the pipe were defined at 50, 100, and 150 mm, respectively. Figure 3-15 (a) indicates air temperature measurement layout. Several thermocouples were used to measure the air around the serpentine copper pipe, as shown in figure. 3-15 (b).

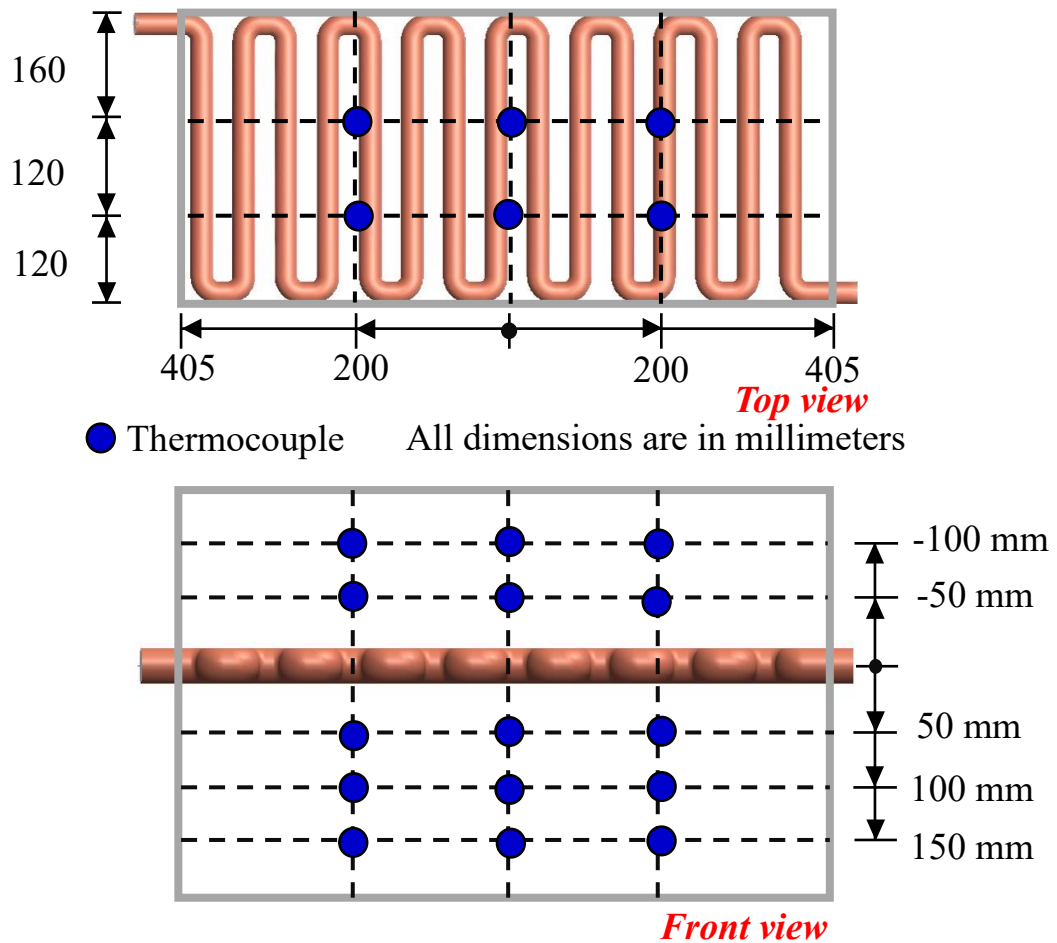
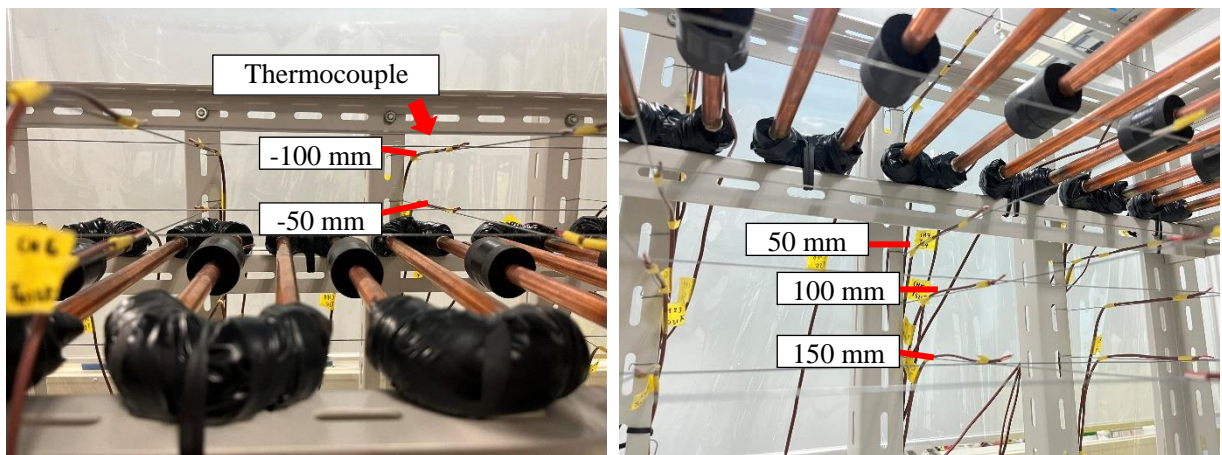


Figure 3-15 (a) Air temperature measurement layout



(i) Measurement above the pipe

(ii) Measurement below the pipe

Figure 3-15 (b) Measurement of air temperatures around the pipe

Surface temperatures of the copper pipe were measured using T-type thermocouple. To reduce heat movements and vapor condensation, thermal insulation cell tubes were used to cover the thermocouple. The length of the

insulating tube wrapped in thermocouple is 4 cm. There were eight sensors used in this experiment. Measurement of surface temperature layout and actual measurement photo are shown in figure 3-16 (a) and figure 3-16 (b), respectively.

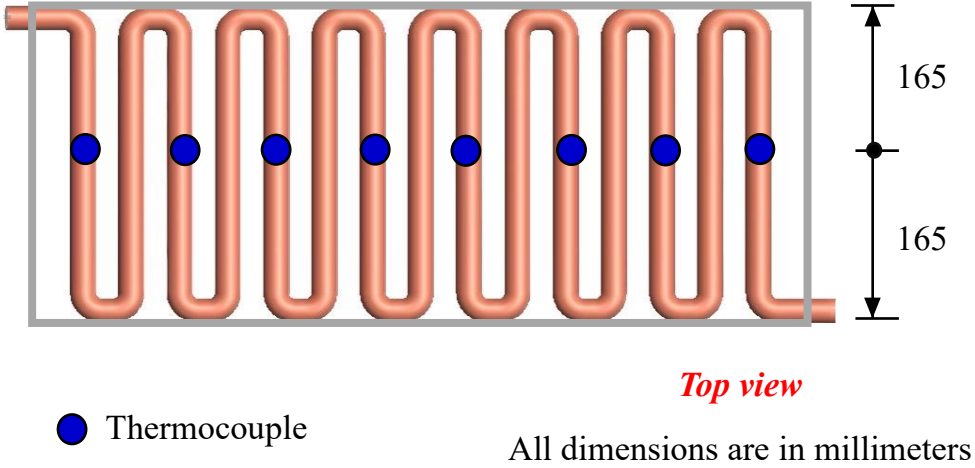


Figure 3-16 (a) Surface temperature measurement layout

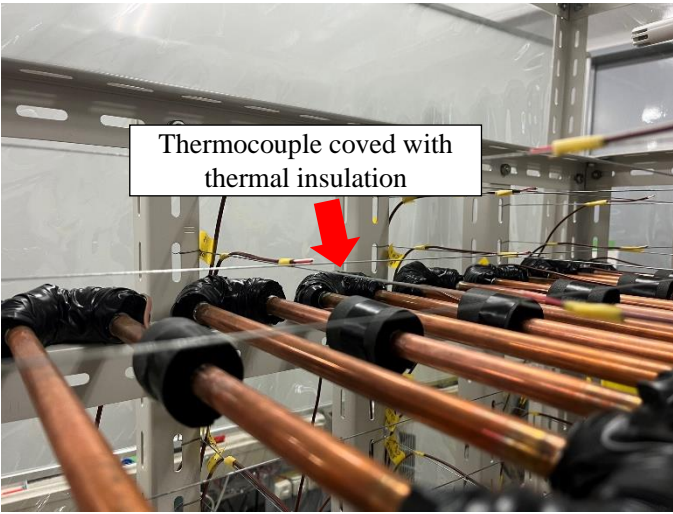


Figure 3-16 (b) Measurement of copper pipe surface temperature

To obtain accurate data, Styrofoam sheets (thermal insulation) were attached around the test section like a box, as shown in figure 3-17 (a). The main purpose was to reduce heat transfer between objects in thermal contact or in the range of radiative influence. Heat flow is an inevitable part of contact objects with differing temperatures. Heat insulation indicates an insulating area in which thermal conduction is reduced or thermal radiation is reflected rather than absorbed by the lower-temperature substance. In this study, the thermal conductivity of the Styrofoam is 0.036 W/m·K and the thickness is 30 mm.

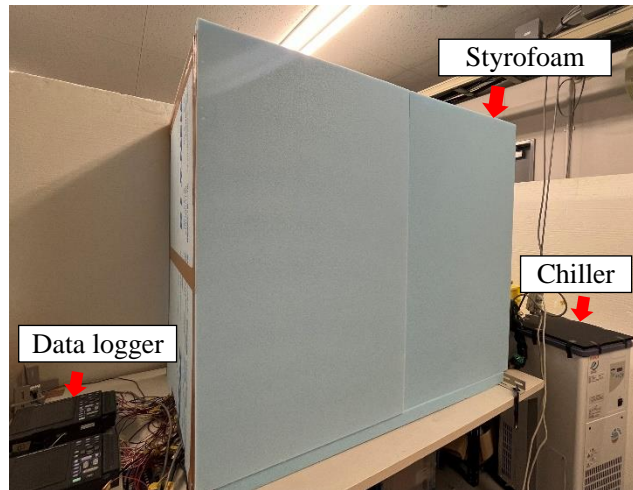


Figure 3-17 (a) Installation picture of Styrofoam sheet (completely closed)

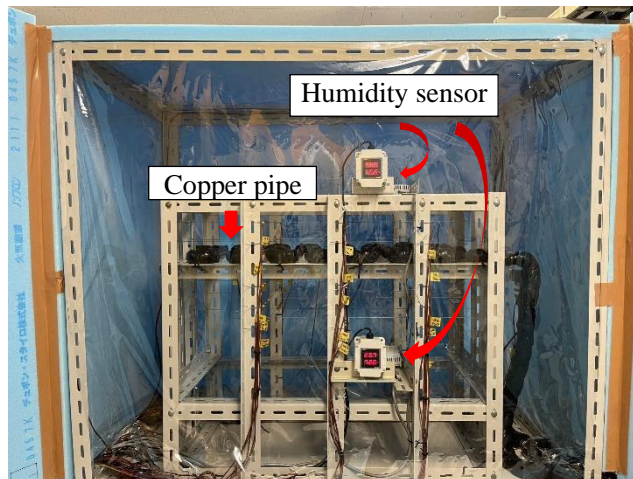


Figure 3-17 (b) Installation picture of Styrofoam sheet (open windows)

The room air temperature was controlled by air-conditioner at specific temperature point. Room air temperatures were also measured by T-type thermocouple. There were two sensors (T_{room1} and T_{room2}) placed on the table near the test section box at a distance of 50 and 15 cm, respectively. The photo of installation is shown in figure 3-18.

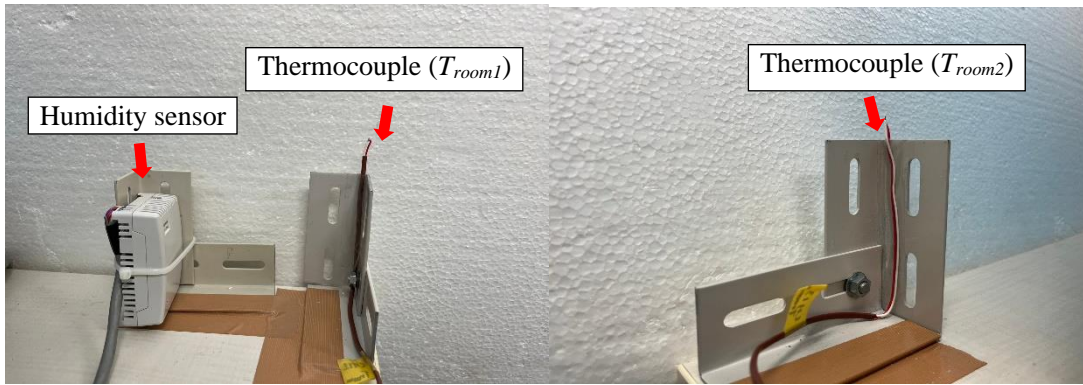


Figure 3-18 Room temperature measurement

Air-cooled chiller was used to generate cold water and to circulate cold water to a serpentine copper pipe heat exchanger. The inlet (T_{wi}) and outlet (T_{wo}) water temperatures were measured using thermocouple to calculate heat flux through a serpentine copper pipe heat exchanger. The measurement installation is shown in figure 3-19.

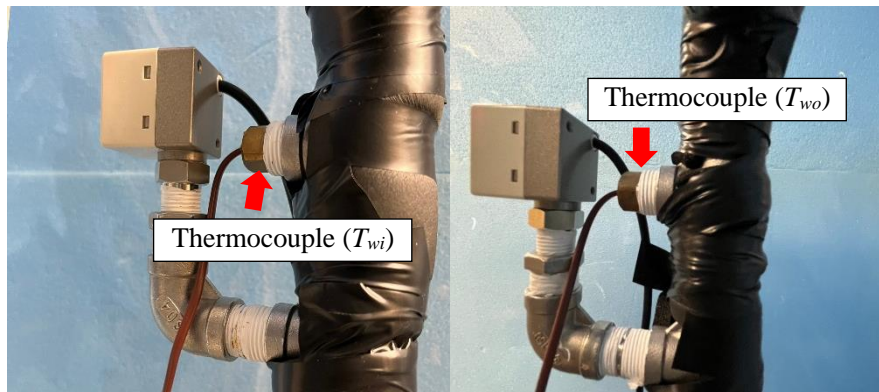


Figure 3-19 Measurement of inlet and outlet water temperature

Volume water flow rate measurement

Volume flow rate of this system was measured by two different flow meters including flow meter with and without monitor, as shown in figure 3-20 (a) and figure 3-20 (b). Volume flow rate was regulated by manually adjusting the globe valve, as shown in figure 3-21.

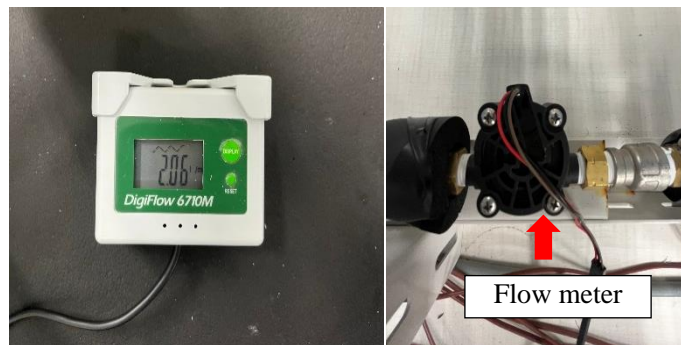


Figure 3-20 (a) Flow meter with monitor

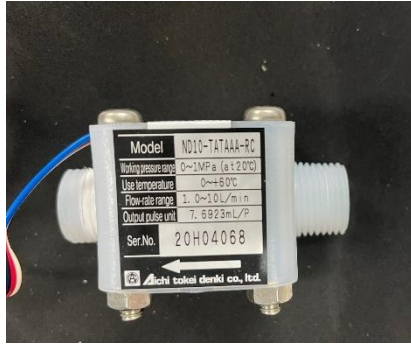


Figure 3-20 (b) Flow meter without monitor



Figure 3-21 Glove valve

Relative humidity measurement

The experiments were conducted in laboratory room with air conditioners. However, relative humidity is an inevitable part and leads to vapor condensation around a copper pipe. Thus, four humidity sensors were installed around a pipe. Two sensors were mounted above the pipe at a distance of 20 cm (sensor with monitor) and 18 cm (sensor without monitor), respectively, as shown in figure 3-22 (a). While, two sensors were mounted below a pipe at a distance of 29 cm (sensor with monitor) and 27 cm (sensor without monitor), respectively, as shown in figure 3-22 (b). For measuring room humidity, another one was placed on the table near a test section box at a distance of 50 cm (see figure 3-18).

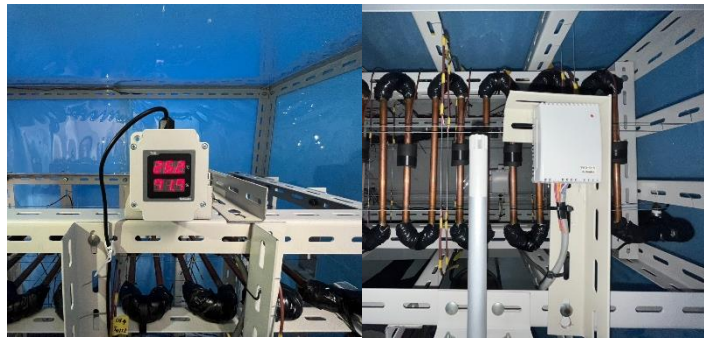


Figure 3-22 (a) Humidity sensor placed above a pipe (with and without monitor)



Figure 3-22 (b) Humidity sensor placed below a pipe (with and without monitor)

Water pressure measurement

To obtain the pressure drop through a pipe, water pressure at inlet and outlet lines were measured by the pressure gauge with monitor, as shown in figure 3-23.



Figure 3-23 Pressure gauge

3.3.3 Equipment and sensor specification

To measure the environmental factors around a serpentine heat exchanger, many measurement sensors were used. The specification and accuracy of the measurement sensors are shown in table 3-8. The details of thermocouple are explained in previous section and other details of the measuring devices will be described below.

Table 3-8 Instruments and sensors

Name of instruments	Model	Measuring range	Accuracy
Thermocouple	Type T	-250 to 350°C	$\pm 1^{\circ}\text{C}$ or ± 0.75 (full-scale)
Humidity sensor	THD-DD2-V	0 to 99.9%	$\pm 2\%$ RH at room temperature
	THD-R-V		$\pm 3\%$ RH at room temperature
Pressure gauge	GC31	-0.1 to 2 MPa	$\pm 1.0\%$ (fs) at 23°C
Flow sensor	ND10-TATAAA-RC	0.8 to 20 L/min	$\pm 2\%$ (rs) at standard installation position
	FS-4400H (Digital output)	1.5 to 25 L/min	$\pm 10\%$

Humidity sensor

Relative humidity both above and below the pipe are measured with two different models, Autonics THD-R-V (without monitor) and Autonics THD-DD2-V (with monitor). The photo of humidity sensors is shown in figure 3-24 and the specifications of the humidity sensor are shown in table 3-9.

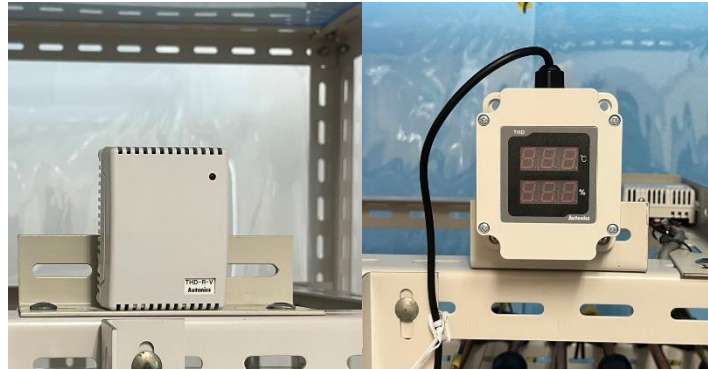


Figure 3-24 Photo of THD-R-V (left) and THD-DD2-V (right) humidity sensors

Table 3-9 Specifications of humidity sensor

Model	THD-R-V	THD-DD2-V
Power supply	24 VDC	
Power consumption	Maximum 2.4 Watts	
Display type	Non-display	7 Segment LED display
Measuring range	0.0 to 99.9%	
Accuracy	$\pm 3\%$ RH at room temperature	$\pm 2\%$ RH at room temperature
Output	1-5 VDC	
Resolution	1/1000	
Environment	-20 to 60°C	
Weight	55 g	160 g

Pressure gauge

Small digital pressure gauge is instrument designed to measure the pressure of water in a system. GC31 digital pressure gauges are used in this experiment due to compact enclosure with LED indication. The photo of pressure gauge is shown in figure 3-25 and the specifications of the pressure gauge are shown in table 3-10.



Figure 3-25 Photo of digital pressure gauge

Table 3-10 Specifications of digital pressure gauge

Item	Description
Pressure range	-0.1 to 2 MPa
Accuracy	$\pm 1.0\%$ (fs) at 23°C
Display	3 ½ digit, 10 mm LED
Units	MPa, kPa
Analog output	Voltage output 1 to 5V DC
Operating temperature	-10 to 50°C
Operating humidity	35 to 85% RH
Weight	100 g

Flow sensor

Cold water will be transferred through the system and water volume flow rate is one of the most important parameters for calculating the heat transfer. As mentioned in previous section, water volume flow rate is controlled by the globe valve and the change of volume flow rate will be monitored by two flow sensors. ND10-TATAAA-RC flow sensor without monitor and FS-44000H flow sensor with monitor are used. Photos of flow sensor are shown in figure 3-20 (a) and figure 3-20 (b) as well as the specifications of flow sensor is shown in table 3-11.

Table 3-11 Specifications of flow sensor

Model	ND10-TATAAA-RC	FS-44000H
Flow rate range	1.0 to 10 L/min	0.8 to 8 L/min
Accuracy	$\pm 2\%$ in the standard installation position	$\pm 10\%$ (fs)
Range of liquid viscosity	0.5 to 2.5 mPa·s (water equivalent)	N/A
Fluid temperature range	-10 to 70°C	0 to 40°C
Output	Pulse constant 7.69 mL/P	Digital display
Weight	120 g	140 g

Chiller

One of important equipment used in this experiment is a chiller. Eyela CA-1116A is used for cooling water circulation device. This chiller can set wide temperature range from -20 to 30°C that is suitable for this study. The photo of chiller is shown in figure 3-26 and the specifications of the chiller are shown in table 3-12.



Figure 3-26 Photo of air-cooled chiller

(Source: <https://eyela-chiller.jp/products/list/ca1116a/>)

Table 3-12 Specifications of chiller

Product Name		Low temperature circulator (Cool Ace)	
Model		CA-1116A	
Circulation method		Circulation for sealed system	
Temperature setting range		-20 to 30°C	
Temperature control accuracy		±2°C	
Cooling capacity	Liquid temperature	Room temperature 20°C	Room temperature 35°C
	at 10°C	1050 W	700W
	at 0°C	800 W	430W
	at -10°C	600 W	200W
Maximum lifting height		9.5/ 13 m (50/60Hz)	
Maximum flow volume		12/ 14 L/min (50/60Hz)	
Temperature setting and display		Sheet key digital setting, LED digital setting	
Refrigerator and coolant		Air cooling, R407C	
Dimension (mm) and weight		340 W × 384D × 851 H, 43 kg	
Power source		4.3 A 950 VA	

3.3.4 Experimental conditions

Experimental conditions were based on the consideration with chiller specification. In this study, the target inlet water temperature ($T_{inlet,t}$) was varied from -6 to 4°C. Thus, the chiller water temperature ($T_{chiller}$) was set from -6 to 4°C. The volume flow rate (\dot{V}) varied from 0.8 to 3.0 L/min, respectively. However, in practice, inlet water temperature (T_{inlet}) was relatively greater than target water temperature. A copper pipe with an inner diameter (D_i) of 11.1 mm was used and internal cross-sectional area (A_i) at 0.000097 m². The serpentine copper pipe heat exchanger was placed on a stand inside the experimental room, and the room air temperature (T_{room}) was set at 25°C. The mixture of ethylene glycol (40%) and water (60%) was used as working fluid. The test conditions and thermal properties of fluid are shown in table 3-13.

Table 3-13 Test cases

Case	Target inlet water temperature ($T_{inlet,t}$), °C	Chiller set-point temperature ($T_{chiller}$), °C	Inlet water temperature (T_{inlet}), °C	Volume flow rate (\dot{V}), L/min	Flow velocity (ϑ), m/s	Density (ρ), kg/m ³	Dynamic viscosity (μ), (N·s)/m ²	Reynolds number (Re)
1	4	4	6.2	0.8	0.14	1069	4.6×10^{-3}	355
2			5.8	1.0	0.18	1069	4.6×10^{-3}	453
3			5.1	1.5	0.26	1069	4.7×10^{-3}	652
4			4.9	2.0	0.34	1069	4.7×10^{-3}	861
5			4.8	2.5	0.43	1069	4.8×10^{-3}	1073
6			4.6	3.0	0.52	1069	4.8×10^{-3}	1277
7	2	2	3.9	0.8	0.14	1070	5.0×10^{-3}	327
8			3.7	1.0	0.18	1070	5.1×10^{-3}	409
9			3.2	1.5	0.26	1071	5.4×10^{-3}	569
10			3.0	2.0	0.34	1071	5.4×10^{-3}	751
11			2.9	2.5	0.43	1071	5.5×10^{-3}	938
12			2.7	3.0	0.52	1071	5.6×10^{-3}	1097
13	0	0	2.4	0.8	0.14	1071	5.7×10^{-3}	287
14			2.0	1.0	0.18	1071	5.9×10^{-3}	354
15			1.2	1.5	0.26	1071	6.3×10^{-3}	487
16			1.0	2.0	0.34	1072	6.4×10^{-3}	634
17			0.9	2.5	0.43	1072	6.4×10^{-3}	807
18			0.7	3.0	0.52	1072	6.5×10^{-3}	946

Table 3-13 Test cases (continue)

Case	Target inlet water temperature ($T_{inlet,t}$), °C	Chiller set-point temperature ($T_{chiller}$), °C	Inlet water temperature (T_{inlet}), °C	Volume flow rate (\dot{V}), L/min	Flow velocity (ϑ), m/s	Density (ρ), kg/m ³	Dynamic viscosity (μ), (N·s)/m ²	Reynolds number (Re)
19	-2	-2	0.8	0.8	0.14	1072	6.5×10^{-3}	252
20			0.0	1.0	0.18	1072	6.8×10^{-3}	307
21			-0.6	1.5	0.26	1072	7.1×10^{-3}	433
22			-0.8	2.0	0.34	1072	7.2×10^{-3}	563
23			-1.1	2.5	0.43	1072	7.3×10^{-3}	707
24			-1.2	3.0	0.52	1072	7.4×10^{-3}	831
25	-4°C	-4°C	-1.7	0.8	0.14	1072	7.6×10^{-3}	216
26			-1.9	1.0	0.18	1073	7.7×10^{-3}	272
27			-2.4	1.5	0.26	1073	7.9×10^{-3}	389
28			-2.7	2.0	0.34	1073	8.1×10^{-3}	501
29			-3.1	2.5	0.43	1073	8.2×10^{-3}	630
30			-3.1	3.0	0.52	1073	8.2×10^{-3}	750
31	-6°C	-6°C	-3.0	0.8	0.14	1073	8.2×10^{-3}	200
32			-3.7	1.0	0.18	1073	8.5×10^{-3}	243
33			-4.2	1.5	0.26	1073	8.6×10^{-3}	358
34			-4.7	2.0	0.34	1073	9.0×10^{-3}	451
35			-4.9	2.5	0.43	1073	9.0×10^{-3}	574
36			-5.0	3.0	0.52	1076	9.1×10^{-3}	678

Here, the Reynolds number is defined by equation (3.3):

$$Re = \frac{\rho \vartheta D_i}{\mu} \quad (3.3)$$

where ρ is the density of the working fluid (kg/m³), ϑ is the fluid velocity (m/s), D_i is the inner diameter of the pipe (m), and μ is the fluid dynamic viscosity ((N·s)/m²).

3.3.5 Experimental procedure

Due to this study focused on a microclimate environmental conditions around plantation area, in order to observe the changes in the temperature of environment around local area. The effect of surrounding environment is very important to this cooling system. Therefore, air-conditioner was used to control room air temperature and air temperature was set at 25°C.

First of all, the air-conditioner was turned on one day before starting the experiment. Then, chiller water temperature ($T_{chiller}$) was set at target water temperature ($T_{inlet,t}$) following experimental conditions. By using the globe valve, water volume flow rate (\dot{V}) will be changed and will be transferred to the test section. After chiller

water temperature reached target water temperature, the experimental data were recorded for an hour at 10-second intervals. After an hour, pictures of the condensation (or water droplets) surrounding a serpentine copper pipe heat exchanger were taken. Finally, the experimental data can be obtained.

References in chapter 3

- [1] Honda, F & Morishita, M. (1977). Commercial Varieties and Differentiation of Cropping Types of Strawberry (*Fragaria x ananassa* (Duch.) Hort.) in Japan. Japan International Research Center for Agricultural Sciences, 11(2), 106–110.
- [2] Kirnak, H., Kaya, C., Higgs, D., Bolat, I., Simsek, M. & Ikinci, A. (2003). Effects of preharvest drip-irrigation scheduling on strawberry yield, quality and growth. *Australian Journal of Experimental Agriculture*, 43(1), 105–111.
- [3] Sudar, R., Jurković, Z., Dugalić K., Tomac, I., & Jurković, V. (2011). Sorbitol and sugar composition of plum fruit during ripening. *The 46th Croatian and 6th International Symposium on Agriculture, Croatia*, 1067–1071.
- [4] Jules, J. *Horticultural reviews*. (1995). John Wiley & Sons: New York, USA.
- [5] Murakami, K. Fukuoka, N. & Noto, S. (2017). Improvement of greenhouse microenvironment and sweetness of melon (*Cucumis melo* L.) fruits by greenhouse shading with a new kind of near-infrared ray-cutting net in mid-summer. *Scientia Horticulturae*, 218, 1–7.
- [6] Pranita, B., Ojas, D., Pranita, D., Rhushabh, G. & Tapobrata, D. (2018). *Procedia Manufacturing (Maharashtra)*, 20, 195–205.
- [7] Timothy, J.R. & Vijjiya, G.S.R. (2005). Experimental studies of a double-pipe helical heat exchanger. *Thermal and Fluid Science*, 29, 919–924.

Chapter 4

Results and discussion of the greenhouse experiment

4.1 Introduction

Strawberries are mostly (>95%) cultivated in the Northern Hemisphere [1], and their annual global production of has steadily increased and has quadrupled to over 8 million tons since 1985. Owing to the increasing demand for strawberries locally and globally, the focus has shifted to enhancing the yield and improving the quality of the strawberry produce. Strawberries are extremely sensitive to the production environment. This makes them an ideal candidate to investigate the effects of environmental and climatic control in a greenhouse on their cultivation.

Environmental factors such as temperature, photoperiod, and light significantly affect the growth, yield, and quality of produce [2]. Therefore, controlled cultivation in greenhouses is a solution to overcome climatic diversity. Strawberry production in Japan is mostly done in greenhouses, which not only provide a suitable environment for cultivation but also prevent any likely damage to the strawberry crop from the extreme environment. Mostly, the climate in the strawberry production areas in Japan is mild. While the temperature in these areas remains above the freezing point during the coldest month, it often goes up to 30°C in summer. Because temperature is one of the key factors that affect the strawberry crop, greenhouses are used to ensure a regulated environment for their cultivation [3][4]. For a high growth rate of strawberries, the desired daytime and nighttime temperature ranges are 23–28°C and 5–10°C [5]. The controlled temperature inside a greenhouse results in the optimal growth of strawberry plants and improves the quality of the crop in terms of its flesh firmness, skin resistance, soluble sugar content (SSC), skin color, and organic acids [6].

For commercial and economic considerations, the quality of strawberry produce and energy consumption for producing it are critical. The ambient temperature can drop suddenly in winter, particularly when there is no solar radiation. This sudden drop in temperature can damage strawberry plants. To mitigate this situation, a heating system can be installed in greenhouses. However, the installation and operation of a heating system in a greenhouse increases the crop production costs. Depending on the location and size of the greenhouse, the cost of installing a heating system can go up to approximately 30–60% of the initial investment needed for a greenhouse [7]. Furthermore, the operation of the heating system accounts for approximately 70–80% of the total energy consumption in the greenhouse [8]. Reducing heat losses from greenhouses can help in decreasing the heating system operating costs. Therefore, it is necessary to study and understand the energy balance in the greenhouse cultivation of strawberries from an economic point of view.

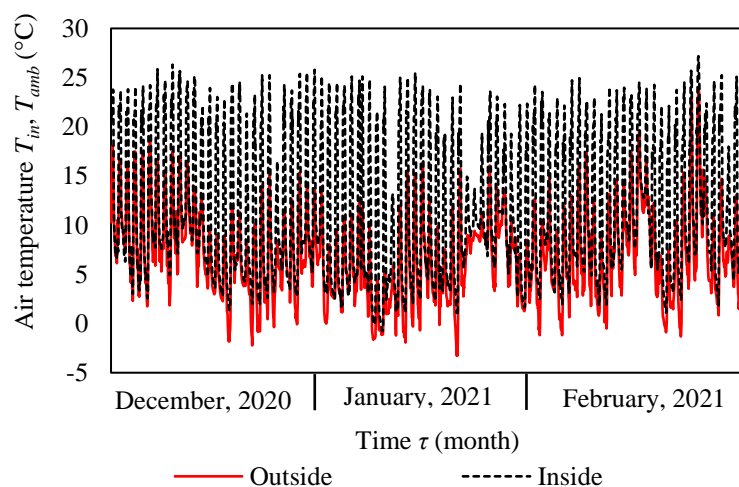
Therefore, in this chapter, the objectives were to perform an energy analysis of an experimental greenhouse and determine how it affected the local environment around the plantation area in terms of temperature, relative humidity, and solar radiation. Furthermore, the energy required to maintain the optimum temperature for strawberry growth in the greenhouse was calculated. In addition, previous studies demonstrated that environmental factors highly affect the quality of strawberries. Thus, in strawberry production in Mie prefecture, Japan, contrasting environmental conditions such as temperature, relative humidity, and solar radiation between the peak and end of the cropping season are differentiated.

In the peak season (between December to late February), the photoperiod is shorter, and the solar radiation and ambient temperature are lower than at the end season (March-May). These environmental differences throughout the season may affect strawberry quality. Most fruit qualities are evaluated by *SSC*. The quality of strawberries in terms of shape and size as well as *SSC* were evaluated in this work. Then, the influence of these effects on the optimum cultivation conditions was proposed. The optimum ranges of environmental conditions for maintaining strawberry quality can be used as a guideline not only in temperate climates, but also in other climates, such as those found in tropical countries.

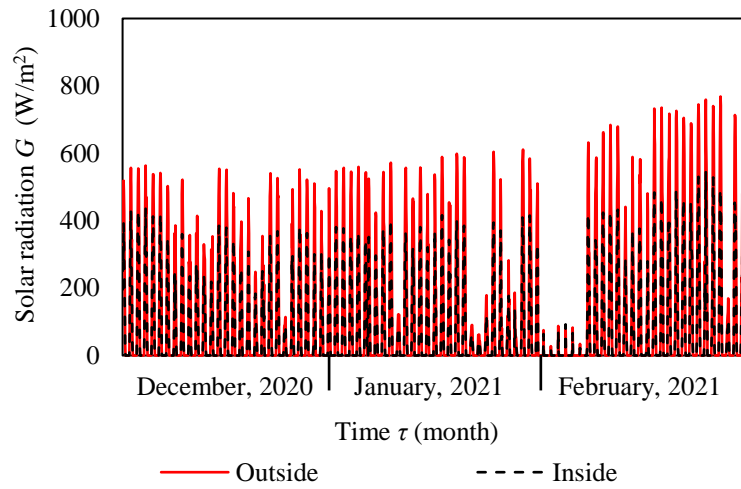
4.2 Climate under the greenhouse

4.2.1 Monthly environmental parameters

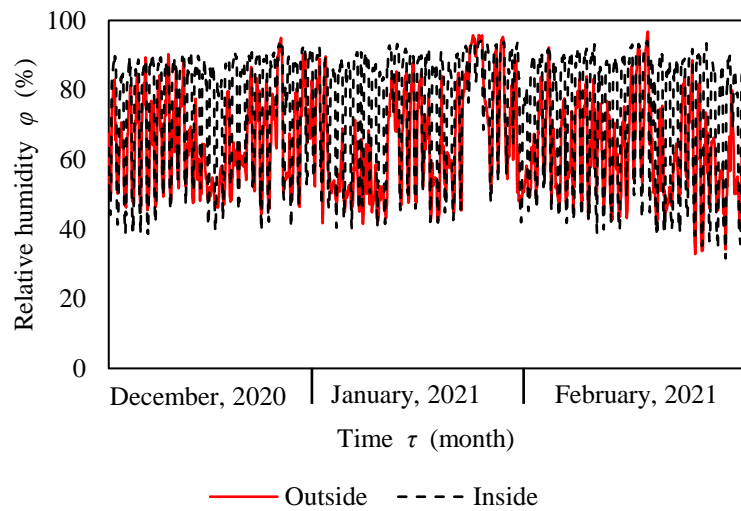
Figure 4-1 shows the monthly outside and inside environmental data of greenhouse during winter periods (December, 2020 to February, 2021) in Matsusaka, Japan. The air temperature outside the greenhouse indicates that the lowest monthly temperature (-4.4°C) was recorded in January. The average air temperature outside the greenhouse was about 7.1°C , whereas the average solar radiation outside the greenhouse was 112.5 W/m^2 . On clear and sunny day ($G > 100\text{ W/m}^2$), the average air temperature inside the greenhouse without supplemental heating was approximately 21.1°C , which is suitable condition for strawberry cultivation. However, when there is no solar radiation ($G = 0\text{ W/m}^2$), the average air temperature inside the greenhouse was about 6.8°C . Thus, a greenhouse may need to be supplemented with a gas- or electricity-based heating system to protect plants against extreme cold conditions. In addition, *RH* of air inside the greenhouse was around 31.4% to 94.2%. *RH* inside the greenhouse during the nighttime was relatively high. It was found that the average was about 86%. Excessive *RH* aids the development of fungal diseases [9]. This reason caused by the outside air temperature dropped dramatically. When air cools down, its capability to hold moisture decreases, and the *RH* increases. *RH* exhibits an increase during the night because there is no solar radiation. Furthermore, there is no need for ventilation to dissipate heat. Conversely, the temperature increased during the daytime and the ventilation fan switched on, so the *RH* recorded minimum values.



(a) Air temperature



(b) Solar radiation



(c) Relative humidity

Figure 4-1 Monthly inside and outside environmental data of greenhouse from December, 2020 to February, 2021

4.2.2 Daily environmental parameters

Temperature, solar radiation, and relative humidity are the major factors that affect the development and quality of strawberries, whereas temperature and solar radiation affect the growth and development of the strawberry plant. Furthermore, the length of the exposure of the crop to sunlight affects the ripening period of the fruit [10].

The “Harunoka” strawberries need two optimum temperature ranges: one for the day (23–28°C), and the other and most important one for the nighttime temperature (5–10°C). This study was conducted during the coldest days of the winter season and because the weather conditions every day during winter were similar. As a result, February 15–18, 2021 was chosen as experimental data.

Figure 4-2 depicts the environmental data recorded at the experimental greenhouse. Figure 4-2 (a) depicts the temperature transitions. The temperature was recorded at 5-s intervals and then averaged on 1-min increments. The

minimum inside and ambient air temperatures reached 1.0°C and -1.6°C, respectively, during the nighttime. The highest daytime ambient and inside temperatures were 18.2°C and 28.0°C, respectively. The average ambient and inside temperatures were 6.7°C and 11.5°C, respectively. Furthermore, the results indicated that the inside temperature was always higher than the ambient air temperature owing to the solar radiation trapping phenomenon. The inside air temperature was stable during the daytime, even when the outside temperature changed owing to the operation of the ventilation fan. The temperature in the greenhouse was regulated for strawberry cultivation in the winter period without a heating system. Nevertheless, the ambient air temperature still affected the inside air temperature. In the absence of solar radiation, a greenhouse may need to be supplemented with a gas- or electricity-based heating system to protect plants against extreme cold conditions.

Figure 4-2 (b) depicts the variation in solar radiation inside and outside the greenhouse. The solar radiation increased steadily from sunrise, reaching a maximum at noon. The highest solar radiation gradually started from 10:30 a.m. to 13:30 p.m. and slightly decreased until the sunset. It is evident that the solar radiation was greater outside than inside the greenhouse. The peak value of outside solar radiation on clear and sunny days was 910 W/m², and it was 627 W/m² inside the greenhouse. On average, approximately 70% of the radiation was transmitted into the greenhouse.

Figure 4-2 (c) depicts the variations in the relative humidity (*RH*) inside and outside the greenhouse. The *RH* inside the greenhouse and outside it varied from 30% to 94%, and 41% to 97%, respectively. The air temperature drop will cause a relative humidity increase. When air cools down, its capability to hold moisture decreases, and the *RH* increases. Because the temperature increases during the daytime and the ventilation fan switches on, the *RH* records minimum values. Therefore, the inside air is exchanged with fresh air. Conversely, *RH* exhibits an increase during the night because there is no solar radiation. Furthermore, there is no need for ventilation to dissipate heat. The results indicate that the *RH* inside the greenhouse follows the trend of the *RH* outside the greenhouse and is slightly less than that outside the greenhouse during the daytime. The *RH* inside the greenhouse fluctuated during day because a ventilation fan whose thermostat was fixed at 25°C automatically turned on to prevent overheating inside the greenhouse. The ventilation fan did not turn on at night; therefore, the *RH* inside the greenhouse was higher than that outside the greenhouse. However, when it rained, the outside and inside *RH* values were similar.

While strawberry plants are sensitive to dry climate, excessive *RH* aids the development of fungal diseases [11]. Maintaining appropriate relative humidity is critical for growing strawberries. The optimal relative humidity is 60–75%. The values measured for internal relative humidity in this study were rather high compared with the optimal values of relative humidity for the development of strawberries when morning aeration can reduce the air humidity and thus remove the water droplets that form on the side windows. Therefore, dehumidification techniques must be used to regulate *RH* in the greenhouse. Although there are various techniques for dehumidification, ventilation dehumidification is a simple technique; however, this technique causes heat loss during the heating period [12]. Moisture can also be removed through condensation on the interior wall of the covering material. However, water droplets may drop on plants and increase their susceptibility to fungal diseases [13]. Mechanical refrigeration and hygroscopic dehumidifiers can provide internal dehumidification without air exchange and heat loss to the outside; however, they are costly [14]. None of the present techniques are technically and economically feasible; therefore, ventilation combined with hygroscopic or mechanical dehumidifiers is desirable for

greenhouses. Selecting a dehumidification system would require the knowledge of the loads as affected by the season, crop, and local climate conditions [15].

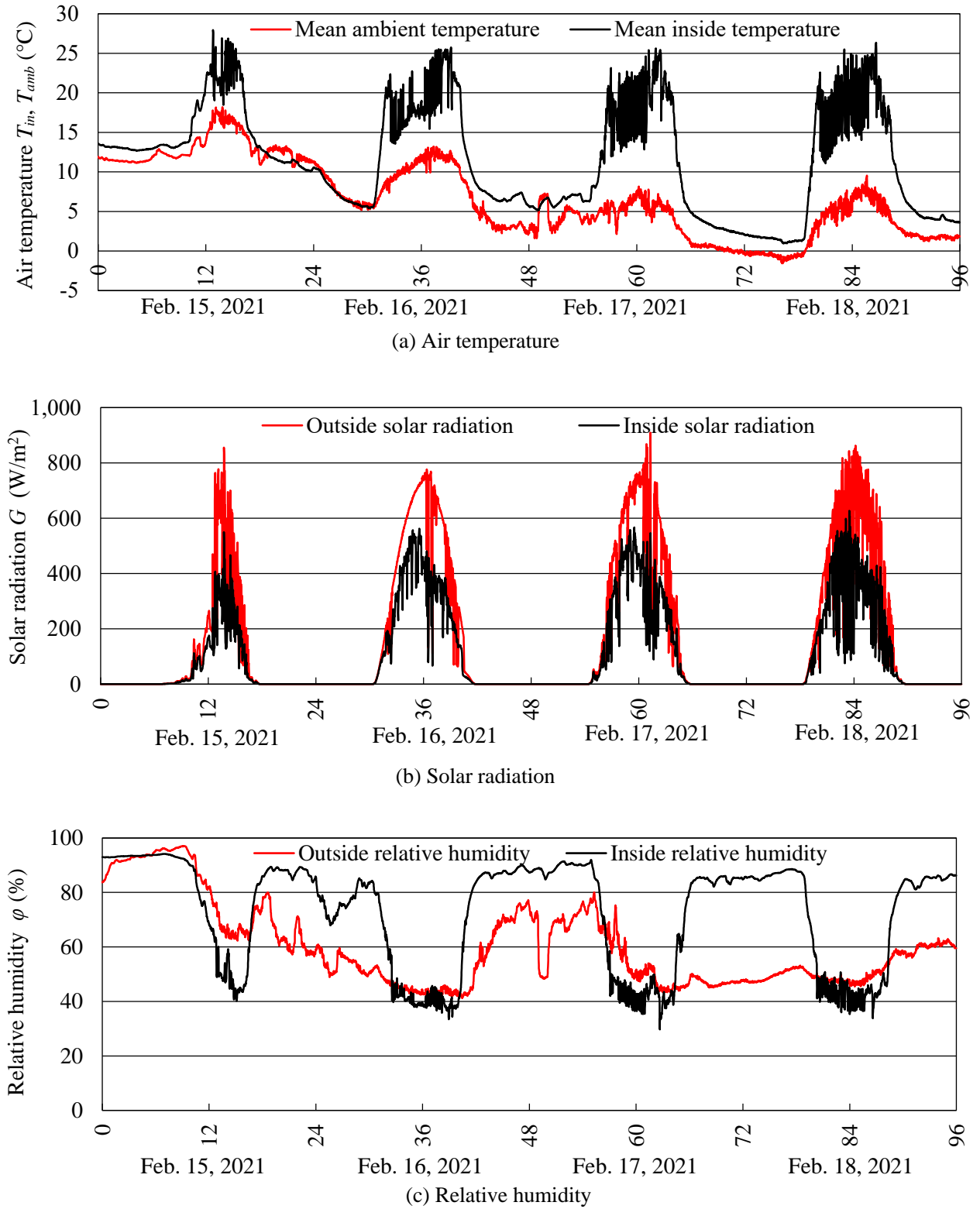


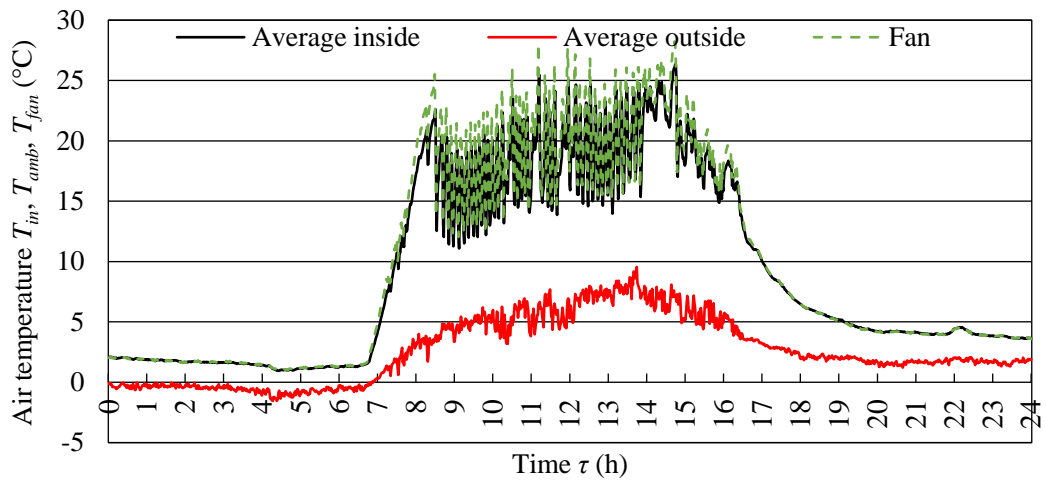
Figure 4-2 Environmental data: (a) air temperature, (b) solar radiation, and (c) relative humidity during February 15–18, 2021

According to the weather graph above (see figure 4-2 (a)), February 18, 2021 is the best day for daily data analysis. This is because there was a significant temperature difference between outside and inside the greenhouse as well as outside solar radiation was on clear and sunny day. The environmental parameters such as the air temperature, solar radiation, and relative humidity in the greenhouse were monitored daily. The values recorded on February 18, 2021 are given in figure 4-3.

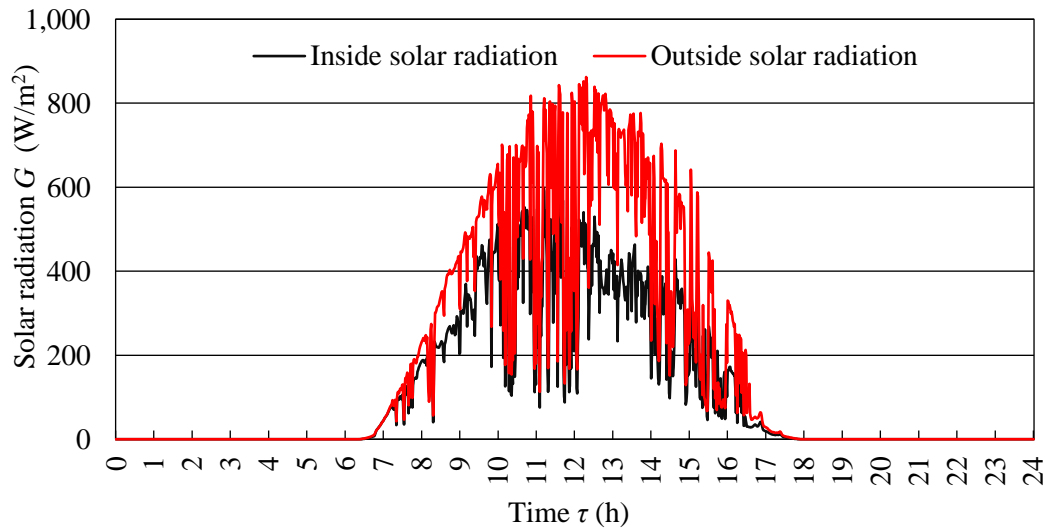
The average inside and ambient temperatures recorded by sensors T_5-T_8 and T_9-T_{14} , respectively, in figure 3-2 are depicted in figure 4-3 (a). The results indicate that the ambient air temperature reached a minimum of -1.6°C , whereas the inside air temperature reached 1.0°C during the night. It is evident that the greenhouse can ensure favorable temperatures for strawberry cultivation at night. The inside air temperature increased slightly from 6:30 a.m., with the availability of solar radiation. The inside air temperature reached a maximum of 26.4°C whereas the ambient temperature reached a maximum of 10.0°C . Therefore, greenhouses with an additional vinyl lining can ensure optimal temperature during the daytime without supplemental heating. Figure 4-3 (a) depicts that the inside air temperature fluctuates because of the effect of the ventilation fan. The ventilation fan automatically switched on when the inside temperature reached approximately 25°C . However, it had a low accuracy and sometimes responded with a delay. Therefore, the working temperature of the fan was approximately $22-28^\circ\text{C}$ and the internal air temperature gradually decreased when the fan was switched on.

As depicted in figure 4-3 (b), the outside solar radiation started increasing from 6:30 a.m. and reached a maximum of approximately 918 W/m^2 at noon on sunny days. At 11:30 a.m., the solar radiation inside the greenhouse with double vinyl lining was 644 W/m^2 . It is evident that the outside solar radiation was always higher than that inside and fluctuated owing to overcast weather. The transmittance between the outside and inside solar radiations was approximately 70%. Because of the difference in the altitude and azimuth of the sun, sensor P_2 was in shade; therefore, its solar radiation probably fluctuated.

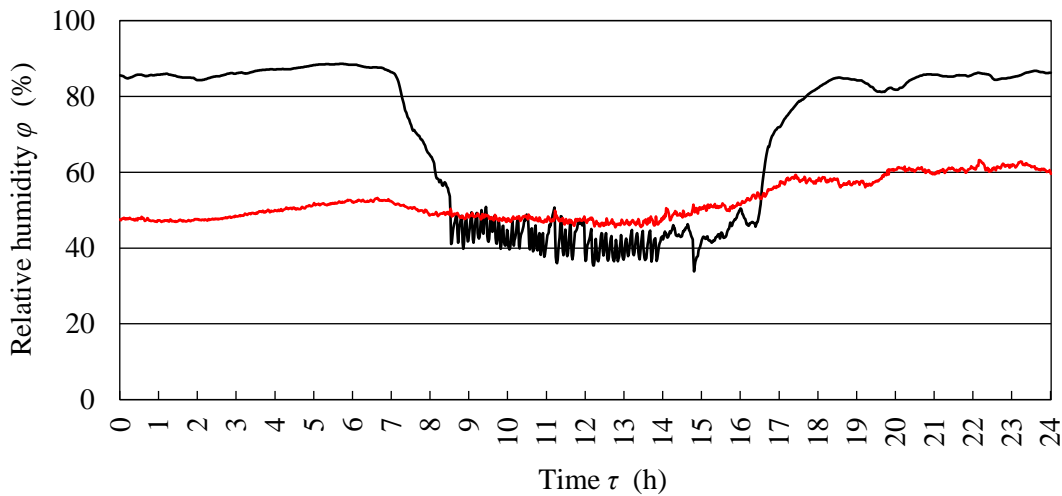
Figure 4-3 (c) depicts the hourly relative humidity evolution inside and outside the greenhouse. It is evident that the relative humidity both inside and outside followed the trend for the variation in air temperature. Moreover, relative humidity decreased during the day to the minimum values and increased at night to the maximum values. The recorded values of relative humidity were 33–89% and 45–64% inside and outside, respectively. The relative humidity at night was rather high compared with the value of approximately 70% for optimal growth. Therefore, morning aeration, such as opening the side windows, can reduce humidity and remove water droplets that form on the side windows.



(a) Air temperature



(b) Solar radiation



(c) Relative humidity

Figure 4-3 Environmental parameters recorded on February 18, 2021

4.3 Heat loss through greenhouse

The energy balance of the greenhouse was derived under steady-state conditions. In this present study, the greenhouse's thermal system is divided into three components: the covering material, ventilation fan and the ground. As the main heat storage media of solar greenhouse, the soil was exposed to solar radiation during the day. The sunlight transmitted through the greenhouse covering material and then arrived at the surface of the soil. Part of heat was transferred to the interior soil or reflected to the inside air. The increased greenhouse air temperature is due to convection heat transfer from the heated inner surface. At night, when ambient air temperature decreased, the heat stored in the soil was transferred back to the inside air. At the same time, heat loss is primarily caused by dissipation through the covering material. Figure 4-4 depicts the heat transfer process in the experimental greenhouse. The energy flow thereof is complicated process. Therefore, the following assumptions are made for estimating heat loss and estimating heating requirement of greenhouse without vegetation.

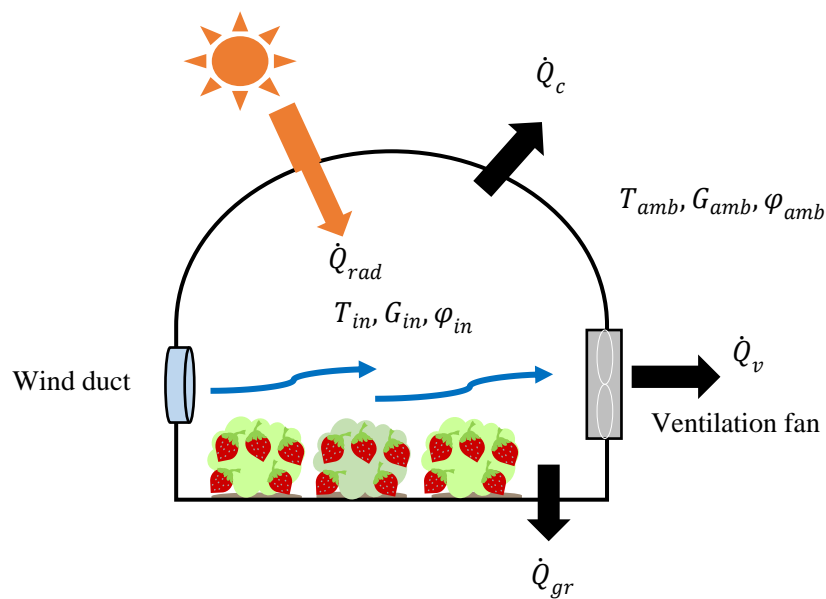


Figure 4-4 Heat transfer process in the greenhouse

Therefore, the following assumptions are made:

- 1) Heat absorption by greenhouse covering material is negligible.
- 2) Evaporation from the ground is negligible.
- 3) Transpiration from strawberry plants is negligible.
- 4) Radiation heat exchange between the greenhouse covering material and inside air is negligible.

4.3.1 Daytime heat loss

The rate of the total heat loss (\dot{Q}_{total}) through the small walk-in tunnel comprised the heat losses through the covering material, ground, and ventilation exhaust and was calculated as follows.

$$\dot{Q}_{total} = \dot{Q}_c + \dot{Q}_{gr} + \dot{Q}_v \quad (4.1)$$

where

$$\dot{Q}_c = U_c A_c (T_{in} - T_{amb}) \quad (4.2)$$

$$\dot{Q}_{gr} = U_{gr} A_{gr} (T_{in} - T_{amb}) \quad (4.3)$$

$$\dot{Q}_v = 0.33 ACHV (T_{in} - T_{amb}) \quad (4.4)$$

where U_c is the overall heat transfer coefficient of the covering material, A_c is the total area of the covering material, T_{in} is the inside air temperature, T_{amb} is the ambient air temperature, U_{gr} is the ground heat transfer coefficient, A_{gr} is the plantation area, ACH is air change per hour, V is the volume of the greenhouse.

The calculated heat loss through the greenhouse on February 18, 2021 (from 8.30 a.m. to 4.30 pm) is presented in figure 4-5. The same trend is observed in all curves in the figure. It is evident that the magnitude of heat loss fluctuated through the day owing to the change in the inside air temperature (see Figure 4-3 (a)). It is also evident that heat loss by ventilation (\dot{Q}_v) plays a significant role in the total heat loss through the greenhouse during the daytime, with the maximum magnitude reaching approximately 110 kW. In addition, the capacity of the ventilation fan was high, and its ACH was excessive compared with the size of the greenhouse. Therefore, heat loss by ventilation can be reduced by selecting an appropriate size for the ventilation fan. Moreover, when the ventilation fan stops, the heat loss by ventilation can be assumed to be 0 kW, particularly at night. This graph also indicates that the heat losses through the ground (\dot{Q}_{gr}) and covering material (\dot{Q}_c) were small compared with the heat loss by ventilation.

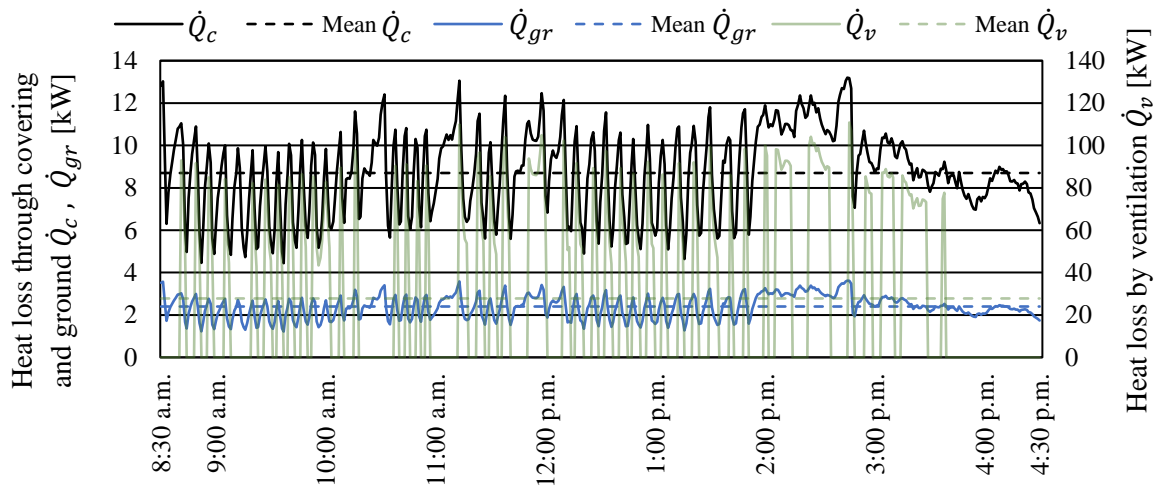


Figure 4-5 Heat loss through the greenhouse as a function of the time of the day (February 18, 2021)

4.3.2 Nighttime heat loss

The calculated heat loss through the greenhouse at the nighttime, is presented in figure 4-6. As stated in chapter 3, to control the greenhouse air temperature, ventilation fan and wind ducts were used. When the inside air temperature exceeded more than 25°C , wind ducts as well as a ventilation fan automatically opened and turned on. However, there was no ventilation at night. Thus, heat loss by ventilation was neglected. It is obvious that heat loss through covering material (\dot{Q}_c) and heat loss through the ground (\dot{Q}_{gr}) were the same trend due to the temperature

difference between inside and ambient air was significantly factor in heat loss calculations. The heat loss through covering material and heat loss through the ground were small and relatively constant at night (from 7.00 p.m. to 7.00 a.m.). This is because of the temperature difference between inside and ambient air was very small (see Figure 4-7). Greenhouse covering material and soil's heat storage capacity was limited and depended on the solar radiation and ambient air temperature. However, when solar radiation presented (see Figure 4-3 (b)), the temperature difference between inside and ambient air temperatures was significant increased (from 7.00 a.m.). This increased heat dissipation through the covering material and the ground. From the agricultural point of view, the desired nighttime temperature range is 5–10°C [5]. In this study, it was observed that inside air temperature was relatively low (about 4.5°C), as shown in figure 4-3 (a). Thus, it is necessary to maintain greenhouse air temperature at night to reduce damage to strawberries. The estimated heating requirement will be described in the next section.

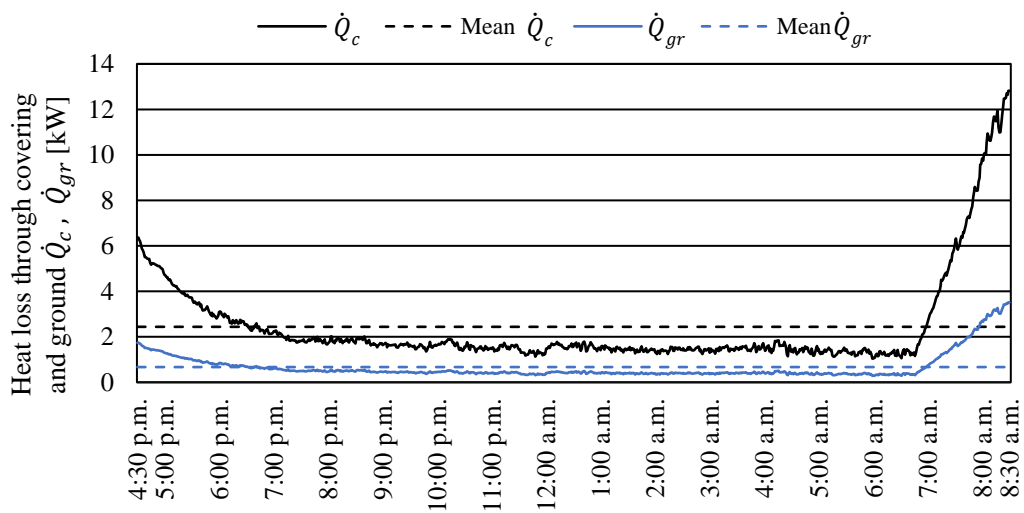


Figure 4-6 Heat loss through the greenhouse as a function of the time of nighttime (February 18, 2021)

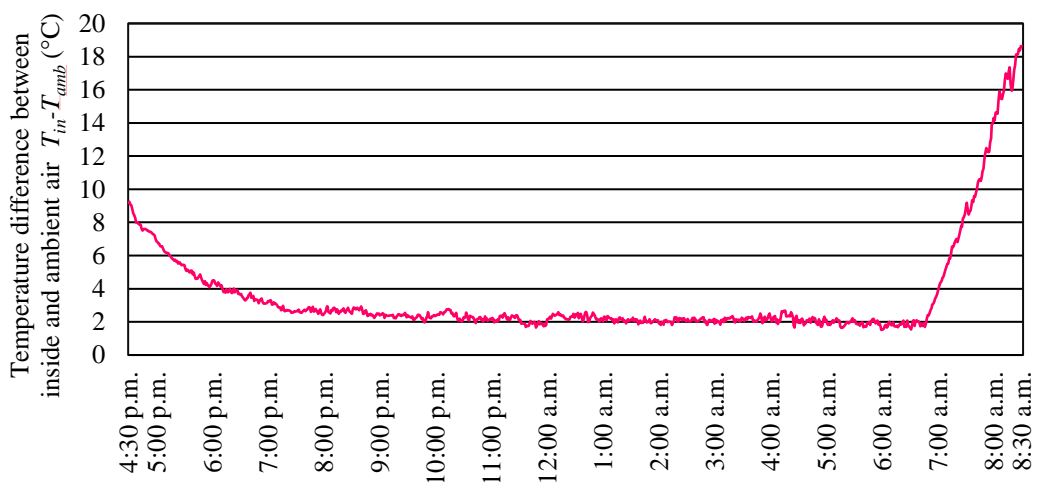


Figure 4-7 The temperature difference between the inside and ambient air temperatures

4.4 Greenhouse heating requirement

Heating is required at night since there is no sun radiation. Similarly, unless the indoor air temperature exceeds 25°C, the ventilation fan does not run. As a result, when the ventilation fan is turned off or the inside air temperature is low, the heat loss by ventilation is ignored. Furthermore, the heat loss or gain to the ground is assumed to be negligible and is ignored. In addition, a single black plastic sheet was also used to cover the ground.

In this study, solar radiation was sufficient to maintain an optimum temperature during the daytime inside the greenhouse for strawberry growth (Fig. 4-2 (b)). Therefore, supplemental heating was required only during the nighttime or when the ambient temperature was significantly low and during the winter period from November to April. The maximum monthly required heating was determined using equation (4.5).

$$e_m = 3.6U_c A_c (T_{de} - T_{amb,min}) \cdot HN/A_{gr} \quad (4.5)$$

where T_{de} is design temperature for optimal growth of the strawberry plants in the greenhouse, $T_{amb,min}$ is the monthly minimum ambient air temperature, H is the daily heating duration, N is the number of days per month, and e_m is monthly heating requirement per plantation area in kJ/(m²·month).

The parameters for the calculation were $A_{gr} = 57$ m², $U_c = 6.2$ W/(m²·K), $T_{de} = 10^\circ\text{C}$ and 8°C (the nighttime optimal strawberry plant temperature) and the daily heating hours per day ranged from 5 to 17 h depending on inside air temperatures (< 10°C) based on the experiment. Table 4-1 lists the details of these calculation parameters.

Table 4-1 Parameters used in calculation for each month

	Nov. 2020	Dec. 2020	Jan. 2021	Feb. 2021	Mar. 2021	Apr. 2021
Overall heat transfer coefficient of covering material; U_c [W/(m ² ·K)]				6.2		
Total area of covering material; A_c [m ²]				111		
Plantation area; A_{gr} [m ²]				57		
Design temperature; T_{de} [°C]				10 and 8		
Minimum ambient air temperature; $T_{amb,min}$ [°C]	0.8	-3.4	-4.4	-2.0	-0.9	3.6
Daily heating time; H [h]	5	15	17	14	11	9
Number of days per month; N [d/month]	30	31	31	28	31	30

Figure 4-8 depicts the estimated maximum monthly heating contribution necessary to maintain the greenhouse temperature at 10°C. The requirement for heat energy for heating was maximum in January (327.6 MJ/m²), because January is the coldest month with the minimum ambient temperature of -4.4°C. The requirement for heat energy for heating was lowest in November (60.0 MJ/m²). Therefore, these amounts of energy must be provided by a heating system to protect strawberry cultivation against extreme cold temperatures.

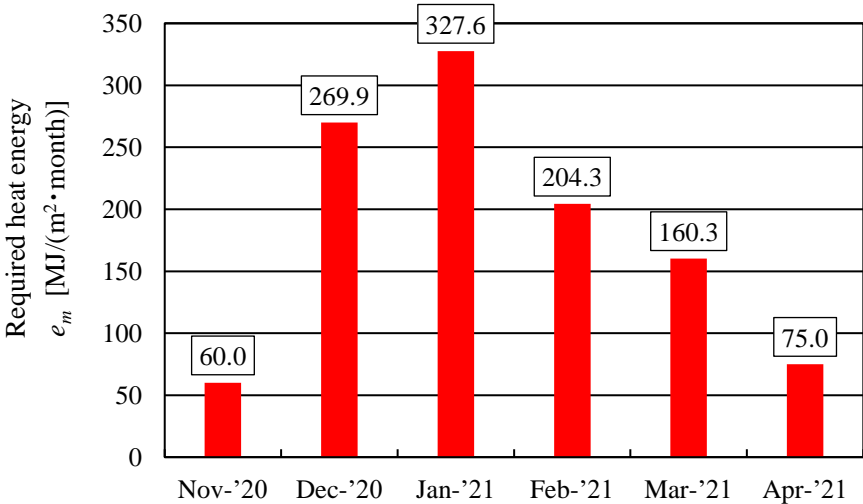


Figure 4-8 Estimated maximum monthly heating required to maintain the greenhouse temperature at 10°C

The “Harunoka” strawberries need nighttime temperature at 5–10°C. To compare the energy reduction in the greenhouse, the design temperature for optimal growth of the strawberry plants was set at 8°C. Other parameters were used as in table 4-1. Figure 4-9 shows the estimated maximum monthly heating required to maintain the greenhouse temperature at 8°C. The graph indicates that the top three maximum heating requirements was in January (281.9 MJ/m²), December (229.6 MJ/m²) and February (170.3 MJ/m²), respectively.

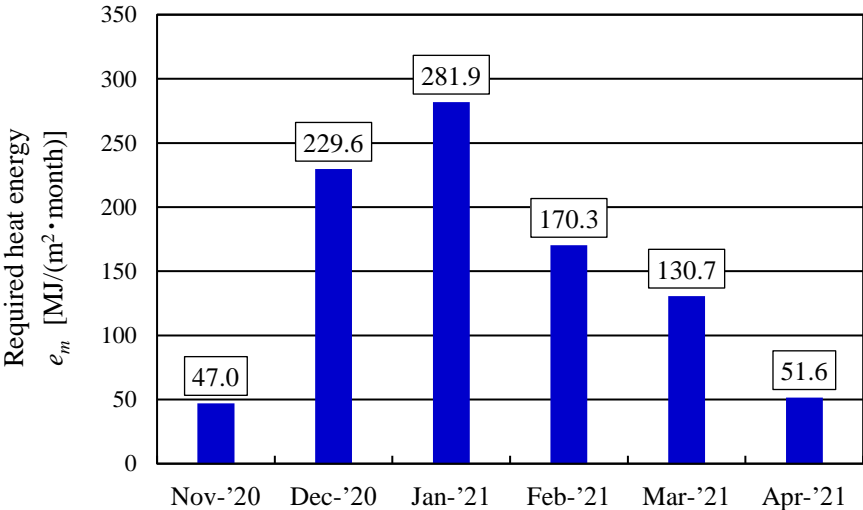


Figure 4-9 Estimated maximum monthly heating required to maintain the greenhouse temperature at 8°C

In addition, it was obvious that when design temperature was set at 8°C, the demand for heating energy was reduced compared to the figure 4-8. Table 4-2 shows the percentage reduction of heating energy. Even when the temperature only dropped by 2°C ($T_{de}=10$ to 8°C), up to 30% more energy was saved. Therefore, design temperature has significant impact on the energy demand in a greenhouse. However, to preserve strawberry cultivation from extreme cold temperatures, significant amounts of energy must be provided by a heating system.

Table 4-2 Required heat energy under different design temperatures and percentage reduction of energy

Month	Required heat energy (e_m), MJ/(m ² ·month)		Percentage reduction, %
	$T_{de} = 10^\circ\text{C}$	$T_{de} = 8^\circ\text{C}$	
Nov. 2020	60.0	47.0	21.7
Dec. 2020	269.9	229.6	14.9
Jan. 2021	327.6	281.9	13.9
Feb. 2021	204.3	170.3	16.4
Mar. 2021	160.3	130.7	18.4
Apr. 2021	75.0	51.6	31.2

Figure 4-10 (a) and figure 4-10 (b) depict the difference between the design and measured values of the ambient and inside temperatures. The average values of the inside air and ambient temperatures were calculated for each month. Monthly temperatures recorded over the experimental period are presented in table 4-3. It is evident from figure 4-10 (a) that the temperature difference from the design temperature was greater than the temperature difference from the measured data. To calculate the heat required for maintaining an optimum temperature in the greenhouse, the temperature difference between the inside and ambient air temperatures is necessary (see equation (4.2) – (4.4)). However, the values of the design temperature of the greenhouse and minimum ambient air temperature are also required because the coldest day leads to the estimated maximum monthly heating. The design temperature of 10°C was appropriate for maintaining and controlling the desired temperature in the greenhouse during winter. Furthermore, figure 4-10 (b) also shows that the temperature difference from the design temperature was greater than the temperature difference from the observed data. However, the difference temperature between design and measured was relatively low in April, 2021 (4.4°C and 4.0°C). An excessively low or high design temperature can result in insufficient heating or consume significant amounts of energy.

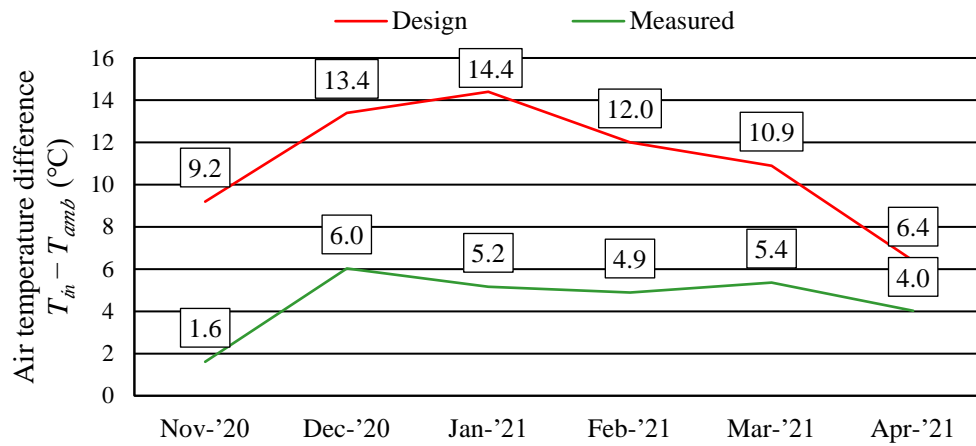


Figure 4-10 (a) Comparison of design and measured temperatures ($T_{de} = 10^{\circ}\text{C}$)

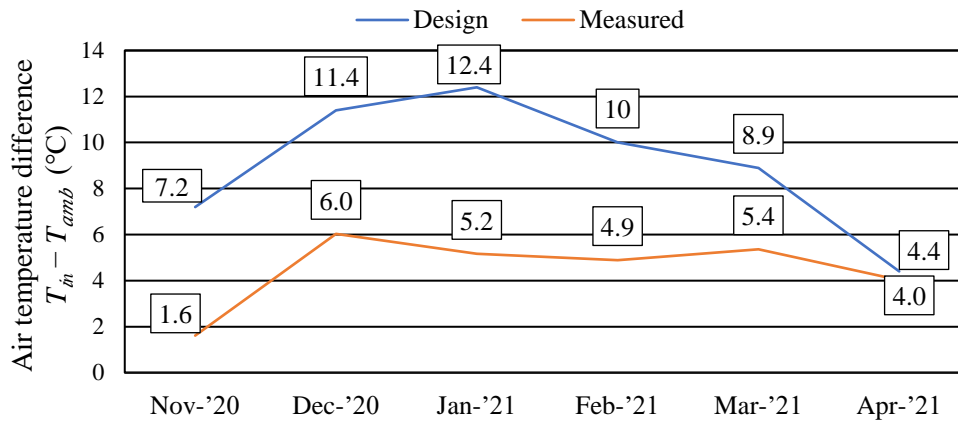


Figure 4-10 (b) Comparison of design and measured temperatures ($T_{de} = 8^{\circ}\text{C}$)

Table 4-3 Mean and design temperatures of the air inside and outside greenhouse

Month	Design		Measured	
	Design greenhouse temperature (°C)	Minimum ambient temperature (°C)	Mean inside air temperature (°C)	Mean ambient temperature (°C)
Nov. 2020	10 and 8	0.8	8.9	10.6
Dec. 2020	10 and 8	-3.4	3.7	9.8
Jan. 2021	10 and 8	-4.4	5.2	10.4
Feb. 2021	10 and 8	-2.0	6.8	11.7
Mar. 2021	10 and 8	-0.9	8.7	14.1
Apr. 2021	10 and 8	3.6	12.7	16.7

4.5 Statistical analysis results

The fluctuation in the inside temperature was evaluated in terms of the standard deviation (SD) σ_i using equation (2.9). The SD should be minimum. The average value ranged from 18.3°C to 19.7°C and SD ranged from 3.4°C to 3.8°C and, as depicted in figure 4-11. The SD of inside air temperature in daytime is relatively low. Since the variance is somewhat low, it can see that air temperatures are performed around the same level. The lower SD indicate a decrease in the fluctuations in the inside air temperature. Greenhouses should be able to maintain inside air temperatures. Therefore, to ensure the optimal environment for strawberry cultivation in greenhouses, air temperature should be steady. According to results, it can see that the greenhouse can maintain inside air temperature in daytime, even in coldest periods without supplemental heating.

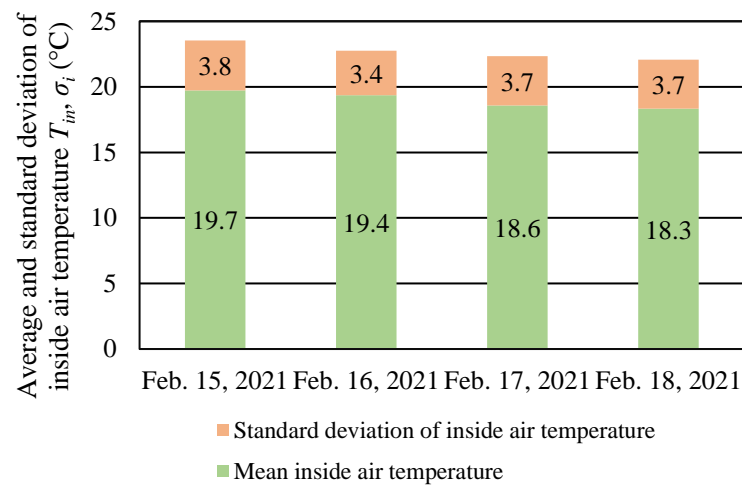


Figure 4-11 Standard deviation and mean value of inside air temperature as a function of day (February 15–18, 2021)

4.6 Effect of environmental on strawberries production

4.6.1 The environment factors on pick up dates

Temperature, solar radiation and relative humidity are the main factors that affect the growth of strawberries and fruit quality. Temperature and solar radiation are basically environmental factors controlling strawberry plant growth and development. A high temperature on the fruit surface caused by prolonged exposure to sunlight hastens ripening. Strawberry fruits exposed to higher sunlight levels ripen faster [16]. In this study, “Harunoka” strawberries were grown under double PVC sheets in the greenhouse. To study the climate changes in the small walk-in greenhouse, environmental parameters were monitored and recorded. Generally, strawberry continue to increase in size during the ripening process. The developmental stages of strawberry ripening are normally divided into four ripeness stages, referred to as green, white, pink (or turning) and red (or ripe) [17]. Strawberries are typically harvested 30-40 days after flowering, depending on the cultivar. The entire ripening process is rapid, generally occurring within a few days following the white stage, depending on air temperature [18]. Thus, in this present study, environmental factors during the three days before harvest were evaluated in each season. Seasons are characterized as peak and end seasons for fruiting, with the peak season lasting from December to February. After that, the season is referred to as the “end season” until May.

Figure 4-12 (a) shows the temperature transition between 17 and 20 February 2021 and between 2 and 5 April 2021. The air temperature was recorded at 5-second intervals and then averaged into 15-minute increments. For 17-20 February 2021, the minimum inside air temperature reached 1.0°C, the ambient temperature reached -1.9°C in the nighttime. The highest daytime ambient temperature was 16.9°C when the inside air temperature was 27.1°C. Moreover, it can be seen from figure 4-12 (a) that the inside air temperature was more than 30°C and reached a maximum of 38°C in the daytime on a sunny day during the period of 2-5 April 2021. Likewise, the differences between the inside and outside air temperatures were small, especially for the nighttime and on cloudy days. The lowest value was found to be 1°C. Due to the changing of the seasons, the outside air temperature was slightly higher throughout the day. This phenomenon resulted in a higher inside air temperature, which may have had an impact on strawberry quality. Furthermore, the results demonstrate that inside temperature was always higher than the ambient air temperature in both periods due to the solar radiation trapping phenomenon. The inside air temperature is very stable in the daytime, even when the outside temperature changes, due to the side windows and ventilation fan. It is also observed that the difference between the optimal high and optimal low temperatures can create suitable conditions for strawberry cultivation. According to these results, the temperature between 17 and 20 February 2021 is more suitable for planting than the period of 2-5 April 2021.

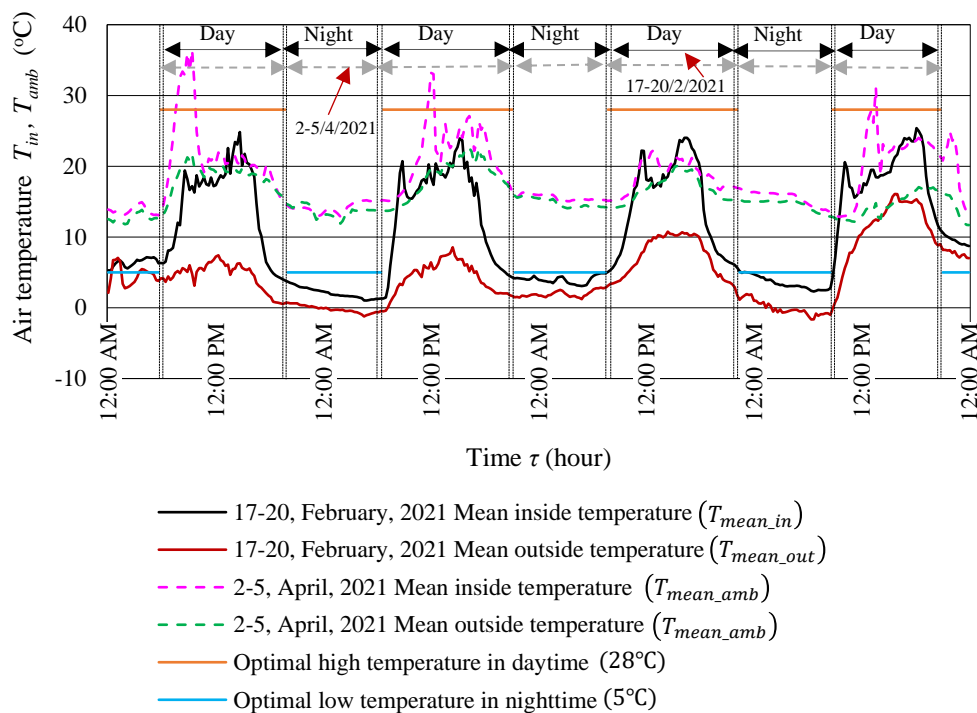


Figure 4-12 (a) The comparison of the temperatures inside and outside the greenhouse at different times

Figure 4-12 (b) presents the variation of solar radiation inside and outside the greenhouse. The solar radiation increases from the sunrise reaching maximum value at noon. The highest solar radiation will gradually start from 10:30 to 13:30 and slightly decrease until the sunset. It is obvious that outside solar radiation was greater than inside solar radiation, the peak value of solar radiation on clear and sunny days was 770 W/m² (outside the greenhouse) and 560 W/m² (inside the greenhouse) during 17-20 February, 2021. Approximately 70% of this radiation is

transmitted to inside the greenhouse. This Figure also shows that outside solar radiation was still higher than inside solar radiation during 2-5 April, 2021. Although, it was mostly cloudy. The maximum was found at 900 W/m² at the outside, while it was 590 W/m² at the inside greenhouse. The average 63% of this radiation is transmitted to inside the greenhouse which was similar to the peak season. Moreover, solar radiation both inside and outside the greenhouse during the end season, fluctuated depending on cloud. Likewise, solar radiation on 4 April, 2021 was quite low compared to other days due to it was a rainy day.

According to this graph, it can see that outside solar radiation was a bell curve in both seasons. However, inside solar radiation fluctuated due to the effect of double vinyl sheets and cloud. Furthermore, even though the seasons were different, two seasons inside solar radiations were not different. It can conclude that polyvinyl chloride sheet and its additional sheet can filter out high solar radiation. In addition, in this study, it was not seen the effect of solar radiation on strawberry quality due to inside solar radiation values were similar.

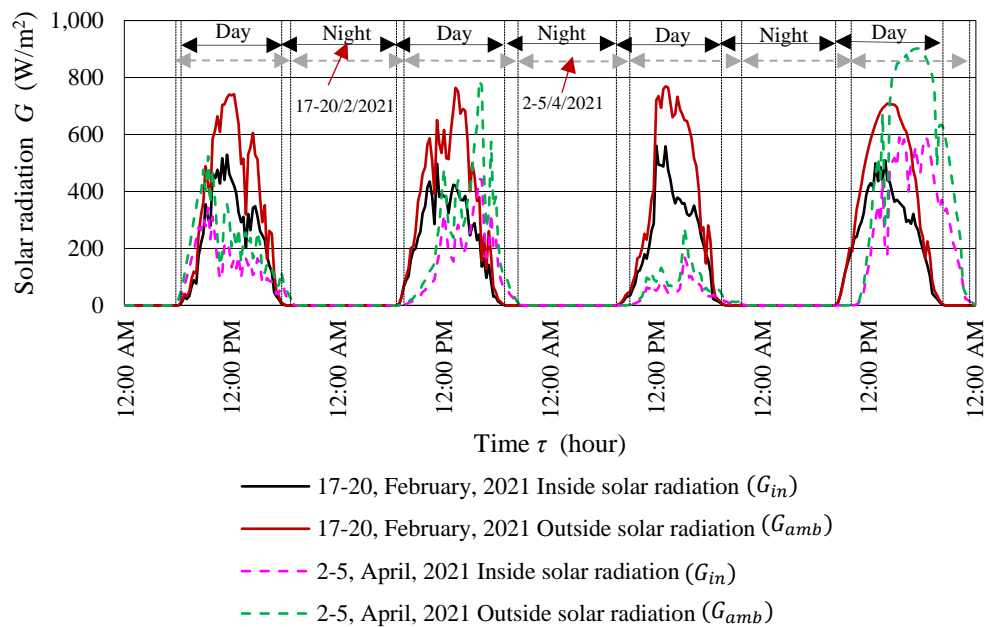


Figure 4-12 (b) The comparison of solar radiation between inside and outside greenhouse at different times

Figure 4-2 (c) shows the variation of relative humidity (*RH*) inside and outside the greenhouse. During the peak season, the *RH* inside the greenhouse varied from 30% to 92%, while the *RH* outside the greenhouse ranged from 43% to 85%. The increase in the relative humidity indicated a decreased air temperature. *RH* decreases during the daytime to its minimum values and increases in the nighttime to its maximum values. The results demonstrate that *RH* inside the greenhouse followed the profile of *RH* outside the greenhouse and was slightly less than the *RH* outside greenhouse during the daytime. Because of the ventilation fan and the side windows, the *RH* inside the greenhouse fluctuated during the day.

Nevertheless, as the ventilation fan did not turn on and side windows were closed in the nighttime, and due to the evapotranspiration of strawberries, the *RH* inside the greenhouse was higher than the *RH* outside the greenhouse. Due to the temperature profile during the period of 2-5 April 2021 being rather high and there being small

differences between day and night temperatures, the RH profile did not differ significantly between day and night. The RH inside the greenhouse varied from 30% to 93%, while the RH outside the greenhouse ranged from 43% to 95%. The humidity range of the end season was not different from that of the peak season.

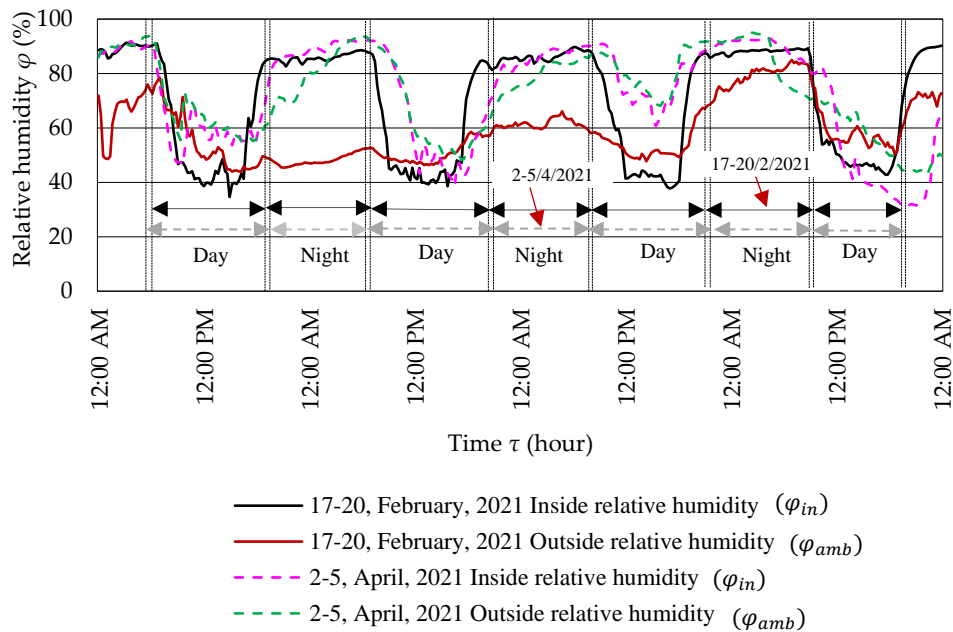


Figure 4-12 (c) The comparison of relative humidity between inside and outside greenhouse at different times

To evaluate the influence of environmental factors on strawberry quality, eight strawberry samples were randomly selected in each period. Additionally, pictures of the samples were taken by a digital camera inside the greenhouse. However, the weather on each day was different. It was sunny and clear on 20 February 2021, while it was cloudy and occasionally drizzly on 5 April 2021. Therefore, the light and shadow levels in the figures was out of our control.

4.6.2 Harvest on 20 February 2021

On the day of harvesting (20 February 2021), the weight, shape, and soluble sugar contents (SSC) of strawberries were recorded. The SSC was measured three times, and we also determined an average value of SSC. Table 4-4 shows the summarized of measured parameters. The results demonstrate that the SSC ranged from 8.8% to 12.8%. The range of SSC was of satisfactory quality. SSC values for the cultivar "Harunoka" range from 8% to 12%, indicating good quality. The taste of the strawberries was very sweet, and fruit firmness was very favorable. The heaviest strawberry was 49.6 g. As shown in figure 4-13 (a), the fruits from the strawberry plants grown under small walk-in greenhouse conditions were rather large (a short-wedge) and had a consistent red color. Furthermore, it is noticed that strawberry shape had no effect on the sweetness, even if the strawberry did not have a good shape.

Table 4-4 Strawberry quality parameters on 20 February 2021

Sample no.	Width (mm)	Hight (mm)	Weight (g)	Mean SSC (%)
1	40	48	24.0	12.8
2	46	51	31.9	9.90
3	50	62	38.5	10.6
4	53	36	19.3	11.6
5	60	55	49.6	12.3
6	50	51	33.3	9.90
7	54	50	37.4	11.2
8	50	55	34.6	8.80

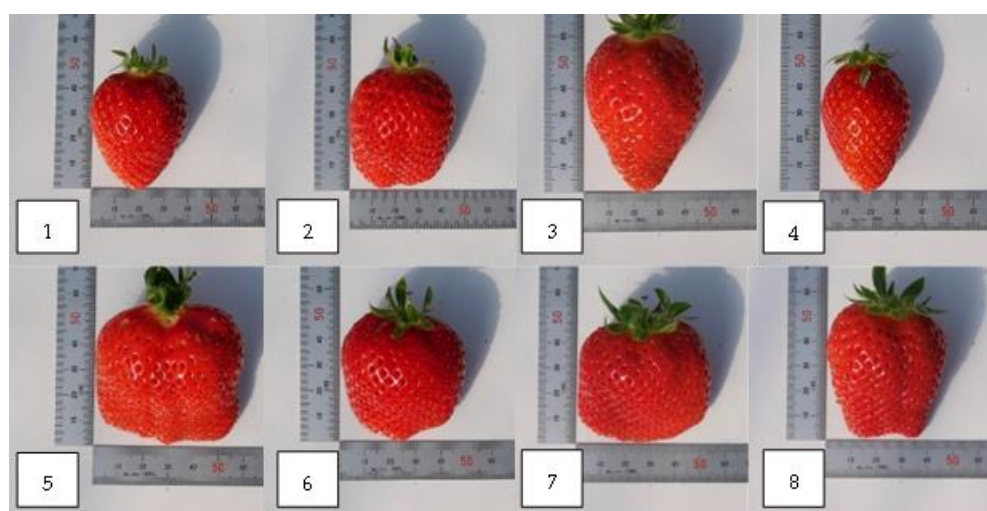


Figure 4-13 (a) Strawberry fruits harvested on 20 February 2021

4.6.3 Harvest on 5 April 2021

Table 4-5 shows a summary of the measured parameters on 5 April 2021. The results show that the soluble solid contents ranged from 7.4% to 8.9%. The range of *SSC* was less than that in the data for 20 February 2021 (see Table 4-4). The taste of strawberries was sweet and slightly sour. The heaviest strawberry was approximately 41 g. Moreover, according to figure 4-13 (b), the shape of strawberries was a beautiful long conical shape, and they had a ruddy red color. However, the firmness was quite sensitive.

Table 4-5 Strawberry quality parameters on 5 April 2021

Sample no.	Width (mm)	Hight (mm)	Weight (g)	Mean SSC (%)
1	45	51	31.0	8.6
2	42	57	36.0	7.9
3	41	55	27.0	8.3
4	39	54	27.0	8.7
5	54	61	40.5	8.9
6	37	58	17.5	7.7
7	45	57	34.0	8.6
8	45	52	30.0	7.4

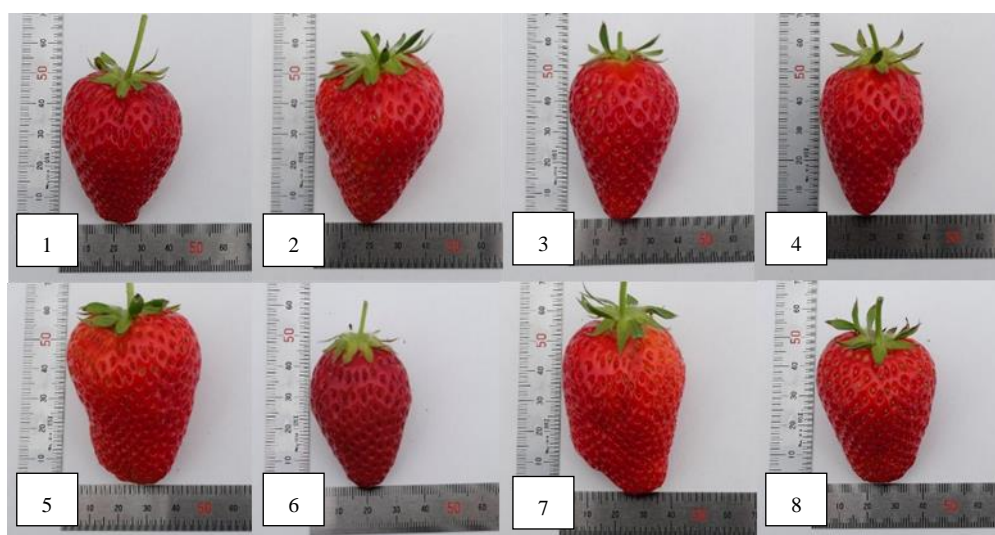


Figure 4-13 (b) Strawberry fruits harvested on 5 April 2021

In these present experiments, eight sample strawberries in each period were harvested to show their typical shape, size and color, and they were then compared. It can be seen that during the peak season, the typical strawberry shape was a short wedge. The width was significantly greater than the height among these strawberries. During the second harvest, strawberries were a beautiful long conical shape. In addition, it was noticed that the sizes were similar but the SSC, firmness and the color of strawberries from the two seasons were different. The average SSCs of fruit grown in the greenhouse covered with double vinyl sheets on 20 February 2021 and 5 April 2021 were $10.9\% \pm 1.3\%$ and $8.3\% \pm 0.5\%$, respectively, as shown in table 4-6. This result indicates that the SSC during the peak season was significantly higher than at the second harvest. It can be inferred that growing strawberries in a greenhouse provided a better microclimate, i.e., a more appropriate temperature during the cold period. In addition, the cultivation of strawberries requires different day ($23-28^{\circ}\text{C}$) and night ($5-10^{\circ}\text{C}$) air temperatures. The difference between day and night air temperatures may cause an increase in fruit SSC. The average difference between day and night air temperatures during the peak season ($\sim 12^{\circ}\text{C}$) was greater than during the end season ($\sim 8^{\circ}\text{C}$).

Table 4-7 indicates the comparison of climatic parameters on different days of harvest. In the peak season, the greenhouse can provide suitable temperatures for the strawberry. At the end of the season, air temperature in the nighttime was rather high, along with the maximum air temperature at night being above the favorable temperature range. In both seasons, it was observed that temperature did not affect strawberry weight. According to the results, in the peak season, the average relative humidity inside greenhouse was about 73%, while it was 63% during the end season. The relative humidity between the two seasons was not significantly different. In addition, it can see that solar radiation during the end season was slightly higher than solar radiation in the peak season, fluctuation in solar radiation is not likely to have a major impact on strawberry SSC.

Table 4-6 Mean and standard deviation of strawberry samples ($s = 8$) on different days of harvest

Traits	20/2/2021		5/4/2021	
	Mean	SD	Mean	SD
SSC	10.9 (%)	1.3	8.3 (%)	0.5

Table 4-7 The comparison of climatic parameters at different days

Characteristics	20/2/2021	5/4/2021
Average inside air temperature at night, T_{in_night} (°C)	5.8	12.7
Average inside air temperature during the day, T_{in_day} (°C)	17.8	21.2
Average difference between day and night inside air temperatures, ΔT (°C)	12.0	8.5
Average inside solar radiation during the day, G_{in} (W/m ²)	255	307
Average inside relative humidity, φ_{in} (%)	73	63

Summary

An experimental study was performed to investigate the effects of environmental factors on strawberry cultivation in a greenhouse and estimate the heat energy required for maintaining an optimum temperature inside the greenhouse during winter. The results of the study indicate that the greenhouse can provide favorable environmental conditions for strawberry plants. Generally, supplemental heating is not required during the daytime because solar radiation is sufficient to maintain the temperature inside the greenhouse high enough for strawberry cultivation even in winter. The maximum temperature difference between the inside and ambient air temperatures was 16.4°C, whereas the maximum reduction in solar radiation was approximately 30% when compared with ambient solar radiation in this greenhouse. The calculated maximum heating requirement was from November 2020 to April 2021. The monthly heating requirement ranged from 60.0 to 327.6 MJ/(m²·month) and 47.0 to 281.9 MJ/(m²·month), when the design temperatures for heating were 10°C and 8°C, respectively and the heat energy requirement was found to be maximum in January, with the lowest nighttime ambient temperature of -4.4°C. The results of this study indicate that passive solar heating may need to be supplemented with gas- or electricity-based heating systems in cold areas with long periods of cloudy weather.

Environmental factors including solar radiation, air temperature and relative humidity were monitored and recorded during the experiment. Additionally, the harvesting time was different; (1) the first harvest was during the

peak season on 20 February 2021, and (2) the second harvest is at the end of the season on 5 April 2021. Eight samples of strawberry were harvested during each period and their size, weight and SSC were measured and compared to each other. The difference between day and night air temperatures may cause an increase in fruit SSC. Based on these results, we conclude that temperature difference is one of major factors responsible for the end-season decline in the SSC, firmness and color of strawberry fruits in a temperate production system. In both seasons, it was observed that temperature did not affect strawberry weight. Increasing temperatures lead to the decline in SSC at the end of the season. The relative humidity was not significantly different between the two seasons. In addition, it can be seen that solar radiation at the end of the season was slightly higher than solar radiation during the peak season. Furthermore, it can be stated that fluctuations in solar radiation are not likely to have a major effect on fruit SSC. In addition, other factors such as the age of plants and the predominant order of harvested fruit could affect fruit SSC independently. Thus, it can be concluded that temperature difference is a major factor responsible for the quality of strawberries.

References in chapter 4

- [1] FAOSTAT (n.d.) Food and Agriculture Organization of the United Nations, Available at: <http://www.fao.org/faostat/en/#search/Strawberries> (accessed 5 April, 2021).
- [2] Ministry of the Environment, Ministry of Education, Culture, Sports, Science and Technology, Ministry of Agriculture, Forestry and Fisheries, Ministry of Land, Infrastructure, Transport and Tourism and Japan Meteorological Agency, Climate Change in Japan and Its Impacts, *Synthesis Report on Observations, Projections and Impact Assessments of Climate Change*, Tokyo, Japan, 2018.
- [3] Singh, M.C., Singh, J.P., Pandey, S.K., Mahay, D. & Shrivastva, V. (2017). Factors Affecting the Performance of Greenhouse Cucumber Cultivation-A Review. *International Journal of Current Microbiology and Applied Sciences*, 6(10), 2304–2323.
- [4] Martzopoulou, A., Vafiadis, D. & Fragos, V.P. (2020). Energy Gain in Passive Solar Greenhouses Due to CO₂ Enrichment. *Energies*, 13(5), 1–7.
- [5] M. Takei, *The Cultivation of Strawberry in Japan*, Nagano, Japan, 2010.
- [6] Atkinson, C.J., Nestby, R., Ford, Y.Y. & Dodds, P.A.A. (2005). Enhancing beneficial antioxidants in fruits: A plant physiological perspective. *BioFactors*, 23(4), 229–234.
- [7] Firfiris, V.K., Fragos, V.P., Kotsopoulos, T.A. & Nikita-Martzopoulou, C. (2020). Energy and environmental analysis of an innovative greenhouse structure towards frost prevention and heating needs conservation. *Sustainable Energy Technologies and Assessments*, 40, 1–17.
- [8] Huang, L., Deng, L., Li, A., Gao, R., Zhang, L. & Lei, W. (2021). A novel approach for solar greenhouse air temperature and heating load prediction based on Laplace transform. *Journal of Building Engineering*, 44, 1 – 12.
- [9] Hao, X., Zheng, J., Celeste, L. & Guo, X. (2017). Liquid desiccant dehumidification system for improving microclimate and plant growth in greenhouse cucumber production. *Acta Horticulturae*, 1170, 861–866.
- [10] Palencia, P., Martínez, F., Medina, J.J. & López-Medina, J. (2013). Strawberry yield efficiency and its correlation with temperature and solar radiation. *Horticultura Brasileira*, 31(1), 93–99.

- [11] Hao, X., Zheng, J., Celeste, L., Guo, X. & Kholsa., S. (2017). Liquid desiccant dehumidification system for improving microclimate and plant growth in greenhouse cucumber production. *Acta Hortic*, 1170, 861–866.
- [12] Han, J., Guo, H., Brad, R., Gao, Z. & Waterer, D. (2015). Dehumidification requirement for a greenhouse located in a cold region. *Applied Engineering in Agriculture*, 31(2), 291–300.
- [13] Sultan, M., Ashraf, H., Miyazaki, T., Shamshiri, R.R. & Hameed, I.A., *Temperature and Humidity Control for the Next Generation Greenhouses: Overview of Desiccant and Evaporative Cooling Systems. Next-generation Greenhouses*, IntechOpen Ltd., London, UK, 2021.
- [14] Liu, H. Yang, H. & Qi, R. (2020). A review of electrically driven dehumidification technology for air-conditioning systems. *Applied Energy*, 279, 115863.
- [15] Rahman, M. S., Guo, H., & Han, J. (2021). Dehumidification requirement modelling and control strategy for greenhouses in cold regions. *Computers and Electronics in Agriculture*, 187, 1–14.
- [16] Palencia, P., Martínez, F., Medina, J. J. & López-Medina, J. (2013). Strawberry yield efficiency and its correlation with temperature and solar radiation. *Horticultura Brasileira*, 31, 93–99.
- [17] Basson, C. E., Groenewald, J. H., Kossmann, J., Cronjé, C. & Bauer, R. (2010). Sugar and acid-related quality attributes and enzyme activities in strawberry fruits: Invertase is the main sucrose hydrolysing enzyme. *Food Chemistry*, 121, 1156–1162.
- [18] Li, H., Li, T., Gordon, R.J., Asiedu, S.K. & Hu, K. (2010). Strawberry plant fruiting efficiency and its correlation with solar irradiance, temperature and reflectance water index variation. *Environmental and Experimental Botany*, 168, 165–174.

Chapter 5

Results and discussion of the experiment in the heat exchanger

5.1 Introduction

Among the various types of heat exchangers, serpentine heat exchangers are the most compact and are minimal in terms of the volume of the microchannel coils, without manifolds in their design. This arrangement allows for serpentine coils that are suitable for compact, lightweight cooling applications. Serpentine tubes can be used in laminar flow heat exchange systems, since straight tube heat exchangers allow limited mixing in the laminar flow regime [1]. In addition, a serpentine heat exchanger does not block light in plant photosynthesis, unlike a fin and tube heat exchanger, which is important in cultivation. One thing to note is that this type of heat exchanger is a simple system that works well in greenhouse applications and is simple to maintain.

Controlling air temperature in a controlled room consumes a large amount of energy. In particular, cooling a large space such as the inside of a plant factory consumes more electricity than a small or local area. Accordingly, there are new techniques that can reduce energy consumption and control local air temperature. Thus, in this study, controlling local air temperatures around a plantation area was experimentally investigated. In addition, a cooling serpentine copper pipe heat exchanger was constructed and designed. Experiments in which the fluid supply temperature, fluid flow rate, and heat transfer surface area were controlled were carried out under various operating conditions (see Table 3-13) to investigate the optimum conditions. The thermal performance and local air temperature distributions around a cooling serpentine copper pipe heat exchanger was also investigated. The local temperature was also contoured by graphs in this study.

5.2 Analysis of serpentine heat exchanger

Typically, the operating conditions of heat exchangers remain constant over long periods of time. They are therefore suitable for modeling as steady-flow devices. As a result, each fluid continues to flow at a constant mass rate, and its temperature and velocity are constant at all inlets and outlets. Additionally, the velocities and elevations of the fluid streams change very little or not at all, which results in negligible kinetic and potential energy changes. In general, temperature affects a fluid's specific heat. But with little loss in accuracy, it can be treated as a constant at some average value within a given temperature range.

When heat energy is added to a substance, the temperature changes significantly. From the first law of thermodynamics, the total of heat lost or heat gained ($\dot{Q}_{total,c}$) can be calculated using the equation,

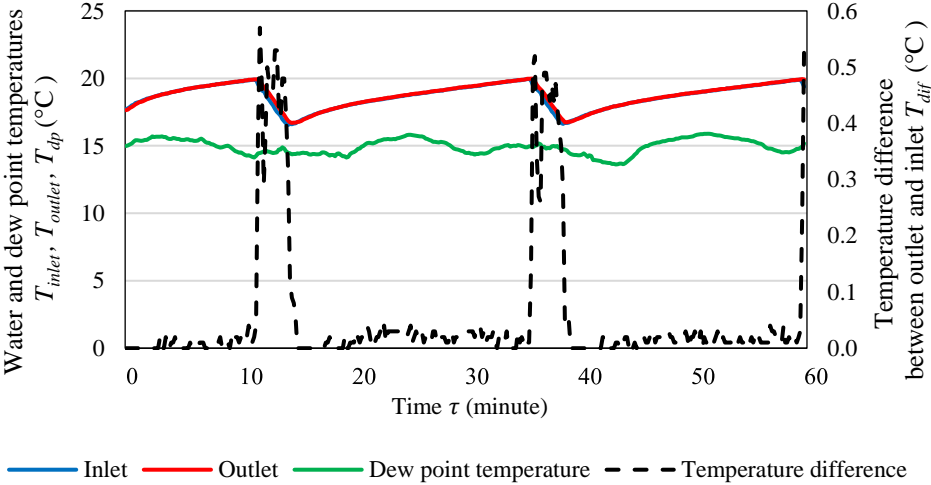
$$\dot{Q}_{total,c} = \dot{m}c_p(T_{outlet} - T_{inlet}) \quad (5.1)$$

where \dot{m} is mass flow rate, c_p is specific heats, T_{outlet} is outlet temperature and T_{inlet} is inlet temperature.

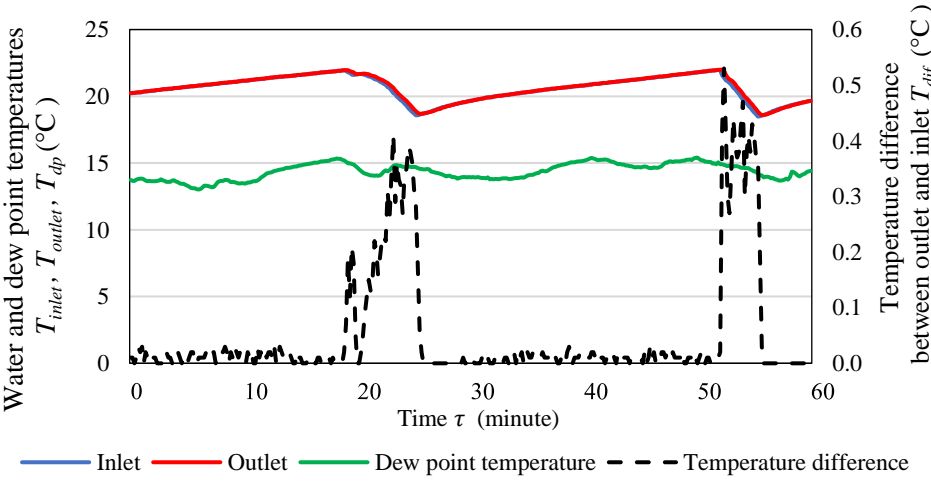
Total heat transfer can also be expressed by the summation of convective heat transfer (\dot{Q}_{conv}) and condensation heat transfer (\dot{Q}_{cond}), equation (5.2) as follows

$$\dot{Q}_{total,c} = \dot{Q}_{conv} + \dot{Q}_{cond} \quad (5.2)$$

In this research, a serpentine copper pipe heat exchanger was built in a laboratory room and the length and width were 870 mm and 330 mm, respectively. To evaluate the heat transfer of this heat exchanger, the temperature difference between outlet and inlet water temperatures (T_{dif}) is significant. Figure 5-1 indicates the temperature difference between outlet and inlet water temperatures when inlet water temperature was set above dew-point temperature ($T_{inlet} = 18.7^{\circ}\text{C}$ and $T_{inlet} = 20.6^{\circ}\text{C}$). From these figures, when delivered inlet water temperature through a serpentine copper pipe within an hour, it was notice that there was no temperature difference between outlet and inlet water temperatures over a period of time. That means there was no heat exchange between water and surrounding. Therefore, the temperature of the inlet water must be set lower than dew-point temperature in this research.



(a) $T_{inlet} = 18.7^{\circ}\text{C}$, $\dot{V} = 2.5 \text{ L/min}$



(b) $T_{inlet} = 20.6^{\circ}\text{C}$, $\dot{V} = 2.5 \text{ L/min}$

Figure 5-1 Showing water and dew-point temperatures along with temperature difference between outlet and inlet water temperatures when inlet water temperature was set above dew-point temperature

5.2.1 Effect of inlet water temperature on water temperature difference

The temperature difference between outlet and inlet water temperatures on volume flow rate was experimentally investigated for different temperatures of inlet water (note that inlet water temperatures were slightly higher than the target inlet water temperature and varied from -5.0 to 6.2°C) as shown in figure 5-2. When the working fluid passed through the serpentine copper pipe heat exchanger, it gained heat from the environment and the outlet water temperature thus increased in all conditions. It was observed that the low volume flow rate (all cases assumed to be a laminar flow, even if the heat exchanger had U-shape curves) resulted in a higher temperature difference between the outlet and inlet water temperatures. The advantages of laminar flow designs include a decrease in thermodynamic and hydrodynamic irreversibility, which leads to an improvement in system effectiveness [2]. The temperature difference between outlet and inlet was low at high volumatic flow rate because if the number of molecules of water flowing through a point is more then it will take more time to heat them up. In addition, it was observed that the inlet water temperature has effect on the conversion of the temperature difference between the outlet and inlet water temperatures at the same flow rate. Furthermore, this graph shows that heat flux through a heat exchanger increases by decreasing inlet water temperature.

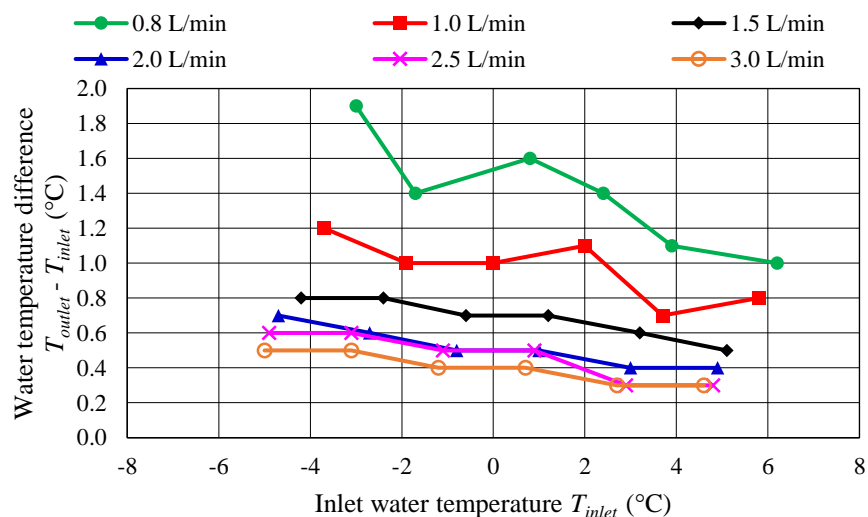


Figure 5-2 The variation of water temperature difference with inlet water temperature for different water flow rates

5.2.2 Pressure drop and pumping power

A pressure drop in the system can be caused by friction or a physical obstruction in the pipe that results in a loss of line pressure. Figure 5-3 (a) and figure 5-3 (b) show the variation of pressure drop and pumping power with inlet water temperature for different water flow rates. The pumping power expenditure is proportional to the total pressure drop, that is experienced by the water across the passage. Figures 5-3 (a) and 5-3 (b) show that pumping power followed the same trend as pressure drop, indicating a direct variation relation. Pressure drop was very small varied from 2 to 76 Pa. It can be seen that the high-volume flow rate resulted in a higher pressure drop. In addition, pressure drop slightly increased at lower inlet water temperature. When pressure drop increases, a proportional need for more pumping. In this study, the water loop is a simple loop. Thus, the pumping power consumption is low. However, the low specific sensible heat can cause the system may work at high inlet water temperatures.

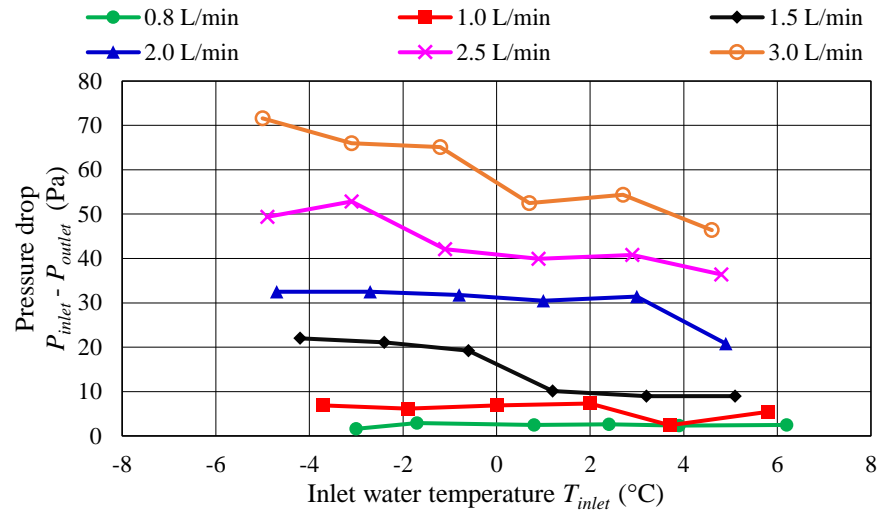


Figure 5-3 (a) The variation of pressure drops with inlet water temperature for different water flow rates

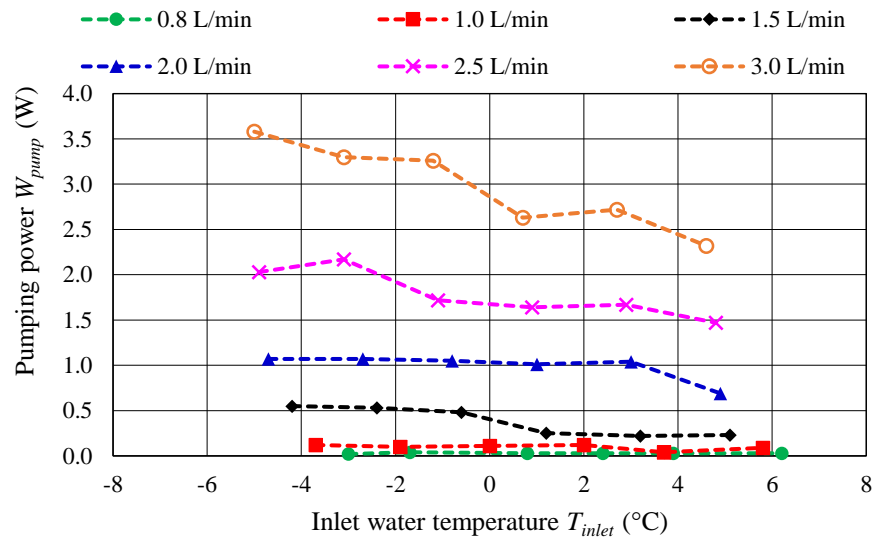


Figure 5-3 (b) Pumping power versus flow rate curves

5.2.3 Rate of heat transfer

Inlet water temperature (T_{inlet}) is an important parameter that significantly influences heat flux and the condensation of the moisture of surrounding air. In this study, room air temperature (T_{room}) was kept at 25°C, while relative humidity (RH) was independent. Thus, dew-point temperature varied from 13 to 18°C (see section 5.3) due to the change in RH during the experiments, and the condensation of moisture occurred. Heat flux through heat exchanger can be calculated using equation (5.1). Figure 5-4 indicates the variation in average heat flux with the inlet water temperature. It can be seen that, because of the difference between the inlet water temperature and the surroundings, the average heat flux significantly increased while the inlet water temperature decreased from 6.2 to -5.0°C. Therefore, a low inlet water temperature was desired for a greater heat flux of the serpentine copper pipe

heat exchanger. This may have been due to the condensation of moisture on the copper pipe surface. From the test results, it was observed that when inlet water temperatures varied from 2.7 to 6.2°C, there was no difference in heat flux under the same flow rate. However, when inlet water temperatures were reduced from 2.7 to -5.0°C, the heat flux significantly increased as volume flow rate increased. Furthermore, when the inlet temperature was lower than the atmospheric dew-point temperature from the chiller, it required more energy (see figure 5-3 (b)) and had insufficient cooling capacity.

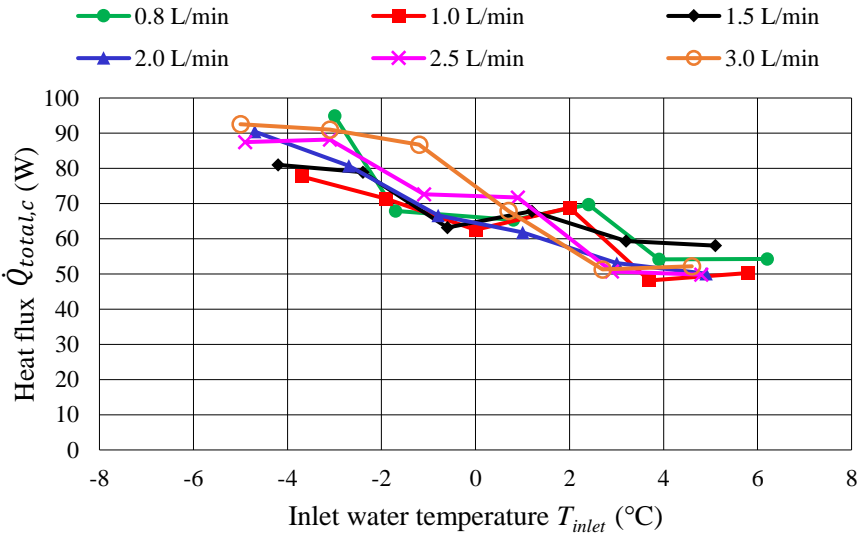


Figure 5-4 Rate of heat transfer versus inlet water temperature at different water flow rates

5.2.4 Convective heat transfer coefficient on the surface

This experiment was carried out in a laboratory room with no solar radiation or induced convection. Thermal insulation sheets were used to cover this system. As a result, it was considered that natural convection is the heat transfer mechanism (or free convection). The convective heat transfer occurred whenever a serpentine copper pipe heat exchanger surface is colder than air surrounding. The convective heat transfer coefficient (h) is commonly utilized in this analysis of external flows around a heat exchanger to express the relevant temperature variation and heat flux. As a result, the convection heat transfer coefficient is affected by, 1) fluid thermophysical characteristics and 2) fluid velocity. Figure 5-5 shows the variation in the convective heat transfer coefficient with inlet water temperature for different flow rates. The values plotted are calculated for a room temperature ($T_{room} \approx 25^\circ\text{C}$) and for a copper pipe with an outer diameter of 12.7 mm. Results can be seen that convective heat transfer coefficient were close to each other under the same water flow rate. The reduction in inlet water temperature slightly affect the convective heat transfer coefficient. Convective heat transfer coefficient increased with inlet water temperature decreased. The convective heat transfer coefficient varied from 6.7 to 7.3 $\text{W}/\text{m}^2\text{K}$ during this study. The air movement surrounding the copper pipe affects the convective heat transfer coefficient as well. Consequently, it can be said that under any conditions, the air movement around copper pipe is the same.

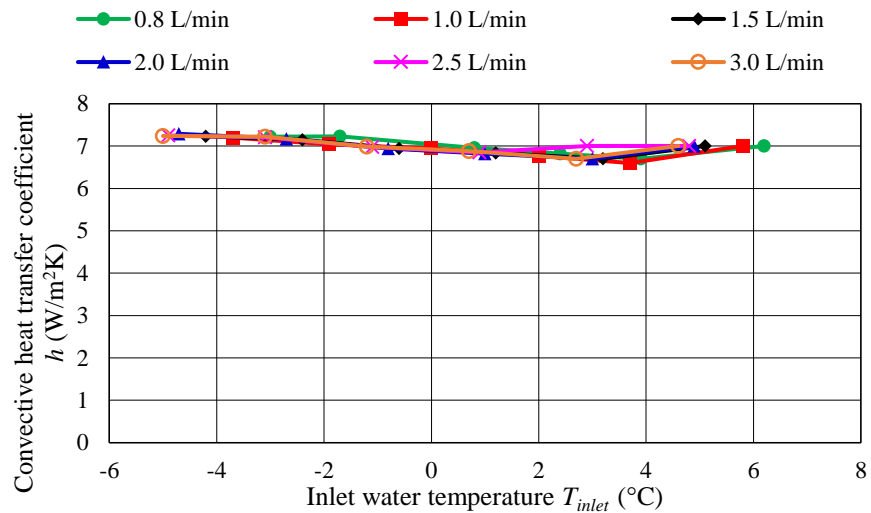


Figure 5-5 Variation in the convective heat transfer coefficient with inlet water temperature for different water flow rate

Convective heat transfer occurs when heat exchanger surface is colder than surrounding fluid. The basic equation for the rate of convection heat transfer is known as

$$\dot{Q}_{conv} = hA_s(T_\infty - T_s) \quad (5.3)$$

where h is the convective heat transfer coefficient, A_s is the surface area of heat exchanger being cooled, T_∞ is the temperature of the surrounding fluid, and T_s is the surface temperature of the heat exchanger. Figure 5-6 can be seen that convective heat transfer trended to be increase while inlet water temperature decreased. A low inlet water temperature resulted in higher convective heat transfer coefficient. Low inlet water temperature strongly influenced on surface temperature of the copper pipe. Thus, this may increase the rate of convective heat transfer.

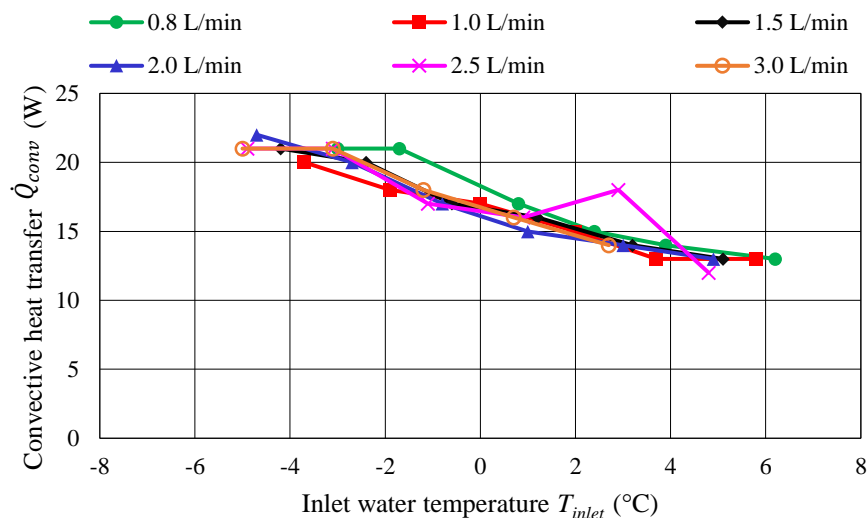


Figure 5-6 Variation in the convective heat transfer with inlet water temperature for different water flow rate

5.3 Condensation heat transfer

Condensation is the process of converting a medium from a vapor to a liquid by removing its heat. The condensation phenomenon occurs when a medium that is initially in the vapor state is cooled and its phase changes from vapor to liquid. Condensation can be divided into film condensation and dropwise condensation depending on the surface wettability. The observation of moist air condensing on copper pipe is shown in figure 5-9 to figure 5-14. It can be observed that the gradual change in condensation mode from dropwise condensation to film condensation. Therefore, the condensation was assumed to be film condensation throughout the experiment. In this study, inlet water temperature all cases were lower than dew-point temperatures. The condensation heat transfer can be expressed by using equation (5.4) and equation (5.5).

$$\dot{Q}_{cond} = \dot{Q}_{total,c} - \dot{Q}_{conv} \quad (5.4)$$

$$\dot{Q}_{cond} = h_{horiz} A_s (T_{\infty} - T_s) \quad (5.5)$$

The evaluation of condensation heat transfer coefficient follows equation (5.6) which considers the effect of free or natural convection.

$$h_{horiz} = \frac{\dot{Q}_{cond}}{A_s (T_{\infty} - T_s)} \quad (5.6)$$

where h_{horiz} is the condensation heat transfer coefficient of a horizontal tube, A_s is the surface area of heat exchanger being cooled, T_{∞} is the temperature of the surrounding fluid, and T_s is the surface temperature of the heat exchanger.

As a result of cooling, condensation is the phase transition from the vapor state to the liquid state. Figure 5-7 indicates the variation in condensation heat transfer with the inlet water temperature. It can be seen that condensation heat transfer profile follows the trend of total heat transfer. At the same inlet water temperature, higher condensation heat transfer is obtained at high water volume flow rate. At constant water volume flow rate the condensation heat transfer decreased with increasing inlet water temperature. Thus, the condensation rate and water flow velocity are higher for the experiments conducted at high water volume flow rate. It is generally known that high water flow rates and velocities have a remarkable impact on heat transfer. High interfacial shear stress causes the water film to thin, resulting in an increase in condensation heat transfer.

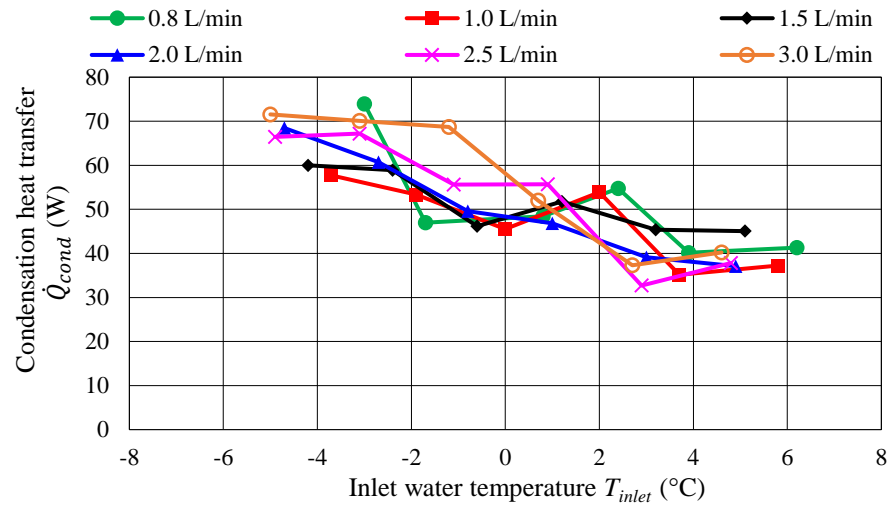


Figure 5-7 Condensation heat transfer with inlet water temperature for different water flow rate

Figure 5-8 indicates condensation heat transfer coefficient with inlet water temperature for different water flow rate. Results show that condensation heat transfer coefficient (h_{horiz}) varied from 16 to 25 W/m²K and it was be noticed that as the inlet water temperature increased, the condensation heat transfer coefficient showed tendency to decrease. It was also found that at the same water volume flow rate, higher condensation heat transfer coefficients are obtained at low inlet water temperatures. Consequently, increasing water volume flow rate led to increase in condensation heat transfer coefficient. From the experiments, it was observed that heat transfer rate is directly proportional to the inlet water temperature and heat transfer rate is related with droplets size, number of droplets as well as film thickness. Thermal resistance increases with increasing film thickness and number of droplets on copper pipe [3]. Therefore, these parameters affect the reduction in condensation heat transfer coefficient. It was observed that low inlet water temperature and high-water volume flow rate resulted in thinner film thickness and small amount of water droplets. The observation of the condensing on the copper pipe is described in details.

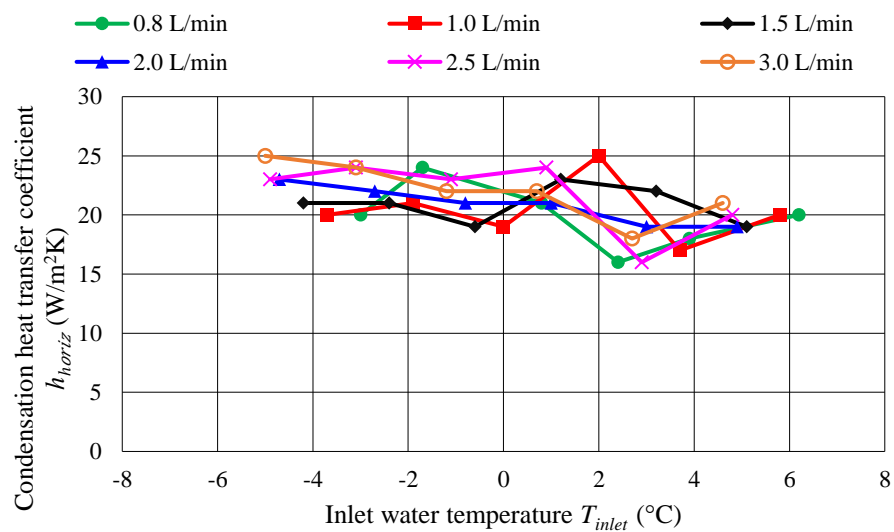


Figure 5-8 Condensation heat transfer coefficient with inlet water temperature for different water flow rate

Figures 5-9 to 5-14 depict the observation of wet air condensing on copper tubing. In this research, the dew-point temperature varied from 13 to 18°C. When surrounding air was cooled to its dew-point temperature, droplets occurred on copper pipe. It can be seen that dropwise condensation can be obviously seen at high inlet water temperature and low volume flow rate (see figure 5-9 to 5-14). When increased the volume flow rate, the droplet sizes increased. Then, the dropwise condensation gradually changed to water film condensation due to flooding.

From figure 5-12 and 5-13, it can be noted that there was no difference in water droplets sizes on the pipe. In addition, film condensation is noticeable without dropwise condensation. A large number of water droplets dripped by gravity. Thus, only a few drops of film can be seen on the pipe. In addition, the thickness of liquid film is very thin compared with tube diameter. Reducing liquid film thickness led to reduced thermal resistance. Therefore, that process led to increase in the condensation heat transfer coefficient and condensation heat transfer.

When reducing the inlet water temperature to -6°C, it can see that the copper pipe was covered by ice (at $T_{inlet} = -4.2^\circ\text{C}$, $\dot{V} = 1.5 \text{ L/min}$) as shown in figure 5-14. Under the conditions of low volume flow rate (low Re) and low inlet water temperatures, the ice gradually increased in thickness and finally all of copper pipes were covered by ice. The formation of ice requires heat and mass transfer due to the latent heat of fusion generated in the process.

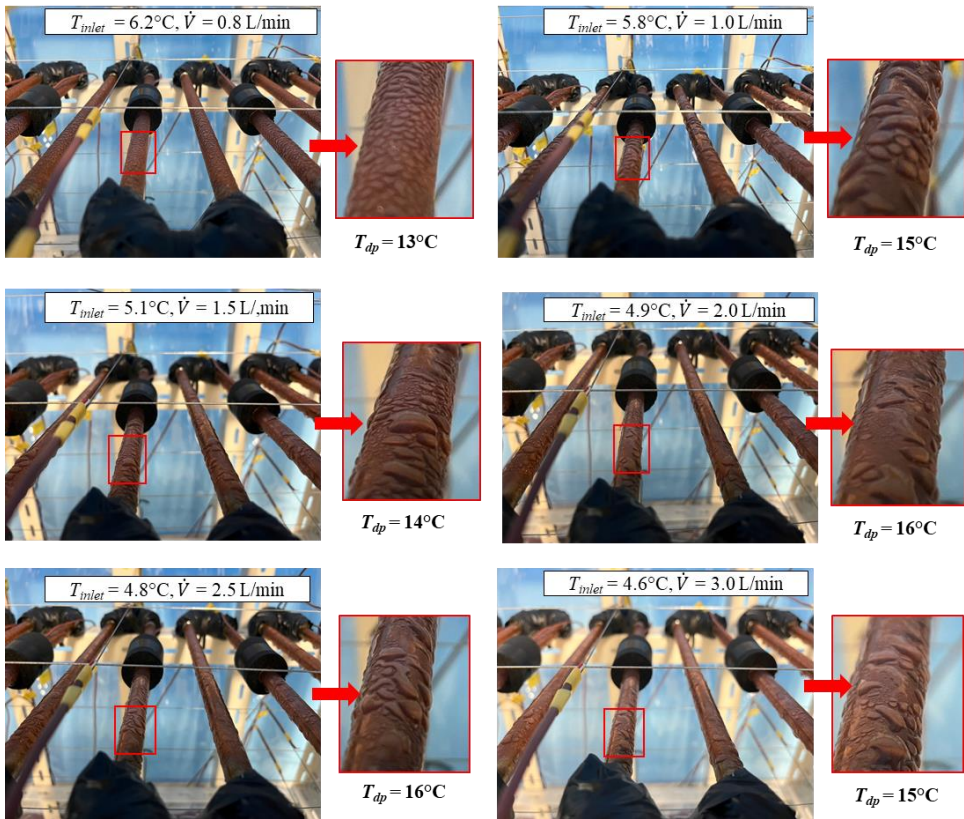


Figure 5-9 Photo of moist air condensing on copper pipe (at $T_{inlet,t} = 4^\circ\text{C}$)

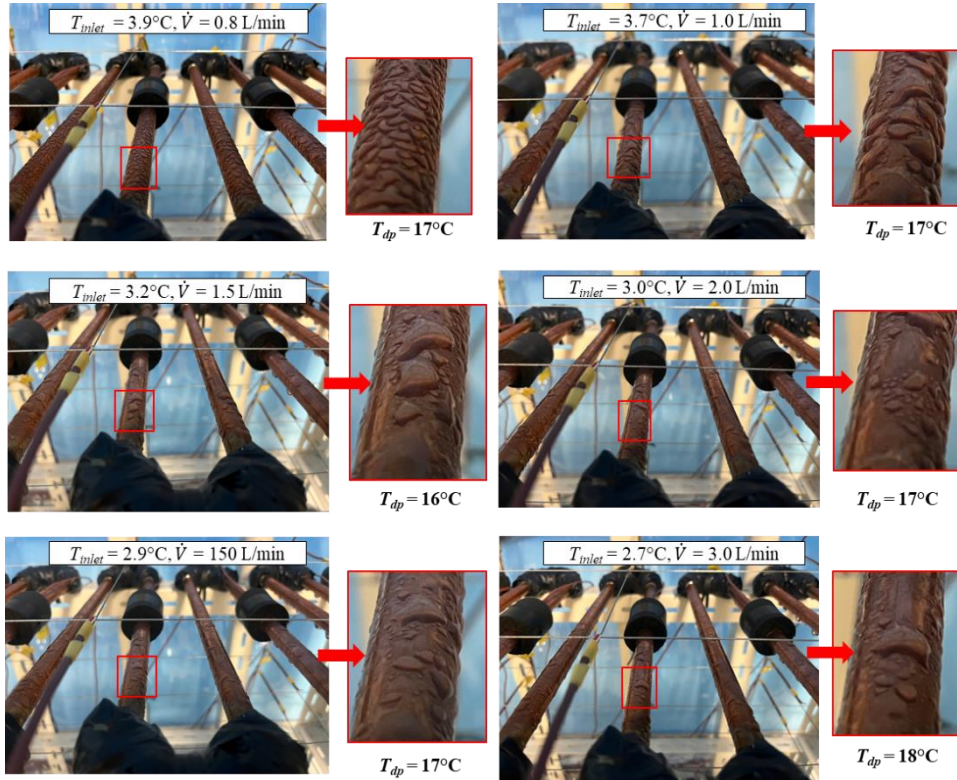


Figure 5-10 Photo of moist air condensing on copper pipe (at $T_{inlet,t} = 2^\circ\text{C}$)

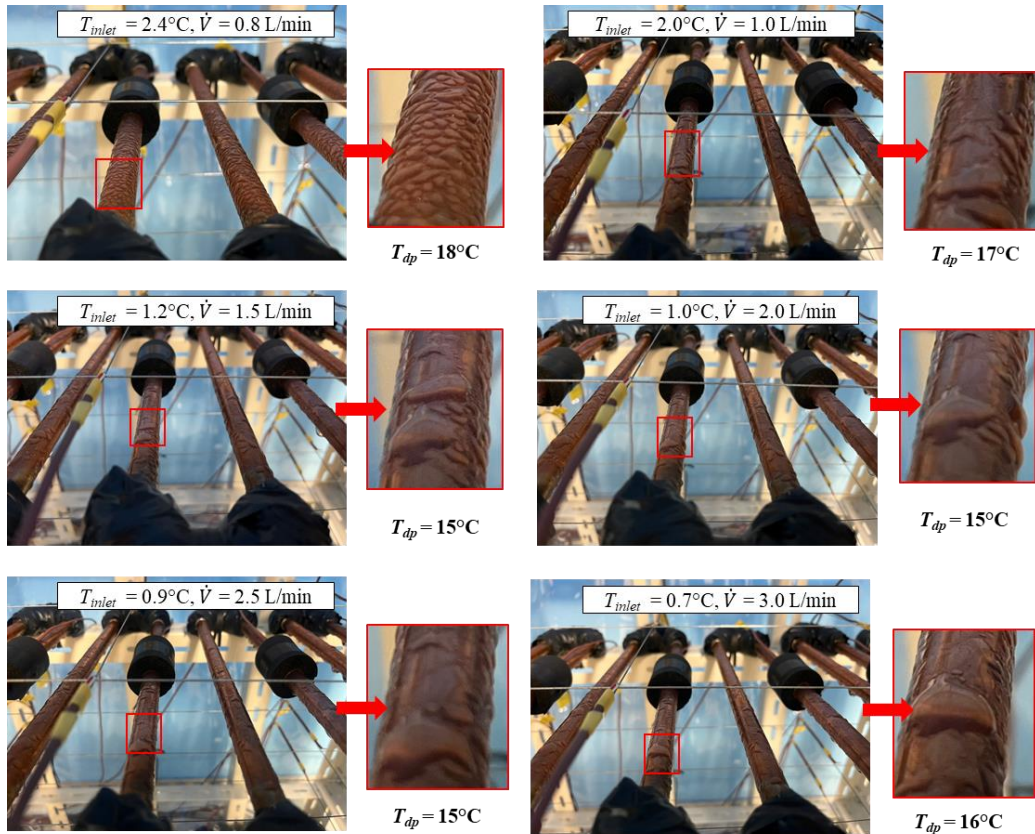


Figure 5-11 Photo of moist air condensing on copper pipe (at $T_{inlet,t} = 0^\circ\text{C}$)

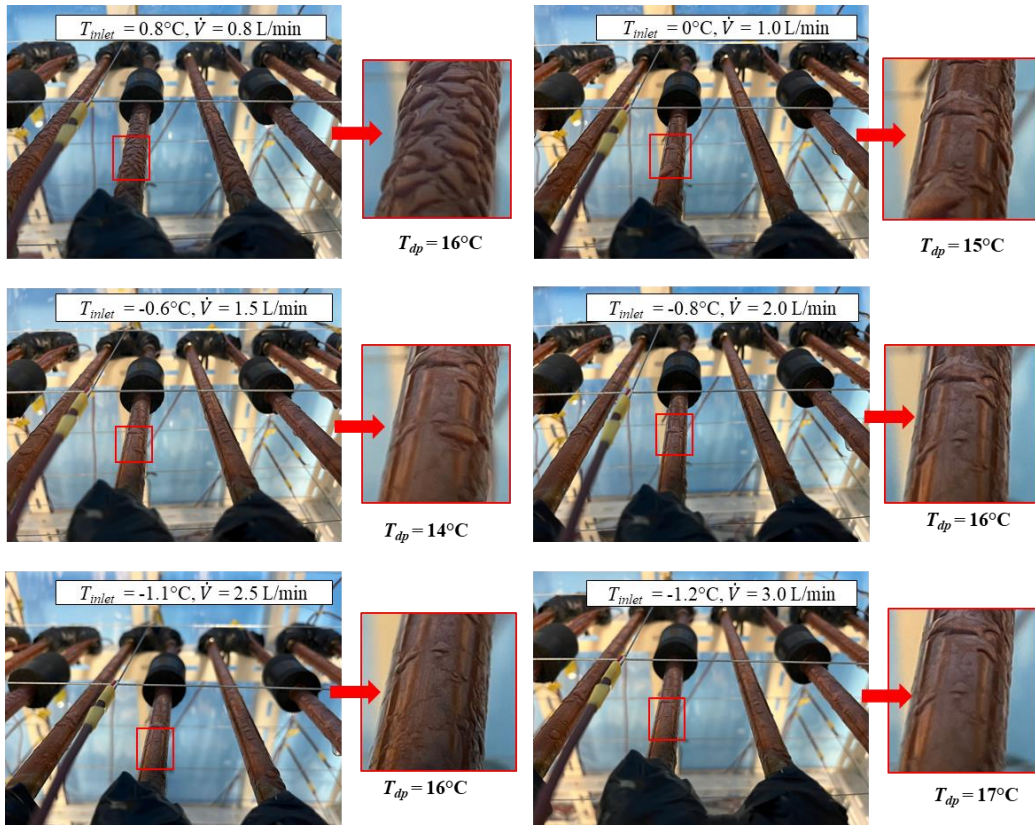


Figure 5-12 Photo of moist air condensing on copper pipe (at $T_{inlet,t} = -2^{\circ}\text{C}$)

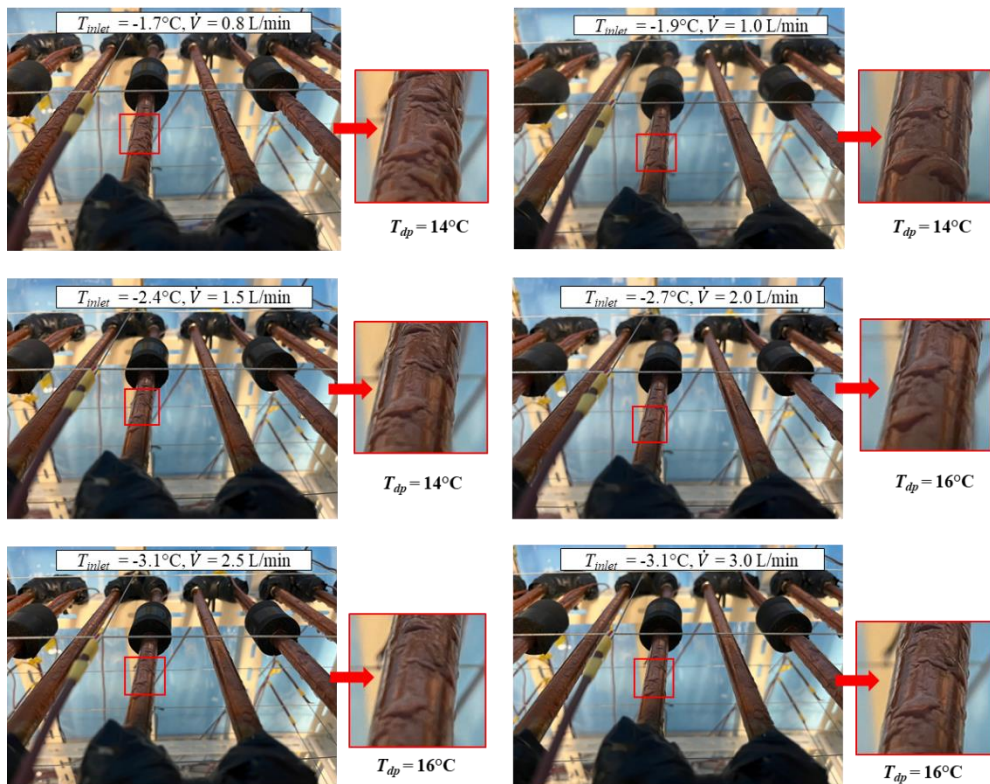


Figure 5-13 Photo of moist air condensing on copper pipe (at $T_{inlet,t} = -4^{\circ}\text{C}$)

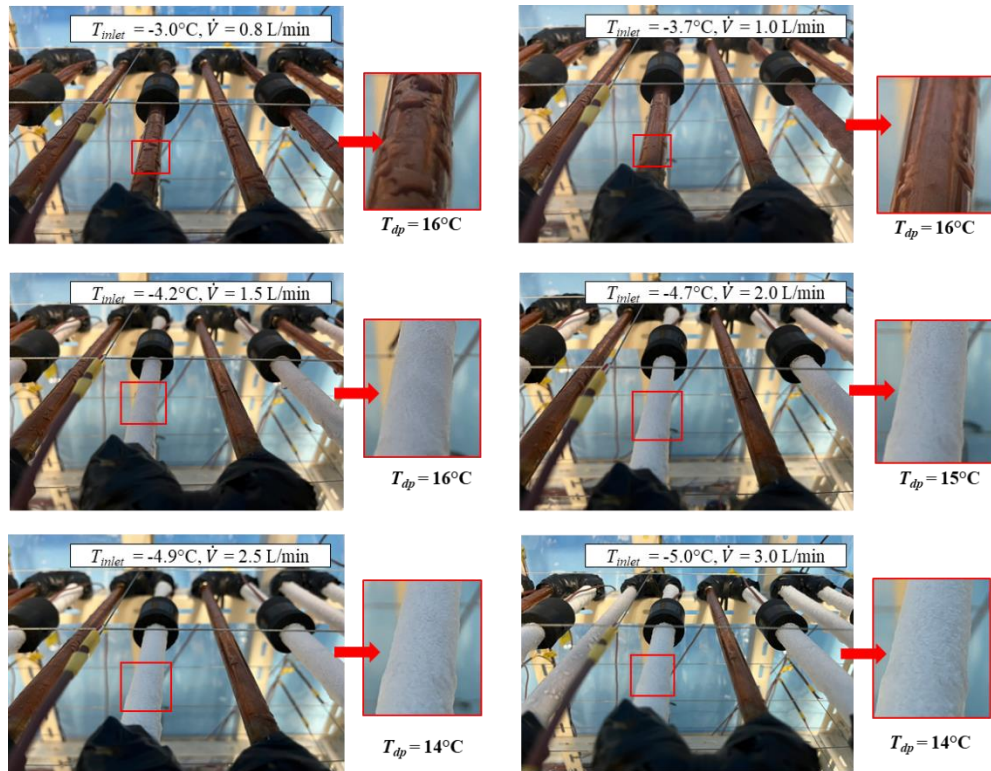


Figure 5-14 Photo of moist air condensing on copper pipe (at $T_{inlet,t} = -6^{\circ}\text{C}$)

5.4 Local air temperature profiles

To investigate local air temperature distributions, air temperatures around the serpentine copper pipe heat exchanger were measured. The inlet water temperature ranged from 6.2 to -5.0°C with different water flow rates in this study. In addition, only four conditions were selected as examples. Figure 5-15 shows air temperature measurement layout and the plotting positions of air temperature contour plots. Air temperatures were measured both above and below the serpentine copper pipe at different vertical positions. There are two vertical different positions above the pipe and three vertical different positions below a pipe. The air temperatures above the pipe were defined at -50 and -100 mm. The air temperatures below the pipe were defined at 50 , 100 , and 150 mm, respectively. For contour plotting, plane A and plane B mean local air temperature at 100 mm and 50 mm above a copper pipe. Plane C, plane D and plane E mean local air temperature at 50 mm, 100 mm and 150 mm below a copper pipe, respectively.

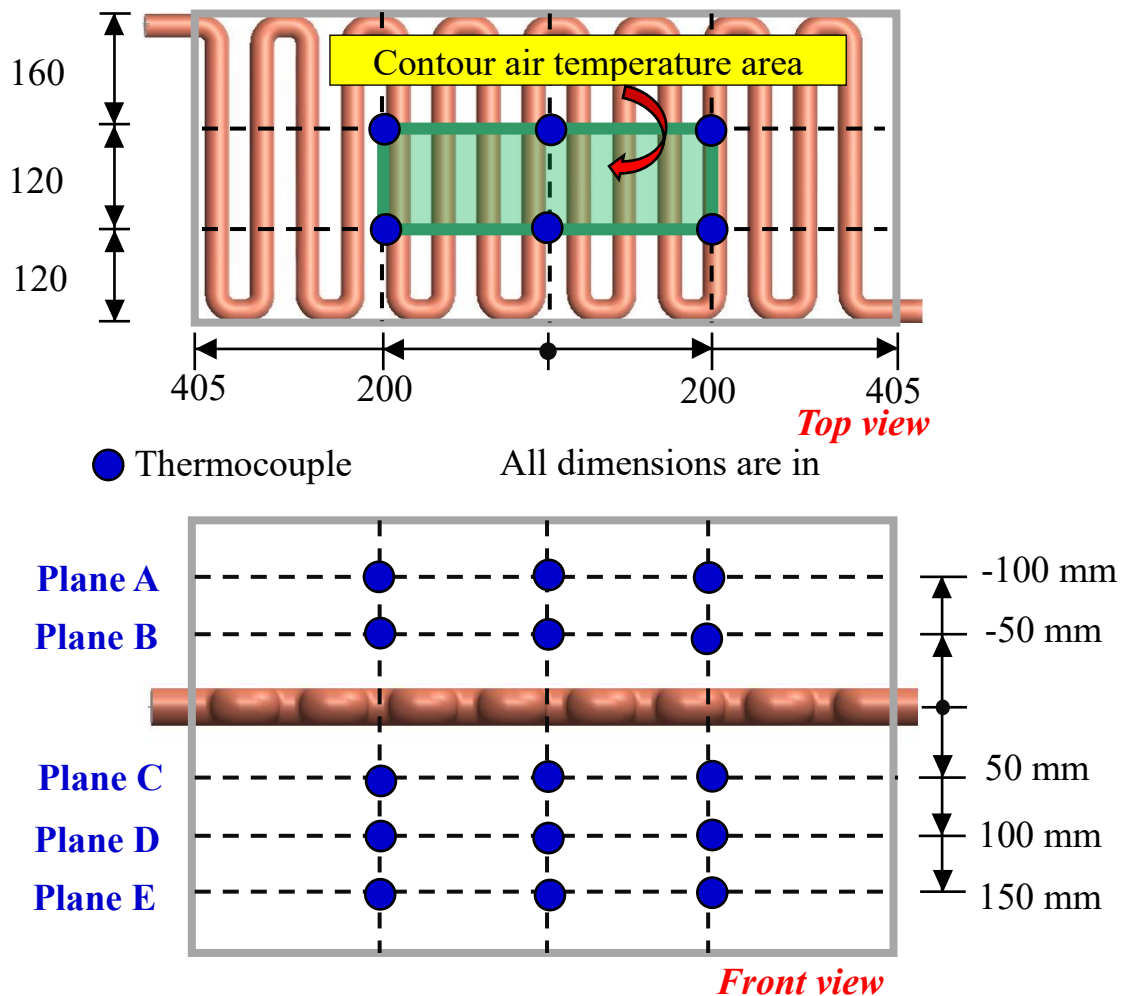
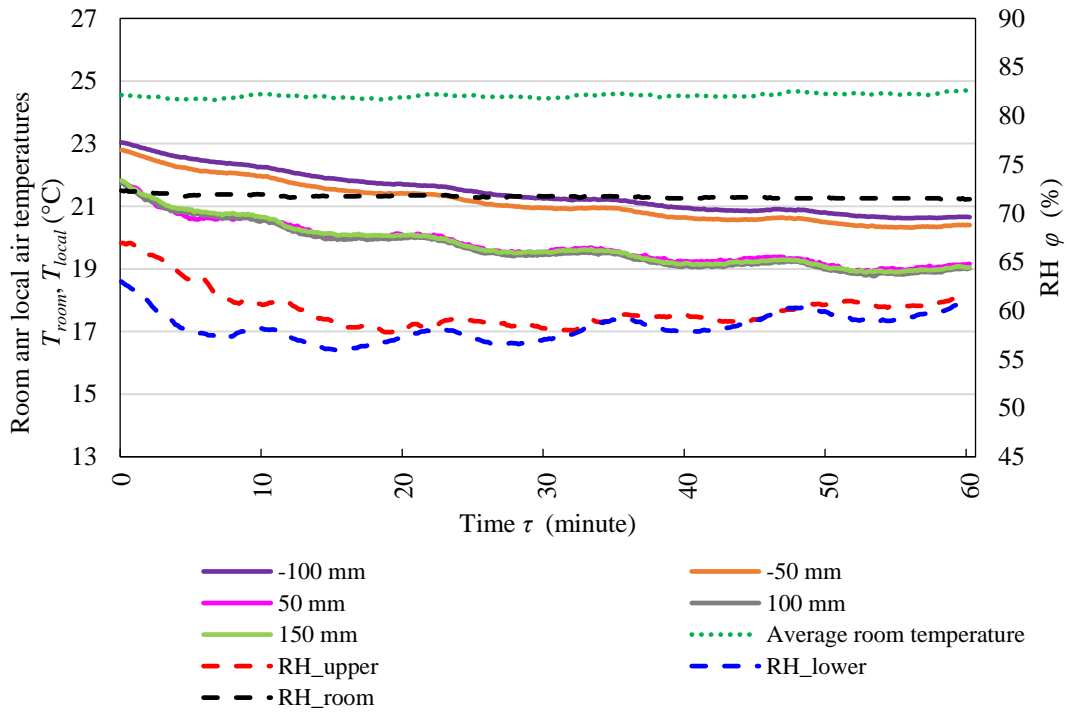


Figure 5-15 Showing the plotting positions of air temperature contour plots

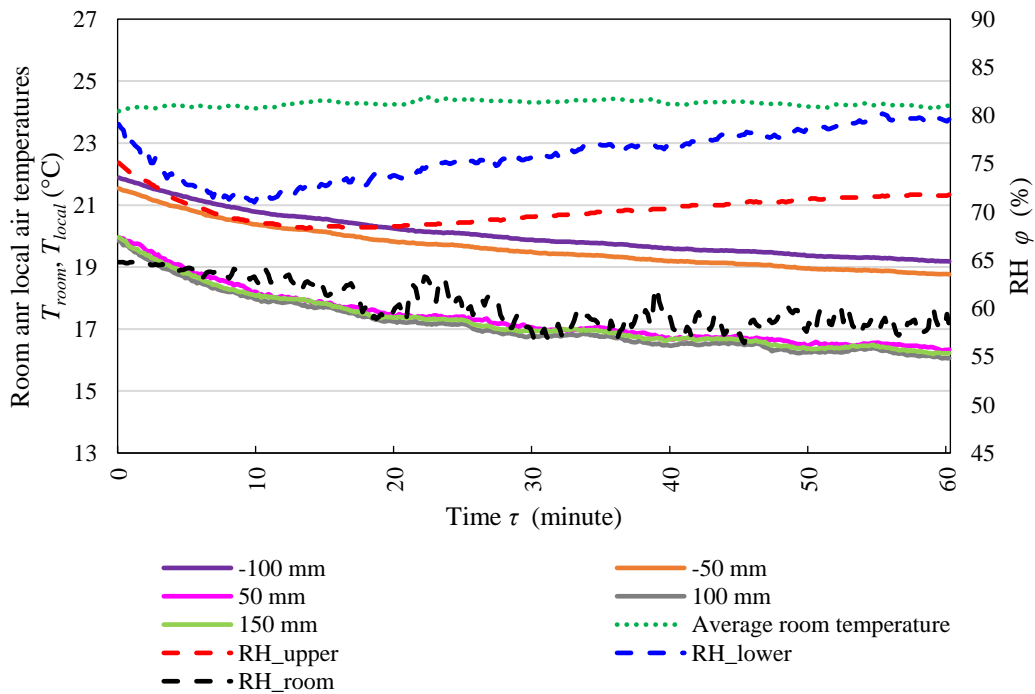
Figure 5-16 shows the comparison of air temperature over time under different inlet water temperatures when the flow rate was unchanged. Note that room air temperature was set at 25°C. A similar trend of air temperature distribution over time was observed both above and below the copper pipe in the four conditions. After the experiment began, the local air temperatures slightly decreased. They reached a steady state when a thermal equilibrium in the indoor environment was achieved. In addition, they were lower than the room air temperature and were separate from each other. The air temperature difference occurred in a vertical direction due to natural convection.

As shown in Figure 5-16 (a), air temperatures above the pipe were approximately 21°C, while air temperatures below the pipe were about 19°C. However, when the inlet water temperature was reduced to -3°C, the local air temperatures below the pipe reached around 16 °C, approximately 8°C less than the room air temperature, as shown in figure 5-16 (b) same as the behavior of figure 5-16 (c) and figure 5-16 (d). When increasing volume flow rate to 3.0 L/min, the lowest local air temperature could reach about 13°C that means approximately 9°C lower than room temperature as seen in figure 5-16 (d). This result may be due to the condensation of moisture on the pipe surface. The pipe surface fell below the dew-point temperature, which varied from 13 to 18°C. These values depended on the *RH*. When air around the pipe contacted the pipe surface, it condensed and created water droplets and frozen

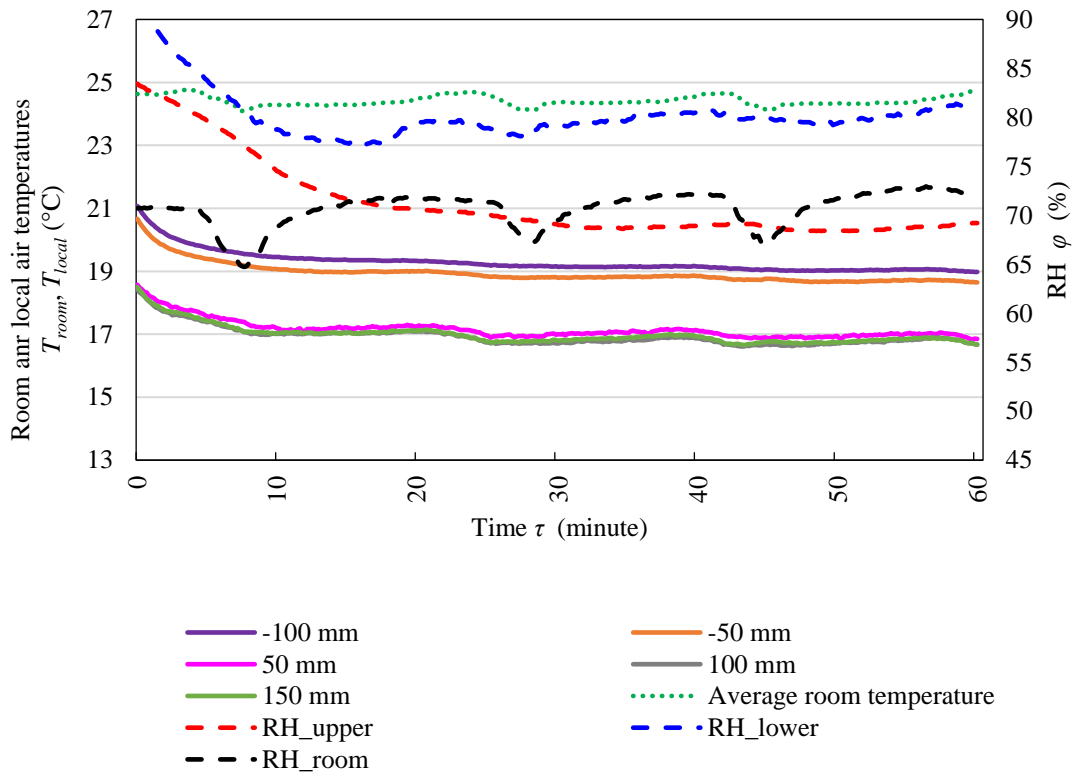
droplets. Moreover, the local air temperatures below the pipe were not significantly different due to the low airflow during the experiments.



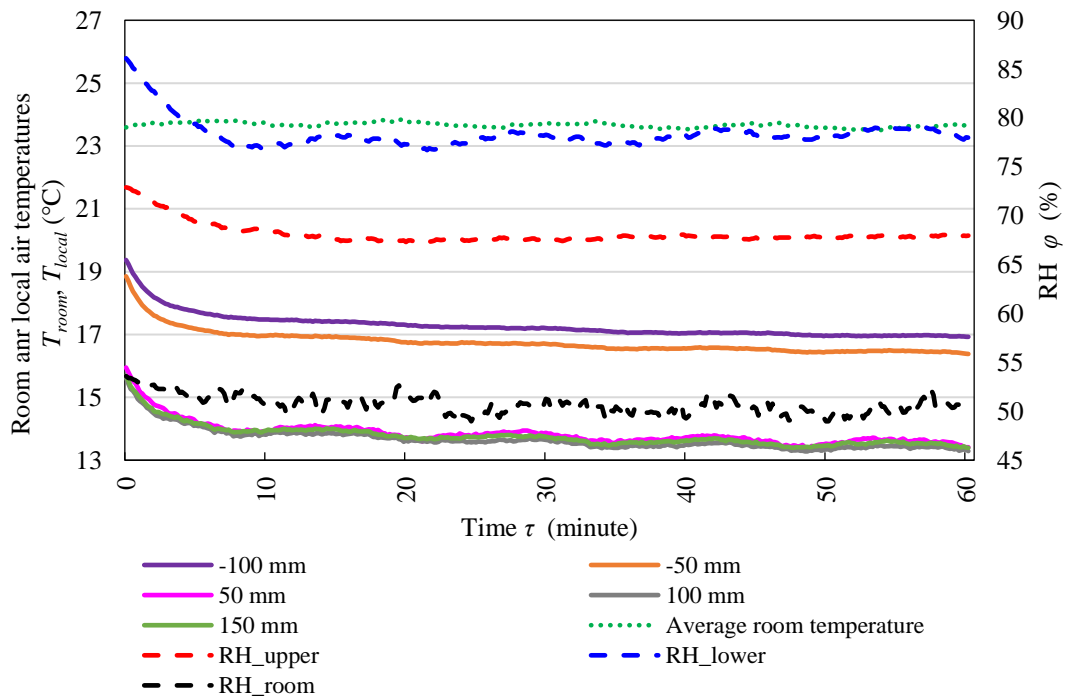
(a) $T_{inlet} = 6.2^{\circ}\text{C}$ ($T_{inlet,t} = 4^{\circ}\text{C}$), $\dot{V} = 0.8 \text{ L/min}$



(b) $T_{inlet} = -3.0^{\circ}\text{C}$ ($T_{inlet,t} = -6^{\circ}\text{C}$), $\dot{V} = 0.8 \text{ L/min}$



(c) $T_{inlet} = 4.6^{\circ}\text{C}$ ($T_{inlet,t} = 4^{\circ}\text{C}$), $\dot{V} = 3.0$ L/min

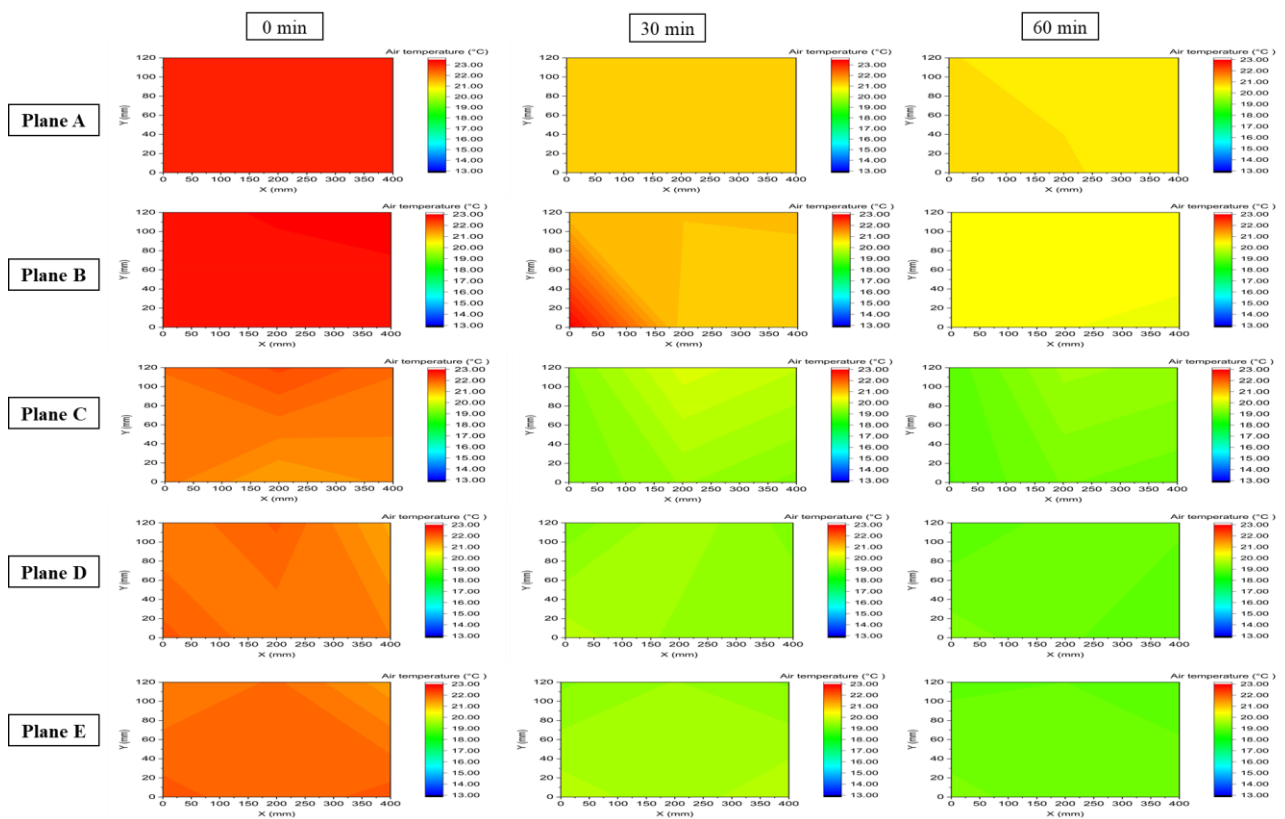


(d) $T_{inlet} = -5.0^{\circ}\text{C}$ ($T_{inlet,t} = -6^{\circ}\text{C}$), $\dot{V} = 3.0$ L/min

Figure 5-16 Air temperature distribution over time τ under different inlet water temperatures and flow rates

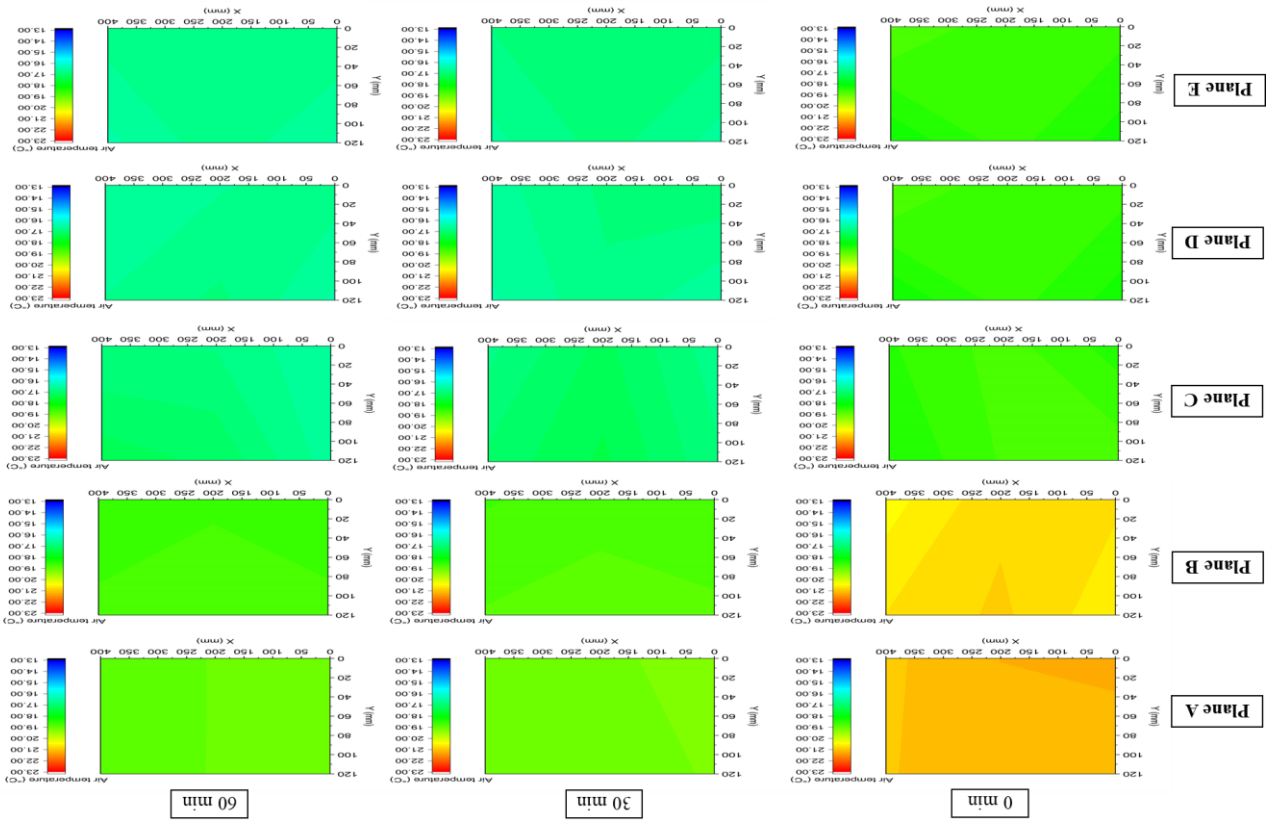
The contour graph was plotted to clearly visualize the temperature difference. The contour graphs were plotted under different vertical positions and were plotted under different time. First of all, graph was plotted before system startup (0 minute) and was plotted after 30 and 60 minutes to examine the change of local air temperature. From figure 5-17, it can be seen that before running cooling system, local air temperatures above (Plane A and Plane B) and below (Plane C, Plane D and Plane E) a copper pipe were slightly different. However, after 30 minutes, local air temperature changed approximately 2°C below the starting point. Then, during 30 to 60 minutes, local air temperature reached a steady state. There was no difference of local air temperature between these periods.

Results show that inlet water temperature greatly affected local air temperature when the flow rate was unchanged. A low inlet water temperature could reduce local air temperature more than a higher water temperature. The comparison results show in figure 5-17 (a) and 5-17 (b) as well as figure 5-17 (c) and 5-17 (d). According to the test results, it can be seen that a serpentine copper pipe has the potential to reduce indoor local air temperatures. However, the observation was made that increasing the water volume flow rate did not strongly affect the air temperature distribution. Thus, choosing an appropriate water volume flow rate and inlet water temperature can provide a desired local air temperature as well as reducing energy consumption.

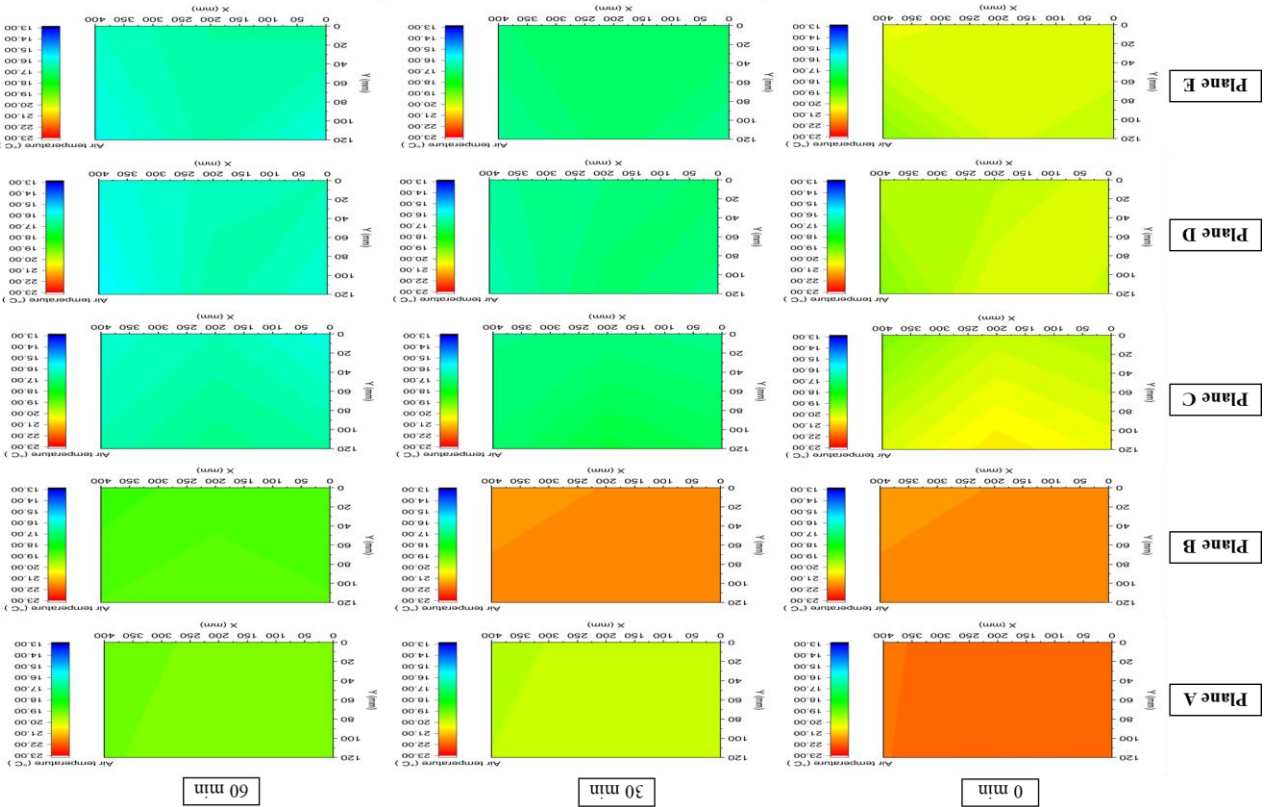


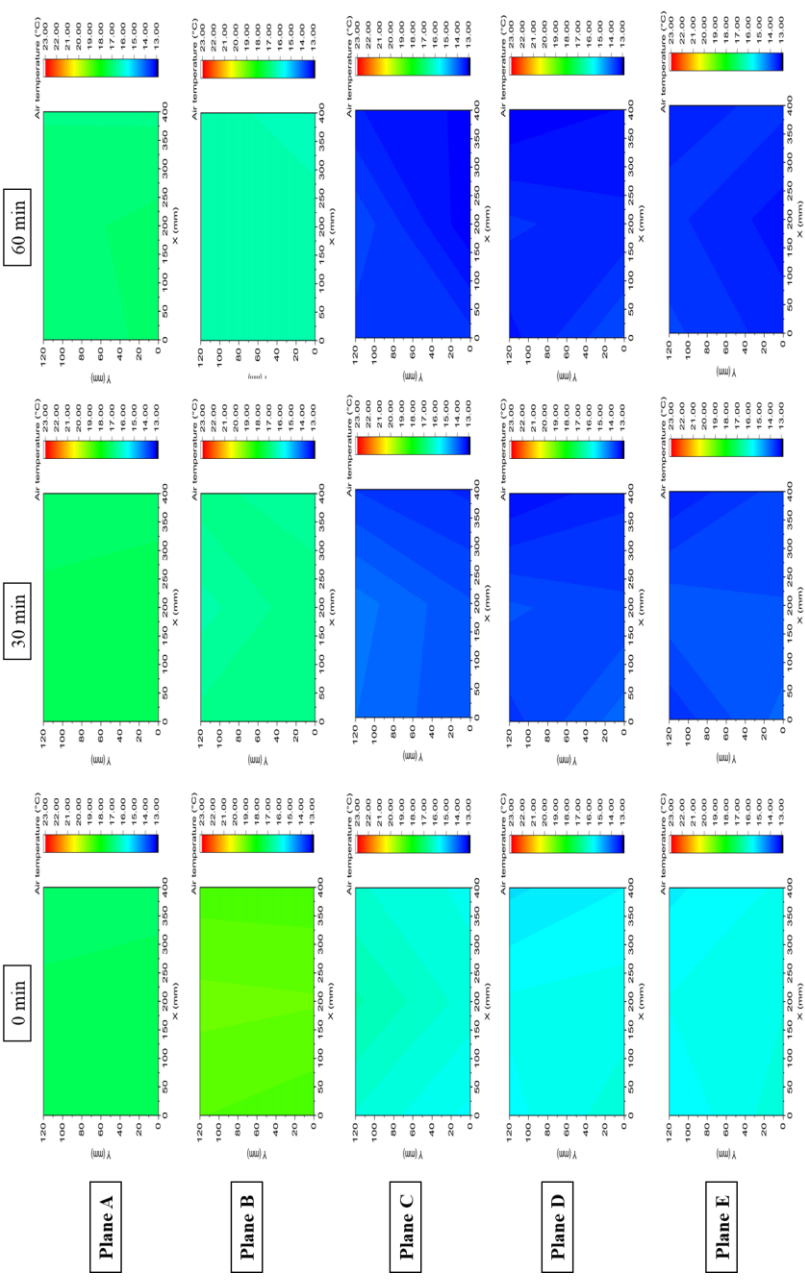
(a) $T_{inlet} = 6.2^{\circ}\text{C}$, $\dot{V} = 0.8 \text{ L/min}$

(c) $T^{inlet} = 4.6^{\circ}\text{C}, V = 3.0\text{L/min}$



(b) $T^{inlet} = -3^{\circ}\text{C}, V = 0.8\text{L/min}$





(d) $T_{inlet} = -5^{\circ}\text{C}$, $\dot{V} = 3.0 \text{ L/min}$

Figure 5-17 Air temperature contour graphs

Summary

In this chapter, controlling local air temperatures around a local area was experimentally investigated. A cooling serpentine copper pipe heat exchanger was constructed. The experiments were conducted in a laboratory-room under various operating conditions. It can be seen that the temperature of inlet water and volume flow rate greatly influenced on total heat flux, condensation heat transfer and convective heat transfer. Increasing water volume flow rate and reducing inlet water temperature led to increase in rate of heat transfer. It was observed that low inlet water temperature and high-water volume flow rate resulted in thinner film thickness and small amount of water droplets. Thermal resistance increases with increasing film thickness and number of droplets on copper pipe. In terms of volume flow rate, a high-volume flow rate has a strong effect to pressure drop as well as pumping power. It can be seen that the high-volume flow rate resulted in a higher pressure drop. In addition, pressure drop increased at lower inlet water temperature. When pressure drop increases, a proportional need for more pumping.

A distribution of air temperatures will occur upon starting the cooling system. In the experiment, air temperatures below and above the serpentine copper pipe were less than room air temperature ($T_{room} = 25^{\circ}\text{C}$). The local air temperatures dropped slightly after the experiment began. They reached a steady state (around 30 minutes) when the indoor environment approached thermal equilibrium. Furthermore, they were cooler than the surrounding air and distinct each other. Natural convection caused the temperature difference in the air to move upward. As the same volume flow rate, inlet water temperature has significantly influenced on local air temperature. The local air temperature was reduced by approximately 5 and 9°C .

From air temperature contour graphs, local air temperatures above (Plane A and Plane B) and below (Plane C, Plane D, and Plane E) a copper pipe were slightly different before the cooling system was turned on. However, after 30 minutes, the local air temperature dropped by about 2°C below the starting point. The local air temperature then stabilized for 30 to 60 minutes. The local air temperature did not change between these times. In conclusion, a serpentine copper pipe is useful for managing local air temperature and lowering energy usage as compared to typical air conditioning.

References in chapter 5

- [1] Timothy, J.R. & Vijaya, G.S.R. (2005). Experimental studies of a double-pipe helical heat exchanger. *Thermal and Fluid Science*, 29, 919–924.
- [2] Doty, F. D., Hosford, G., Jones, J. D. & Spitzmesser, J. B. (1990). Proceedings of the 25th Intersociety Energy Conversion Engineering Conference (Reno), 4, 1–7.
- [3] Arslan, G. & Eskin, N. (2015). Heat transfer characteristics for condensation of R134a in a vertical smooth tube. *Experimental Heat Transfer*, 28(5), 430–445.

Chapter 6

Conclusions

An experimental study was performed to investigate the effects of environmental factors on strawberry cultivation in a greenhouse and estimate the heat energy required for maintaining an optimum temperature inside the greenhouse during winter. The experimental site was located in Mie prefecture, Japan. The results of the study indicate that the greenhouse can provide favorable environmental conditions for strawberry plants. Generally, supplemental heating is not required during the daytime because solar radiation is sufficient to maintain the temperature inside the greenhouse high enough for strawberry cultivation even in winter. The maximum temperature difference between the inside and ambient air temperatures was 16.4°C, whereas the maximum reduction in solar radiation was approximately 30% when compared with ambient solar radiation in this greenhouse. These values depend on the quality of the vinyl sheet and weather conditions. The measured weather data indicated that the inside temperature was rather low during nighttime in winter; therefore, the use of a heating system is recommended during in this period.

The calculated maximum heating requirement was from November 2020 to April 2021. The monthly heating requirement ranged from 60.0 to 327.6 MJ/(m²·month) and 47.0 to 281.9 MJ/(m²·month), when the design temperatures for heating were 10°C and 8°C, respectively and the heat energy requirement was found to be maximum in January, with the lowest nighttime ambient temperature of -4.4°C. The results of this study can serve as a reference for agricultural greenhouses in temperate and tropical climates. Because some plants are sensitive to temperature differences, greenhouses can offer a means of controlling the environment for optimal plant growth in such cases. Based on the temperature conditions, a climate-controlling system, such as a heating or cooling system, may be required to grow plants in greenhouses. Therefore, having access to calculations/estimates of the energy requirements in greenhouses is essential. The estimation of the greenhouse energy balance can be used as a reference point for calculating the energy requirements of both heating and cooling systems. Moreover, the estimate may be useful for calculating the energy costs. The results of this study indicate that passive solar heating may need to be supplemented with gas- or electricity-based heating systems in cold areas with long periods of cloudy weather.

Environmental factors including solar radiation, air temperature and relative humidity were monitored and recorded during the experiment. Additionally, the harvesting time was different; (1) the first harvest was during the peak season on 20 February 2021, and (2) the second harvest is at the end of the season on 5 April 2021. Eight samples of strawberry were harvested during each period and their size, weight and SSC were measured and compared to each other. The difference between day and night air temperatures may cause an increase in fruit SSC. Based on these results, we conclude that temperature difference is one of major factors responsible for the end-season decline in the SSC, firmness and color of strawberry fruits in a temperate production system. In both seasons, it was observed that temperature did not affect strawberry weight. Increasing temperatures lead to the decline in SSC at the end of the season. The relative humidity was not significantly different between the two seasons. In addition, it can be seen that solar radiation at the end of the season was slightly higher than solar radiation during the peak season. Furthermore, it can be stated that fluctuations in solar radiation are not likely to have a major effect on fruit SSC. In addition, other factors such as the age of plants and the predominant order of harvested fruit could

affect fruit SSC independently. Thus, it can be concluded that temperature difference is a major factor responsible for the quality of strawberries.

In this study, a cooling serpentine copper pipe heat exchanger was constructed and designed in a laboratory-scale room. Moreover, heat flux and local air temperature distributions around this exchanger was investigated. The experiments were carried out under various operating conditions, in which the fluid supply temperature, fluid flow rate, and heat transfer surface area were controlled. The calculation and measurements showed that a cooling serpentine copper pipe heat exchanger can reduce local air temperatures. When room air temperature was 25°C, the cooling serpentine copper pipe heat exchanger could reduce the local air temperatures around it. The local air temperature was 5 to 9°C below room air temperature under different inlet water temperatures and water flow rates. Based on the results, it can be seen that the temperature of inlet water and volume flow rate greatly influenced on total heat flux, condensation heat transfer and convective heat transfer. Increasing water volume flow rate and reducing inlet water temperature led to increase in rate of heat transfer. In addition, heat transfer rate is directly proportional to the inlet water temperature and heat transfer rate is related with droplets size, number of droplets as well as film thickness. Thermal resistance increases with increasing film thickness and number of droplets on copper pipe. It was also observed that condensation around the pipe could increase the reduction in local air temperature. According to the local air temperature profiles, there was no variation in air temperature at the same horizontal level. However, there was a temperature difference between vertical positions due to natural convection. That means this cooling system could reduce local air temperature below it and can be applied to cool air temperature in the local space. In summary, this novel cooling technique can help to control local air temperature. However, decreasing the inlet water temperature below the atmospheric dew-point temperature from the chiller requires more pumping power and insufficient cooling capacity.

Appendix

1. Thermal properties of ethylene glycol 40% by volume (Freezing point = -23.5°C)

1.1 Dynamic viscosity (μ) of ethylene glycol-based water solutions at any temperature

Temperature (°C)	μ (N·s/m ²)
-17.8	0.015
4.4	0.0048
26.7	0.0022

1.2 Density (ρ) of ethylene glycol-based water solutions at any temperature

Temperature (°C)	ρ (kg/m ³)
-8	1,075
-4	1,073
0	1,073
20	1,063

1.3 Specific heat (c_p) of ethylene glycol-based water solutions at any temperature

Temperature (°C)	c_p (kJ/kg·K)
-10	3.569
0	3.595
10	3.621

2. Thermal properties of air at 1 atm pressure

T Temp.(K)	ρ density(kg/m ³)	c_p specific heat (kJ/kg·K)	μ viscosity(10 ⁻⁷ N·s/m ²)	ν kinematic viscosity (10 ⁻⁶ m ² /s)	k thermal conductivity (10 ⁻³ W/m·K)	Prandtl number
100	3.5562	1.032	71.1	2.00	9.34	0.786
150	2.3364	1.012	103.4	4.426	13.8	0.758
200	1.7458	1.007	132.5	7.59	18.1	0.737
250	1.3947	1.006	159.6	11.44	22.3	0.72
300	1.1614	1.007	184.6	15.89	26.3	0.707
350	0.995	1.009	208.2	20.92	30.0	0.700
400	0.8711	1.014	230.1	26.41	33.8	0.690
450	0.7740	1.021	250.7	32.39	37.3	0.686
500	0.6964	1.030	270.1	38.79	40.7	0.684
550	0.6329	1.040	288.4	45.57	43.9	0.683
600	0.5804	1.051	305.8	52.69	46.9	0.685
650	0.5356	1.063	322.5	60.21	49.7	0.690
700	0.4975	1.075	338.8	68.10	52.4	0.695
750	0.4643	1.087	354.6	76.37	54.9	0.702
800	0.4354	1.099	369.8	84.93	57.3	0.709
850	0.4097	1.110	384.3	93.80	59.6	0.716
900	0.3868	1.121	398.1	102.9	62.0	0.720
950	0.3666	1.131	411.3	112.2	64.3	0.723
1000	0.3482	1.141	424.4	121.9	66.7	0.726
1100	0.3166	1.159	449	141.8	71.5	0.728
1200	0.2902	1.175	473	162.9	76.3	0.728
1300	0.2679	1.189	496	185.1	82	0.719
1400	0.2488	1.207	530	213	91	0.703
1500	0.2322	1.23	557	240	100	0.685
1600	0.2177	1.248	584	268	106	0.688
1700	0.2049	1.267	611	298	113	0.685
1800	0.1935	1.286	637	329	120	0.683
1900	0.1833	1.307	663	362	128	0.677
2000	0.1741	1.337	689	396	137	0.672
2100	0.1658	1.372	715	431	147	0.667
2200	0.1582	1.417	740	468	160	0.655
2300	0.1513	1.478	766	506	175	0.647
2400	0.1448	1.558	792	547	196	0.63

List of publications

1. Peer-reviewed journals

- 1) Napassawan Khammayom, Naoki Maruyama and Chatchawan Chaichana, Simplified model of cooling/heating load prediction for various air-conditioned room types, *Energy Reports*, Vol. 6, pp. 344-351, 2020.
- 2) Napassawan Khammayom, Naoki Maruyama and Chatchawan Chaichana, The Effect of Climatic Parameters on Strawberry Production in a Small Walk-In Greenhouse, *AgriEngineering*, Vol. 4, pp. 104-121, 2022.
- 3) Napassawan Khammayom, Naoki Maruyama, Chatchawan Chaichana and Masafumi Hirota, Impact of environmental factors on energy balance of greenhouse for strawberry cultivation, *Case Study in Thermal Engineering*, Vol. 33, 101945, 13 pages, 2022.
- 4) Napassawan Khammayom, Naoki Maruyama, Chatchawan Chaichana and Masafumi Hirota, Experimental Analysis of Local Air Temperature and Thermal Performance of a Serpentine Copper Pipe, *Energy Reports*, Vol. 9, pp. 653-661, 2023.

2. Peer-reviewed international conference proceedings

- 1) Napassawan Khammayom, Chatchawan Chaichana and Naoki Maruyama, A Comprehensive Review of Cooling Systems for Agricultural Greenhouse, *Proceedings of The 1st International Conference on Smart Community Development in the Asia Pacific (iSCAP2020)*, 2020-2, pp. 129-137, Chiang Mai, Thailand.
- 2) Napassawan Khammayom, Naoki Maruyama, Chatchawan Chaichana and Masafumi Hirota, Thermal Performance and Local Air Temperature Analysis of a Cooling Serpentine Copper Pipe, *The TSME 12th International Conference on Mechanical Engineering*, 2022-12, 9 pages, Phuket, Thailand. (In print)

3. National conferences

- 1) Napassawan Khammayom, Chatchawan Chaichana, Naoki Maruyama and Masafumi Hirota, An Experimental Study of Radiant Cooling for Greenhouse in Thailand, *Proceedings of Japan Society of Refrigerating and Air Conditioning Engineers (JSRAE2020)*, Paper No. E-134, 2020-9, 5 pages, Tsu, Japan.
- 2) Napassawan Khammayom, Chatchawan Chaichana, Naoki Maruyama and Masafumi Hirota, A FIELD STUDY OF COPPER PIPE RADIANT COOLING FOR GREENHOUSE IN THAILAND, *Proceedings of the 20th National Conference on Heat and Mass Transfer*, 2021-3, pp. 22-26, Songkla, Thailand.
- 3) Napassawan Khammayom, Naoki Maruyama, Chatchawan Chaichana and Masafumi Hirota, Filed test and analysis of copper pipe radiant cooling for greenhouse in tropical countries, *Proceedings of the Symposium on Environmental Engineering*, Paper No. 404, 2021-7, 4 pages, Online, Japan.
- 4) Napassawan Khammayom, Naoki Maruyama, Masafumi Hirota and Chatchawan Chaichana, Experimental Study of Local Microclimate and Heat Transfer Performance of a Serpentine Copper Pipe, *Tokai Engineering Complex 2022 (TEC22)*, 2022-3, 1 page, Online, Japan.

- 5) Napassawan Khammayom, Naoki Maruyama, Masafumi Hirota and Chatchawan Chaichana, The Estimation of Heat Loss and Energy Consumption Required of Strawberry Cultivation in Greenhouse, *The 59th Japan Heat Transfer Symposium*, 2022-5, 6 pages, Gifu, Japan.
- 6) Napassawan Khammayom, Naoki Maruyama, Masafumi Hirota and Chatchawan Chaichana, Experimental and Evaluation of Local Air Temperature and Thermal Performance of a Serpentine Copper Pipe, *Proceeding of 32nd Environmental Engineering Division Symposium 2022*, 2022-7, 4 pages, Takamatsu, Japan.

4. Oral presentations

- 1) Napassawan Khammayom, Chatchawan Chaichana and Naoki Maruyama, Simplified Model of Cooling/Heating Load Prediction for Various Air-Conditioned Room Types, *Lecture Meeting, The Heat Transfer Society of Japan*, Tokai Chapter, 2019-2, Nagoya, Japan.
- 2) Napassawan Khammayom, Naoki Maruyama and Chatchawan Chaichana, Simplified model of cooling/heating load prediction for various Air-conditioned room types, *The 6th International Conference on Power and Energy Systems Engineering (CPESE 2019)*, Paper ID: SE19-624E, 2019-9, 7 pages, Okinawa, Japan.
- 3) Napassawan Khammayom, Naoki Maruyama, Chatchawan Chaichana and Masafumi Hirota, Energy and environmental analysis for strawberry cultivation in small walk-in tunnel, *Lecture Meeting, The Heat Transfer Society of Japan*, Tokai Chapter, 2021-10, Nagoya, Japan.
- 4) Napassawan Khammayom, Naoki Maruyama, Chatchawan Chaichana and Masafumi Hirota, Experimental Analysis of Local Air Temperature and Thermal Performance of a Serpentine Copper Pipe, *The 9th International Conference on Power and Energy Systems Engineering (CPESE 2022)*, 2022-9, 10 pages, Kyoto, Japan